Participation of PMCA-Neuroplastin complexes in neuronal Ca^{2+} regulation, signaling and plasticity

Thesis

for the degree of

doctor rerum naturalium (Dr. rer. nat.)

approved by the Faculty of Natural Sciences of Otto von Guericke University Magdeburg

by **M.Sc. Ayse Malci**

born on 31.08.1991 in Söke (Turkey)

Examiners: apl. Prof. Dr. Constanze Seidenbecher
Prof. Dr. med. Dipl.-Phys. Stefan Hallermann

submitted on 01.06.2021
defended on 19.11.2021

Dedicated to my favorite young human being,

also known as İdil…

Summary

The calcium ion (Ca^{2+}) is a second messenger responsible for the initiation and expression for multiple forms of synaptic plasticity in neurons. The plasma membrane Ca^{2+} ATPase (PMCA) plays a capital role in Ca^{2+} clearance which is essentially important for intracellular Ca^{2+} homeostasis. Recent studies have shown that PMCA forms protein complexes with the glycoprotein Neuroplastin which leads to the stabilization of the calcium pump in the plasma membrane. In fact, in Neuroplastin-deficient mutant mice, the protein levels of the PMCA isoforms are downregulated along with the occurrence of an impaired synaptic plasticity. However, the importance of PMCA-Neuroplastin complex function in Ca^{2+} clearance and plasticity remained unrevealed. In my thesis, I focus on the role of PMCA-Neuroplastin complexes in Ca^{2+} regulation and downstream signaling ultimately associated to plastic changes in dendrites and spines of mature hippocampal neurons. I characterized high-frequency stimulation (HFS)-induced structural plasticity and PMCA-Neuroplastin levels using immunocytochemistry, confocal microscopy and live-cell calcium imaging, Neuroplastin65 overexpression and several pharmacological reagents to confirm the hypothesis that PMCA-Neuroplastin complexes regulate Ca^{2+} clearance in dendrites and spines during low and high levels of neuronal activity. Using super resolution STED microscopy and live-cell calcium imaging, I found that the synaptic localization and also function of PMCA-Neuroplastin complexes require ionotropic glutamate receptor activity. Supporting the link between PMCA-Neuroplastin complexes and ionotropic glutamate receptors, PMCAs and GluN2A-containing N-methyl-D-aspartate receptor (NMDAR2A) levels were reduced in the hippocampus of Neuroplastin-deficient mutant mice. Further, I studied Ca^{2+}-mediated downstream events and could show that PMCA-Neuroplastin complexes modulate the phosphorylation of downstream signaling molecules, i.e., extracellular signal-regulated kinase 1/2 (ERK1/2) and Ca^{2+}/calmodulin-dependent protein kinase II alpha (CaMKIIα) using PMCA inhibitors, immunocytochemistry and STED microscopy. ERK1/2 phosphorylation was increased in the hippocampus of Neuroplastin-deficient mutant mice. In this thesis, I also tested the effect of the pro-inflammatory cytokine tumor-necrosis factor-alpha (TNF-α) on Ca^{2+} restoration and found altered HFS-induced or spontaneous Ca^{2+} transients upon TNF-α treatment. Taken together, PMCA-Neuroplastin complexes are closely linked with ionotropic glutamate receptors regulating their localization and function. The participation of PMCA-Neuroplastin complexes in Ca^{2+} regulation and Ca^{2+}-dependent signaling serves a candidate mechanism underlying activity-dependent synaptic plasticity.

Zusammenfassung

Das Calzium-Ion (Ca^{2+}) ist ein sekundärer Botenstoff, welcher verantwortlich ist für die Initiierung und Ausprägung diverser Formen von synaptischer Plastizität in Neuronen. Die Plasma Membrane Ca^{2+} ATPase (PMCA) spielt eine zentrale Rolle in der Extrusion von Ca^{2+}, welche von essentieller Bedeutung für die intrazelluläre Calcium-Homöostase ist. Neuste Studien zeigen, dass PMCA mit dem Glycoprotein Neuroplastin Proteinkomplexe formt, welche zur Stabilisation der Kalzium-Pumpe in der Plasmamembran führen. In Neuroplastin-defizienten Mäusen ist das Proteinniveau von PMCA-Isoformen tatsächlich herunterreguliert, und die synaptische Plastizität ist beeinträchtigt. Welche funktionelle Bedeutung der PMCA-Neuroplastin-Komplex für die synaptische Ca^{2+} -Clearance und Plastizität hat, ist jedoch bisher unbekannt. In der vorliegenden Arbeit fokussiere ich mich auf die Rolle des PMCA-Neuroplastin-Komplexes in der Ca^{2+}-Regulation und dem nachfolgenden Signalweg, welcher mit plastischen Veränderungen in Dendriten und Spines (zu Deutsch „Dornenfortsatz“) in maturen hippocampalen Neuronen assoziiert ist. Um meine Hypothese zu verifizieren, dass PMCA-Neuroplastin-Komplexe die Ca^{2+}-Extrusionin Dendriten und Spines während niedriger und hoher neuronaler Aktivität regulieren, charakterisierte ich die durch Hochfrequenzstimulation induzierte strukturelle Plastizität und PMCA-Neuroplastin-Level durch die Anwendung von Immunzytochemie, konfokaler Mikroskopie und Life Cell-Calzium-Imaging, Neuroplastin-Überexpression und Pharmakologie. Mittels hochauflösender STED-Mikroskopie und Life Cell-Calzium-Imaging konnte ich herausfinden, dass die synaptische Lokalisierung und Funktion des PMCA-Neuroplastin-Komplexes die Aktivierung ionotroper Glutamatrezeptoren benötigt. Im Hippocampus von Neuroplastin-defizienten Mäusen waren die Mengen an PMCAs und GluN2A-enthaltenden N-methyl-D-aspartat-Rezeptoren (NMDAR2A) reduziert, was eine Verbindung zwischen den PMCA-Neuroplastin-Komplexen und ionotropen Glutamatrezeptoren unterstützt. Des Weiteren untersuchte ich Ca^{2+}-gesteuerte intrazelluläre Signalwege und konnte mittels PMCA-Inhibitoren, Immunzytochemie und STED Mikroskopie zeigen, dass PMCA-Neuroplastin-Komplexe die Phosphorylierung der nachgeschalteten extrazellulären Signal-regulierten Kinase 1/2 (ERK1/2) und Ca^{2+}/Calmodulin-abhängigen Proteinkinase II alpha (CaMKIIα) regulieren. Die ERK1/2-Phosphorylierung war im Hippocampus der Neuroplastin-defizienten Mäuse erhöht. In meiner Arbeit testete ich auch den Effekt des pro-inflammatorischen Zytokins Tumor-Nekrose Faktor-Alpha (TNF-α) bei der synaptischen Ca^{2+}-Clearance und entdeckte in TNF-α-behandelten Neuronen veränderte Ca^{2+}-Transienten sowohl nach hochfrequenter Stimulation als auch bei spontaner Aktivität. Zusammengenommen zeigt meine Arbeit eine funktionelle Verknüpfung von synaptischen PMCA-Neuroplastin-Komplexen mit ionotropen Glutamatrezeptoren, welche die Lokalisation und Funktion der PMCA regulieren. Die Beteiligung von PMCA-Neuroplastin-Komplexen in der Ca^{2+}-Regulierung und der Ca^{2+}-abhängigen Signalgebung könnte einen Kandidaten-Mechanismus für die aktivitätsabhängige synaptische Plastizität darstellen.

Table of Contents

1. Introduction

1.1. The calcium ion – its function and regulation

More than two decades ago, the calcium ion (Ca^{2+}) was described as “a life and death signal” (Berridge et al., 1998). Emphasizing its complexity and versatility, Ca^{2+} is involved in a large number of cellular processes including neuronal transmission, synaptic activity and how neurons operate the learning and memory processes in the brain. At the basal state, the cytosolic Ca^{2+} concentration oscillates around 50-100 nanomolar levels whereas at the extracellular space and intracellular stores it reaches millimolar levels (Lisek et al., 2018). The entry of Ca^{2+} into the cytosol from either external space through the plasma membrane or from the intracellular Ca^{2+} stores, elevates the Ca^{2+} concentration and acts as a signal to initiate and regulate further signal transduction. In neurons, Ca^{2+} as a signaling ion regulates various cell functions such as triggering neurotransmitter release, activation of signaling pathways, gene transcription and plasticity (Higley & Sabatini, 2012). Neuronal plasticity requires Ca^{2+} for both the strengthening and the weakening of neuronal connections (long-term potentiation or long-term depression, LTP or LTD, respectively) (Evans & Blackwell, 2015). However, within milliseconds to seconds, elevated Ca^{2+} levels are buffered by Ca^{2+}-binding proteins and cleared by Ca^{2+} extrusion mechanisms (Berridge et al., 2003). In case of any failure during Ca^{2+} handling, the Ca^{2+} homeostasis is disturbed and this can be toxic and even lethal (Berridge et al., 1998). The impairment of Ca^{2+} homeostasis has been associated with neurodegenerative diseases including amyotrophic lateral sclerosis (Grosskreutz et al., 2010), Alzheimer’s disease (Hermes et al., 2010) and neuropsychiatric disorders including schizophrenia and bipolar disorder (Lisek et al., 2018).

Molecular mechanisms of Ca^{2+} machinery is orchestrated by a number of functionally interconnected channels, receptors, pumps and exchangers (Fig. 1). A part of this Ca^{2+} regulatory machinery, Ca^{2+} clearance is executed by Ca^{2+} binding proteins, Ca^{2+} uptake into the endoplasmic reticulum by the sarco-endoplasmic reticulum Ca^{2+} ATPase (SERCA) and the other clearance mechanisms located in the plasma membrane (Higley & Sabatini, 2012). In the cell plasma membrane, Ca^{2+} clearance is carried out from the cytosol towards the external space by the plasma membrane Ca^{2+} ATPases (PMCAs) and the Na^{+}/Ca^{2+} exchangers (Blaustein & Lederer, 1999; Scheuss et al., 2006; Strehler & Zacharias, 2001). Compared to the Na^{+}/Ca^{2+} exchangers (NCX), PMCA has lower transport rates but high Ca^{2+} affinity which allows PMCA to respond to modest elevations in Ca^{2+} levels (Berridge et al., 2003). While NCX uses ion gradient to extrude Ca^{2+}, PMCA uses ATP hydrolysis to pump Ca^{2+} to the extracellular milieu.

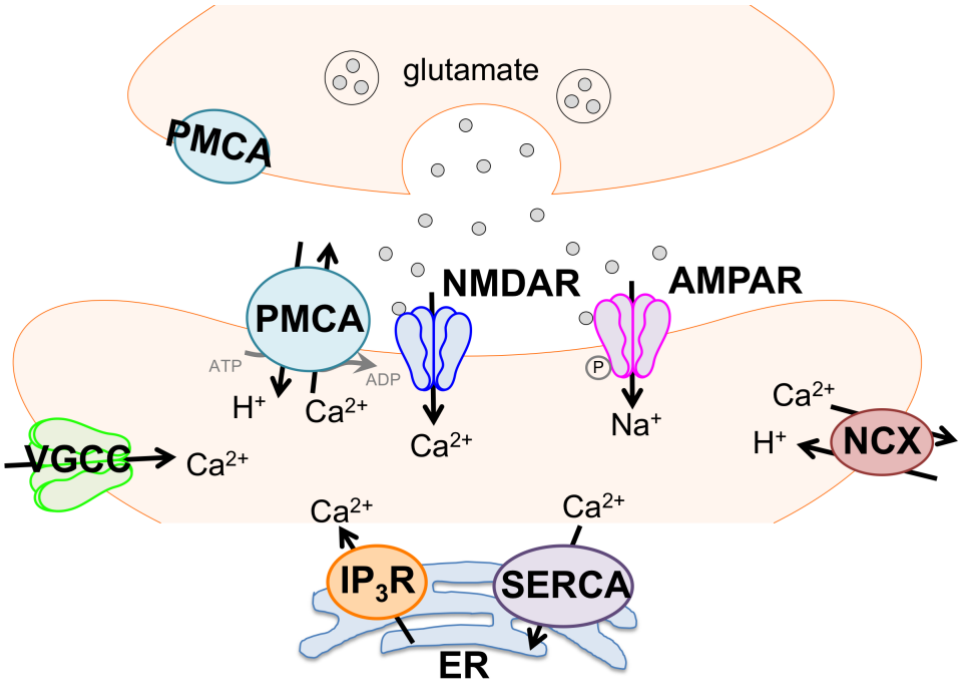

Figure 1. Simplified representation of the Ca^{2+}-managing machinery in neurons. Ca^{2+} influx is mediated through the voltage-gated Ca^{2+} channels (VGCCs) and ionotropic glutamate receptors (N-methyl-D-aspartate receptor, NMDAR and α-amino-3-hydroxy-5-methyl-4-isoxazolepropionic acid receptor, AMPAR). Ca^{2+} extrusion across the plasma membrane is carried out by the plasma membrane Ca^{2+} ATPase (PMCA) or the Na^{+}/Ca^{2+} exchangers (NCX). The endoplasmic reticulum (ER) also contributes to Ca^{2+} machinery by uptaking Ca^{2+} via the sarco/endoplasmic reticulum Ca^{2+} ATPase (SERCA) and releasing Ca^{2+} via the inositol 1,4,5-trisphosphate receptor (IP_3R). The diagram was created using Neuroscience-PPT-Toolkit-Suite (Copyright © motifolio.com).

1. 2. Plasma membrane Ca^{2+} ATPases and Ca^{2+} clearance

1.2.1. The structure of PMCAs

The plasma membrane Ca^{2+} ATPases were first characterized in erythrocytes in 1961 (Dunham & Glynn, 1961) and shown that they use the ATP hydrolysis to pump Ca^{2+} out of the human red cells across the plasma membrane (Schatzmann, 1966). After molecular cloning of PMCAs from human (Verma et al., 1988) and rat (Shull & Greeb, 1988) tissues, the protein structure of PMCA came to light. Structurally, PMCA contains 10 transmembrane domains, two large intracellular loops and N- and C-terminal tails located in the cytosol (Fig. 2). The first cytosolic loop between transmembrane domains two and three contains a phospholipid binding site also known as PL domain (Zvaritch et al., 1990). The cytosolic loop between transmembrane domains four and five contains a catalytic region including the ATP binding site and a P domain for the aspartyl-phosphate formation (Brini & Carafoli, 2011). The C-terminal tail contains the calmodulin-binding domain, consensus sites for protein

kinases A (PKA), and C (PKC) and high affinity allosteric Ca^{2+} binding sites. The calmodulin-binding domain is able to bind to the "receptor" sites in the first (A site) and second (N site) cytoplasmic loops and acts as auto-inhibition (Fig. 2A). Upon calmodulin binding, the C-terminal tail is separated from the receptor sites and is relieved of auto-inhibition (Fig. 2B). PMCA becomes active and functions in the transport of Ca^{2+}.

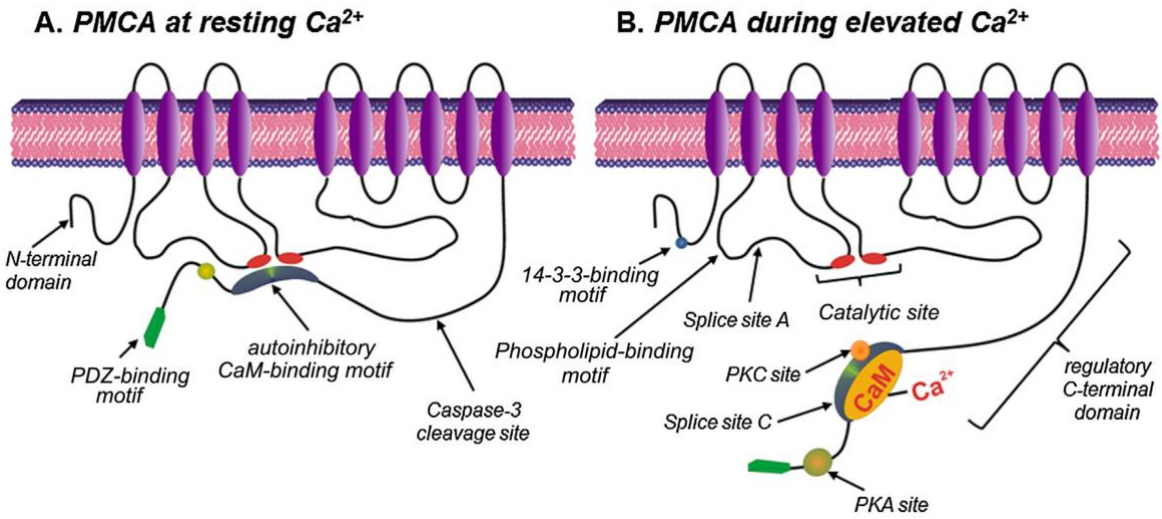

Figure 2. Schematic representation of two-dimensional topological model of the structure of the PMCA during resting state and following activation. **A)** At low Ca^{2+} levels during resting state, the autoinhibitory calmodulin (CaM) binding motif within the C-terminal tail of the PMCA associates with the catalytic motif and prevents Ca^{2+} binding. **B)** Upon Ca^{2+} rise, Ca^{2+}/calmodulin binds to the autoinhibitory CaM binding motif and induce a conformational change. This change allows dissociation from the catalytic motif and transport of Ca^{2+}. Additional regulatory motifs include an inhibitory 14-3-3-binding site in the N-terminal region, a stimulatory phospholipid-binding motif in the first cytosolic loop and PKA/PKC phosphorylation consensus sites and a PDZ binding motif in the C-terminal tail. Splice sites A and C can generate various alternative splice variants. Illustration was taken from Bruce J. (Bruce, 2018).

1.2.2. The ATPase function of PMCAs

PMCAs belong to the P-type ATPases which are known by forming a phosphorylated high-energy intermediate resulting in the formation of an acyl-phosphate which supplies required energy for Ca^{2+} pumping. PMCAs operates with a 1:1 Ca^{2+}/ATP ratio (Niggli et al., 1981). The pump has a relatively high Ca^{2+} affinity, with 10 to 20 μM K_d for Ca^{2+} in the resting state and 1 μM K_d for Ca^{2+} in calmodulin-binding state (Brini, 2009). PMCA is activated by Calmodulin (Niggli et al., 1979), acidic phospholipids (Niggli et al., 1981), oligomerization

(Kosk-Kosicka & Bzdega, 1988) and also phosphorylation (Caroni & Carafoli, 1981; Smallwood et al., 1988).

As a member of P-type ATPase family, PMCA has two major conformations, namely the E1 and E2 states. In the E1 state, PMCA would bind Ca^{2+} with high affinity at the cytosolic side of the plasma membrane. On the other hand, in the E2 state the affinity of PMCA for Ca^{2+} would drastically decrease, leading to its release to the extracellular milieu.

1.2.3. Alternative splice variants of PMCAs

In mammals, four genes encode four different PMCAs and alternative RNA splicing of each of them generates more than 20 distinct PMCA variants (and/or isoforms) (Strehler & Zacharias, 2001). The differential expression of PMCA isoforms in different tissues also during developmental stages suggests the requirement of PMCAs for the spatial and temporal control of Ca^{2+} homeostasis. PMCA1 and PMCA4 are mainly found in all tissues in the mammalian adults including mouse and rat, whereas PMCA2 and PMCA3 are more specific to excitable cells of the nervous system and also skeletal muscles (Burette et al., 2003; Strehler et al., 2007). With certain levels of overlap, all isoforms are differentially expressed in various cells and tissues and they may display different transport kinetics. The PMCA2 and PMCA3 variants display fast kinetics and stay active for a long time (Caride et al., 2001). PMCA4b binds Ca^{2+}/CaM slowly and it remains bound for minutes (Caride et al., 1999; Penheiter et al., 2003) whereas PMCA4a binds Ca^{2+}/CaM rapidly and it dissociates also quickly.

Alternative splicing occurs at two major sites of the PMCAs: site A in the first intracellular loop and at site C in the calmodulin binding domain at the C-terminal tail. The splicing at site A does not considerably alter the PMCA structure. Alternative splice variants occurring at site C results in variants termed “a” and “b”. One variant causes a shift in the open reading frame, produces a premature stop codon and results in a truncated splice variant, i.e. “a” form (Brini et al., 2013). Unlike the “a” form, the “b” form contains a C-terminal PDZ (post-synaptic density (PSD) 95/Dlg/ZO-1) binding motif (DeMarco & Strehler, 2001). This domain is important for interaction of PMCAs with other PDZ binding proteins, especially at the PSD of the synapse. Also, alternative splicing results in a significant difference in calmodulin and kinase regulation, leading to different affinity for Ca^{2+} and even different kinetics (Penniston & Enyedi, 1998).

1.3. PMCAs and their protein-protein interactions

A rapid and local Ca^{2+} influx requires PMCAs to be localized and function in a spatially and temporally specialized manner. In order to operate Ca^{2+} extrusion in the right place at the right time, PMCAs bind to various interaction partners intracellularly. These interaction partners act as a link between specific PMCA isoforms and particular signaling pathways (Strehler et al., 2007). The currently known protein-protein interactions seem to be specific for each subgroups of PMCA isoforms and/or splice variants. The protein 14-3-3ε was identified as an interaction partner of the N-terminal tail of PMCA4 (Rimessi et al., 2005). At least three different signaling proteins have been identified to physically interact with the large catalytic loop of PMCA4b. These are the Ras effector protein RASSF1 (Armesilla et al., 2004), the catalytic A-subunit of the Ca^{2+}/CaM-dependent phosphatase calcineurin (Buch et al., 2005) and α-1 syntrophin (Williams et al., 2006). Calmodulin is a well-known interaction partner and major regulator of PMCA activity (Jarrett & Penniston, 1978). In addition to calmodulin, members of the membrane-associated guanylate kinase (MAGUK) family such as the synapse-associated proteins PSD95/SAP90, SAP97/hDlg, SAP102, and PSD93/ chapsyn-110 (DeMarco & Strehler, 2001; Kim et al., 1998) as well as the Ca^{2+}/CaM-dependent serine protein kinase CASK (Schuh et al., 2003) were also found to bind to the C-terminal tail of the PMCA. PMCA2b also interacts with the ania3-Homer complex within the hippocampal neurons (Sgambato-Faure et al., 2006) and with Homer 3 in the cerebellum (Kurnellas et al., 2007). The interaction of PMCA with synapse-associated proteins are important for their anchoring, targeting and signaling at the synapse.

Regardless the importance of PMCA at the synapse, little is known about PMCA and its relationship with synaptic cell adhesion molecules (CAM). Very recently, the CAM Neuroplastin was found to be a prominent interaction partner of PMCAs in neurons (Herrera-Molina et al., 2017) and immune cells (Korthals et al., 2017). Neuroplastin overexpression promoted PMCA protein levels and their plasma membrane localization in both HEK cells and cultured rat neurons (Herrera-Molina et al., 2017). This study also showed that reduced PMCA levels were correlated with elevated basal Ca^{2+} levels and slow and inefficient restoring of Ca^{2+} levels in Neuroplastin-deficient neurons. Right after, Neuroplastin together with Basigin, a paralog of Neuroplastin, were shown as an essential auxiliary subunit of PMCAs in different tissues and cell types (Schmidt et al., 2017). The exclusive protein complex of PMCA together with the two Ig domain containing proteins (Neuroplastin or Basigin) was shown as obligatory for stability of PMCAs and their plasma membrane localization. A detailed affinity purification assay revealed that Neuroplastin-PMCA assemblies are splice-variant independent, widely exclusive in the brain (>95% of total PMCA binds to Neuroplastin) and stochiometric (Schmidt et al., 2017). Later, the crystal

structure of the human PMCA1 and Neuroplastin complexes was reported by using the cryo-electron microscopy (cryo-EM). The single transmembrane helix of Neuroplastin was shown to interact with the transmembrane helices 8-9-linker and transmembrane helices 10 of human PMCA1 (Go & Soboloff, 2018; Gong et al., 2018). This interaction is important for adjusting PMCA conformation and accessibility of cytosolic Ca^{2+} to PMCA.

1.4. Features, expression and localization of Neuroplastin

1.4.1. Structure, expression and subcellular localization of Neuroplastin

Neuroplastins are transmembrane glycoproteins that belong to immunoglobulin (Ig) superfamily. They were first identified as glycoprotein components of synaptic membranes and postsynaptic density fractions in rat brain (Hill et al., 1988). Neuroplastin65 and Neuroplastin55 are raised from a single gene by alternative splicing (Langnaese et al., 1997). Neuroplastin55 contains two N-terminal Ig domains and enables only molecular interactions *in cis* whereas Neuroplastin65 has an additional Ig domain which allows interaction *in trans* (Owczarek et al., 2011; Smalla et al., 2000). Next to Ig domains, Neuroplastins have a single-pass transmembrane region followed by a short cytosolic C-terminal tail (Fig. 3). An alternative four amino acids insertion (Asp-Asp-Glu-Pro (DDEP)) in the cytosolic tail creates +DDEP and -DDEP isoforms creating four Neuroplastin isoforms in total (Langnaese et al., 1997). Ig2 and Ig3 domains of Neuroplastin contains six N-glycosylation sites.

The developmental expression profile of the Neuroplastin transcripts reveals highest mRNA levels during the first postnatal month in the rat. In human progenitor cells, *NPTN* gene expression was found to be increased during the first 7 days of differentiation *in vitro* (Desrivieres et al., 2015). In the rodent brain, Neuroplastin55 seems to be dominant in the embryonic brain whereas Neuroplastin65 levels increase rapidly during the second and third postnatal weeks (Hill et al., 1988; Langnaese et al., 1997).

In the mature brain, Neuroplastin65 is exclusively expressed in neurons with highest levels in forebrain regions such as the cerebral cortex, the hippocampus, the amygdala and the striatum. On the other hand, Neuroplastin55 is widely expressed in other tissues as well (Hill et al., 1988; Langnaese et al., 1997; Smalla et al., 2000). In the hippocampus, Neuroplastin65 expression is the higher in the CA1 and DG region compared to other regions namely CA2 and CA3 (Herrera-Molina et al., 2014; Smalla et al., 2000). The levels of Neuroplastin65 are lower in the other brain areas for instance thalamus and hypothalamus. In the cerebellum, 95% of total Neuroplastin is Neuroplastin55 (Marzban et al., 2003). Outside of the brain, Neuroplastin65 is detected in the inner and outer plexiform layers of rat

retina (Kreutz et al., 2001) and also in the cochlea of the mouse inner ear (Carrott et al., 2016; Lin et al., 2021). Additionally, Neuroplastin65 was detected in keratinocytes and lesions of atopic dermatitis skin together with S100A9 (Sakaguchi et al., 2016).

Both Neuroplastins are present at the synapse (Hill et al., 1988; Smalla et al., 2000). Neuroplastin65, but not Neuroplastin55 were found in the postsynaptic density protein fraction (Langnaese et al., 1997; Smalla et al., 2000). Biochemically isolated fractions from rat brain homogenates revealed that Neuroplastin, also PMCA1 and PMCA2, are present in docked synaptic vesicles in the active zone (Boyken et al., 2013). Neuroplastins were shown in both excitatory and inhibitory synapses (Herrera-Molina et al., 2014). A reduced number but also mismatched excitatory synaptic contacts were shown in both Neuroplastin-deficient and Neuroplastin65-Fc-treated CA1 and DG neurons whereas inhibitory synaptic contacts were unaltered (Herrera-Molina et al., 2014). Synaptically located Neuroplastin65 colocalizes with $GABA_A$ receptor α1 and α2 subunits and VIIAAT at inhibitory synapses (Sarto-Jackson et al., 2012). In the ear, Neuroplastin65 localizes at the presynaptic region of inner hair cells (IHC) and the colocalization of presynaptic IHC ribbons and postsynaptic afferent terminals were significantly reduced in the absence of Neuroplastin65 (Carrott et al., 2016). Very recently, our research showed that Neuroplastin promotes synaptogenesis together with its interaction partner TRAF6 and deletion of TRAF6 binding site in Neuroplastin or TRAF6 inhibitor prevents the progression of synaptogenesis (Vemula*, Malci* et al., 2020) (further explained and discussed later). Altogether, these facts highlight that Neuroplastin is important for the formation and maintenance of spines.

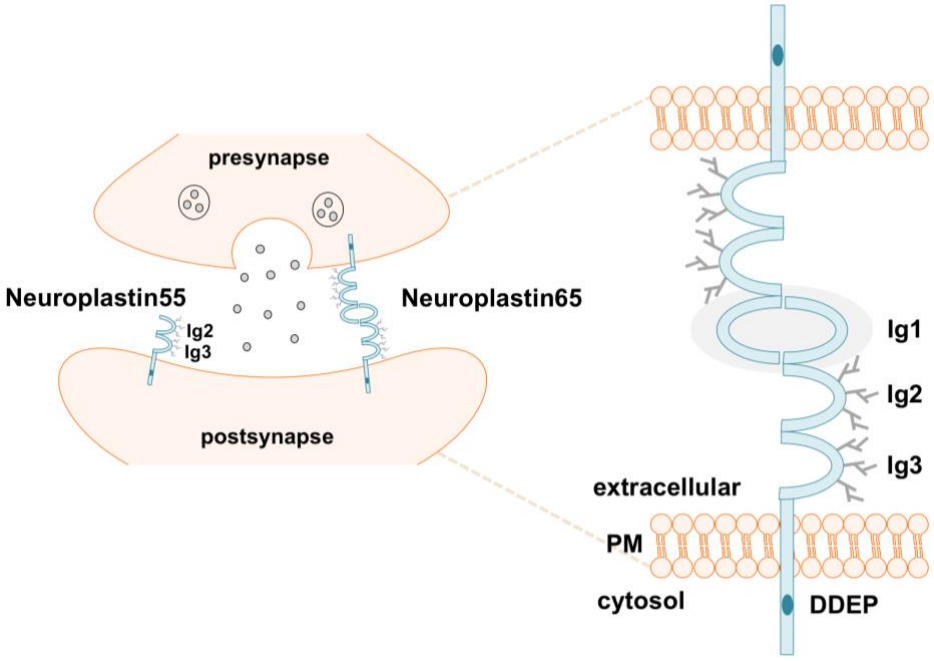

Figure 3. Structural features of Neuroplastin65 and Neuroplastin55 at the synapse. Neuroplastin65 contains three N-terminal immunoglobulin (Ig) domains and Neuroplastin55 have two Ig domains. The first Ig domain (Ig1) is specific for Neuroplastin65 and mediates *trans*-homophilic binding. The Ig domains are followed by a single membrane-spanning sequence and a short C-terminal tail which can display a DDEP insertion or not (Np + DDEP and Np – DDEP, respectively). Ig2 and Ig3 domains of Neuroplastin65 contain six N-glycosylation sites. PM stands for the plasma membrane. The diagram was created using Neuroscience-PPT-Toolkit-Suite (Copyright © motifolio.com).

1.4.2. Neuroplastin's binding partners in neurons

Several binding partners of Neuroplastin were discovered in recent years interacting with extracellular, intracellular and/or transmembrane binding regions. One of the early discoveries was fibroblast growth factor receptor type-1 (FGFR1). The interaction of FGFR1 with Neuroplastin55 occurs in the Ig2 domain of Neuroplastin55. A direct interaction of the α1, α2 and α5 subunits of $GABA_A$ receptor with Neuroplastin in the cell membrane was shown by affinity chromatography, immunoprecipitation and FRET experiments (Sarto-Jackson et al., 2012). Both Neuroplastin isoforms were shown to chaperone the monocarboxylate transporter 2 (MCT2) allowing their localization in the cell surface of HEK cells (Wilson et al., 2013). Our recent work discovered TRAF6 as a novel interaction partner of Neuroplastin binding through TRAF6 binding motif (i.e., (Basic residues)-X-X-P-X-E-X-X-(Ar/Ac)) in the C-terminal tail of Neuroplastin65 and Neuroplastin55 (Vemula*, Malci* et al., 2020). The TRAF6 binding motif in Neuroplastin was not found in other known synaptic CAMs suggesting that TRAF6 interaction is specifically required by Neuroplastin to promote formation of dendritic protrusions in immature neurons. Interestingly, during the early stage of development, PMCA activity was not required by Neuroplastin-TRAF6 to form new dendritic protrusions.

During the finalization of my thesis work, it was published that the amino-terminal domain of the GluA1 subunit of AMPAR selectively interacts with the isoform-specific Ig1 Domain of Neuroplastin65, but not Neuroplastin55 (Jiang et al., 2021). This novel extracellular interaction was described as important for LTP maintenance (Jiang et al., 2021). As mentioned above, Neuroplastin is a prominent interaction partner of PMCAs and their interaction takes place in the interface of hydrophobic residues in the transmembrane region of Neuroplastin (Go & Soboloff, 2018; Gong et al., 2018).

1.4.3. Neuroplastin in disease

The regulation of Neuroplastin function in cognition- and emotion-related brain regions such as the cortex, the hippocampus and the amygdala raises an obviously important question. Is Neuroplastin potentially associated with cognitive or neuropsychiatric disorders? Indeed, disease-related single nucleotide polymorphism (rs7171755) located in the downstream of human *NPTN* gene is associated with reduced cortical thickness and impaired intellectual ability in adolescents (Desrivieres et al., 2015). The human *NPTN* gene is also associated with schizophrenia. Three SNPs located in the 5'-upstream regions of human NPTN gene were detected in schizophrenic patients (Saito et al., 2007). Also, upregulation of Neuroplastin and Basigin were found in two animal models for schizophrenia (Sato et al., 1983). Anxiety-like behavior has been reported in mice lacking constitutively the expression of Neuroplastin65 and 55 or only Neuroplastin65 (Amuti et al., 2016; Bhattacharya et al., 2017). Neuroplastins are essential for learning and memory. Retrograde amnesia of light-clued associative memories was found in inducible Neuroplastin-deficient adult mice ($Nptn^{\Delta lox/loxPr\text{-}CreERT}$) when the *Nptn* gene was excised after learning (Bhattacharya et al., 2017). In addition to brain-associated alterations, an impairment of hearing was observed via behavioral experiments in constitutive Neuroplastin-deficient mice (Bhattacharya et al., 2017) and severe hearing deficits were shown in the cochlea in the absence of Neuroplastin (Carrott et al., 2016; Lin et al., 2021; Zeng et al., 2016).

1.5. Roles of PMCA and Neuroplastin in neuronal plasticity

Synaptic plasticity as a form of neuronal plasticity includes changes in synaptic transmission and strength, and it is proposed as a mechanism for the information storage leading to learning and memory. Upon synaptic transmission, elevated intracellular Ca^{2+} concentrations demand an appropriate timing and extent of Ca^{2+} clearance. PMCA has been found to be a major contributor of Ca^{2+} clearance at the synapse (Scheuss et al., 2006) involved in different forms of plasticity (Empson et al., 2007; Jensen et al., 2007; Simons et al., 2009).

As mentioned, PMCA is present in both pre- and post-synapses. The finding of enhanced paired-pulse facilitation in PMCA2-knockout mice suggests that PMCA2-mediated Ca^{2+} clearance is important for presynaptic short-term plasticity at cerebellar Purkinje neurons (Empson et al., 2007). In addition to the cerebellum, a functional role of PMCA2a and PMCA2-mediated Ca^{2+} clearance in excitatory synaptic transmission was also shown at hippocampal CA3 presynaptic terminals (Jensen et al., 2007). CA2 neurons of the hippocampus express a large number of Ca^{2+}-regulating proteins and characteristically do not generate long-term potentiation (LTP). However, pharmacological inhibition of PMCA with Carboxyeosin led to the induction of LTP in CA2 neurons (Simons et al., 2009).

Together with NCX, PMCAs were found as the major Ca^{2+} extrusion pathways in spines and dendrites (Scheuss et al., 2006). Pharmacological inhibition of PMCA with a calmodulin blocker Calmidazolium supported the role of PMCA-mediated Ca^{2+} extrusion in spike-timing dependent plasticity (Scheuss et al., 2006).

Neuroplastin is also present at the synapse and involves in neuronal plasticity. Neuroplastin65 is localized in the postsynaptic region of CA1 synapses and its presence is significantly enhanced following to LTP induction (Smalla et al., 2000). The contribution of Neuroplastin65 to long-term synaptic plasticity first became evident by impairing LTP upon treatment with Neuroplastin antibodies or recombinant extracellular fragments of Neuroplastin65, i.e. the most N-terminal Ig domain (Empson et al., 2006; Smalla et al., 2000). Treatment with extracellular fragments of Neuroplastin65 also caused a reduction in the surface expression of GluA1 subunit of AMPAR which is a key component of neurotransmission (Empson et al., 2006). Neuroplastin deficiency (both constitutive and induced) affects electrophysiological properties of excitatory and inhibitory synapses (altered frequency and amplitude of mEPSCs and mIPSCs) and LTP expression in CA1 neurons (Bhattacharya et al., 2017). Later, impaired LTP maintenance was also confirmed in CA1 neurons in Neuroplastin65-deficient mice (Li et al., 2019). Very recently, neurons lacking Neuroplastin65 showed severely impaired LTP maintenance (Jiang et al., 2021). The specific association of Neuroplastin65 with AMPAR was shown to be essential for the synaptic anchoring of AMPAR during LTP suggesting the isoform-specific requirement for Neuroplastin in LTP maintenance. Given their individually discovered contribution to neuronal plasticity, PMCA-Neuroplastin complexes are the candidates modulating synaptic plasticity. In the line with PMCA-Neuroplastin interaction (Go & Soboloff, 2018; Gong et al., 2018; Herrera-Molina et al., 2017; Korthals et al., 2017; Schmidt et al., 2017), reduced levels of PMCAs were found in Neuroplastin-deficient mouse brain (Bhattacharya et al., 2017) and also in Neuroplastin-deficient cultured neurons (Herrera-Molina et al., 2017). The absence of Neuroplastin results in elevated cytosolic Ca^{2+} levels and impaired Ca^{2+} clearance which is a consequence of reduced PMCA levels (Herrera-Molina et al., 2017). This finding in neurons was also confirmed in other cells types or by using different experimental tools (Korthals et al., 2017; Schmidt et al., 2017).

1.6. Crosstalk between PMCA and ionotropic glutamate receptors

In order to efficiently control local levels of intracellular Ca^{2+}, Berridge *et al*., introduced a balanced concept between the “on” reactions that introduce Ca^{2+} into the cytoplasm and the “off” reactions through which Ca^{2+} is removed by the orchestra of buffers, pumps and exchangers (Berridge et al., 2003). In the context of microdomains of spatially confined Ca^{2+}

signaling, PMCAs are expected to be recruited into close proximity of Ca^{2+} entry sites, such as NMDA-type glutamate receptors (Strehler et al., 2007).

As a biochemical evidence of coupling of Ca^{2+} clearance and Ca^{2+} entry, the previously suggested interaction of PMCA2 with PSD95 (DeMarco & Strehler, 2001) was confirmed *in vivo* in synapse-enriched tissue from cerebellum (Garside et al., 2009). Also, the authors of this study showed that NMDARs are in close proximity with PMCA2 using GST-pull down, immunoprecipitation and immunohistochemistry assays (Garside et al., 2009). The PMCA2-PSD95 coupling was stated as an efficient way to limit the spread of local Ca^{2+} by coupling PMCA2-mediated Ca^{2+} extrusion with Ca^{2+} entry through NMDAR.

A couple of studies have suggested the existence of a functional coupling between PMCA and NMDARs. It has been shown that hyperactivation of synaptic NMDARs by glutamate uncaging produced depression of Ca^{2+} extrusion via PMCA in hippocampal neurons (Scheuss et al., 2006). The protease calpain-mediated internalization of PMCA was shown to be triggered by NMDAR activation (Ferragamo et al., 2009; Pottorf et al., 2006). PMCA is also known to be a source of alkalinization via H^+ movement across the postsynaptic membrane which is able to cause a rapid rise of extracellular pH during evoked neuronal activity (Makani & Chesler, 2010). Also, the PMCA is found near postsynaptic NMDARs and acts in an autocrine fashion to boost synaptic NMDAR currents in hippocampal slices (Chen & Chesler, 2015). In a recent study, NMDAR EPSCs were reduced when PMCA activation was prevented by the PMCA inhibitor Carboxyeosin. Thus, PMCA was confirmed for causing pH changes and influencing extracellular microdomains of NMDARs at the postsynapse (Stawarski et al., 2020). Also, recently, ketamine-treated (NMDAR antagonist) animal model of experimental psychosis revealed altered mRNA and protein levels of PMCA isoforms in various brain regions. Moreover, treatment of cortical synaptosomal membranes with ketamine inhibited rapidly the PMCA enzymatic activity (Boczek et al., 2019; Lisek et al., 2018; Lisek et al., 2017).

1.7. Cell signaling modulated by either PMCA or Neuroplastin

PMCA does not only act as Ca^{2+} extruding pump but also as regulator of cellular signaling. PMCA's large catalytic loop in the cytosol interacts with at least three different proteins: RASSF1, calcineurin A and alpha-1 syntrophin. PMCA4b was shown to regulate extracellular signal-regulated kinase 1/2 (ERK1/2) activation via its interaction with the RASSF1 in HEK 293 cells (Armesilla et al., 2004). PMCA4b also interacts with calcineurin A catalytic subunit and inhibits the calcineurin/nuclear factor of activated T-cell (NFAT) pathway (Buch et al., 2005). As third, PMCA (isoforms 1 and 4) and alpha-1 syntrophin and nitric-oxide synthase-1 (NOS-1) form complexes and regulate NO signaling in skeletal and heart muscle (Williams et

al., 2006). However, physiological relevance of these interactions is not well understood yet as most of the studies were done in cells overexpressing PMCA and other constructs.

Protein-protein interaction in the C-terminal tail of PMCA is also important for signaling. PMCA is activated by the Ca^{2+} signaling protein calmodulin (CaM) by binding of CaM to an autoinhibitory domain of PMCA (Jarrett & Penniston, 1978). As described above, the b-splice variant of PMCA isoforms is able to interact with PDZ proteins including members of the membrane-associated guanylate kinase (MAGUK) family such as the synapse-associated proteins PSD95/SAP90, SAP97/hDlg, SAP102, and PSD93/ chapsyn-110 (DeMarco & Strehler, 2001) and the Ca^{2+}/CaM-dependent serine protein kinase CASK (Schuh et al., 2003) as a multi-protein signaling hub at pre-synaptic nerve terminals and post-synaptic spines. Besides the activation of PMCA with Ca^{2+}-CaM, PMCA function is also increased by acidic phospholipids. Relatively low concentrations of phosphatidylinositol 4,5- bisphosphate [PtdIns(4,5)P_2] are required for their activation (Choquette et al., 1984; Lehotsky et al., 1992; Missiaen et al., 1989). In addition to PMCA function in Ca^{2+} clearance, PMCAs also protect PtdIns(4,5)P_2 in the plasma membrane from hydrolysis by phospholipase C (PLC) and lead to decreased production of inositol 1,4,5-triphosphate ($InsP_3$), and subsequently Ca^{2+} signal (Penniston et al., 2014). Considering the abundance of PMCAs in dendritic spines, a fine balance of PtdIns(4,5)P_2 and PMCAs should be essential for proper neuronal physiology and transmission.

Neuroplastin can interact with various proteins including intracellular proteins or cell surface receptors to serve its numerous functions through the activation of downstream signaling molecules. Indeed, it has been shown that Neuroplastin55 binds to and signals through fibroblast growth factor receptor 1 (FGFR1) (Owczarek et al., 2011), inducing neurite outgrowth. Neuroplastin55-induced signaling involves ERK1/2 and p38 mitogen activated protein kinase (MAPK) (Owczarek et al., 2010). On the other hand, Neuroplastin65-induced downstream signaling was first studied in the context of synaptic plasticity. The treatment of hippocampal neurons with Neuroplastin65-specific fusion protein activates p38 MAPK signaling to regulate synaptic strength by altering surface glutamate receptor expression (Empson et al., 2006). Later, recombinant proteins derived from the ectodomain of Neuroplastin65 (ectoNp65) and the first Ig domain (enplastin) was found to increase neurite outgrowth in cultured rat hippocampal neurons (Owczarek et al., 2011). Neuroplastin65 and enplastin-induced neurite outgrowth depends on activation of FGFR, MAP kinases and Ca^{2+}/calmodulin-dependent protein kinase II (CaMKII) (Empson et al., 2006; Owczarek et al., 2011; Smalla et al., 2000). Neuroplastin65 and enplastin also induce Ca^{2+} responses in hippocampal neurons, suggesting that activation of these kinases is dependent on synaptic Ca^{2+} signaling (Owczarek et al., 2011). In addition to above described findings using

treatment with peptides, another study using a mouse model lacking Neuroplastin65 revealed increased phosphorylation levels of ERK1/2 and CREB in the forebrain (Amuti et al., 2016). In the same animal model, they also found altered synaptic proteins including an increased level of GluN2A-containing NMDAR, whereas GluN1 and GluN2B levels were unchanged. All of this evidence indicates that Neuroplastin is required for synapse formation, neurotransmission and plasticity through cascaded signaling pathways. In the context of ER stress, Neuroplastin interacts with the mesencephalic astrocyte-derived neurotrophic factor (MANF) regulating inflammatory response and apoptosis via suppression of NF-κB signaling (Yagi et al., 2020).

In the view of these previous findings linking separately PMCA and Neuroplastin to synaptic plasticity and the existence of the recently identified PMCA-Neuroplastin complexes, it can be postulated that they participate in Ca^{2+} clearance that contribute to the regulation of synaptic plasticity. This hypothesis is diagramed in Figure 4 and tested in this thesis.

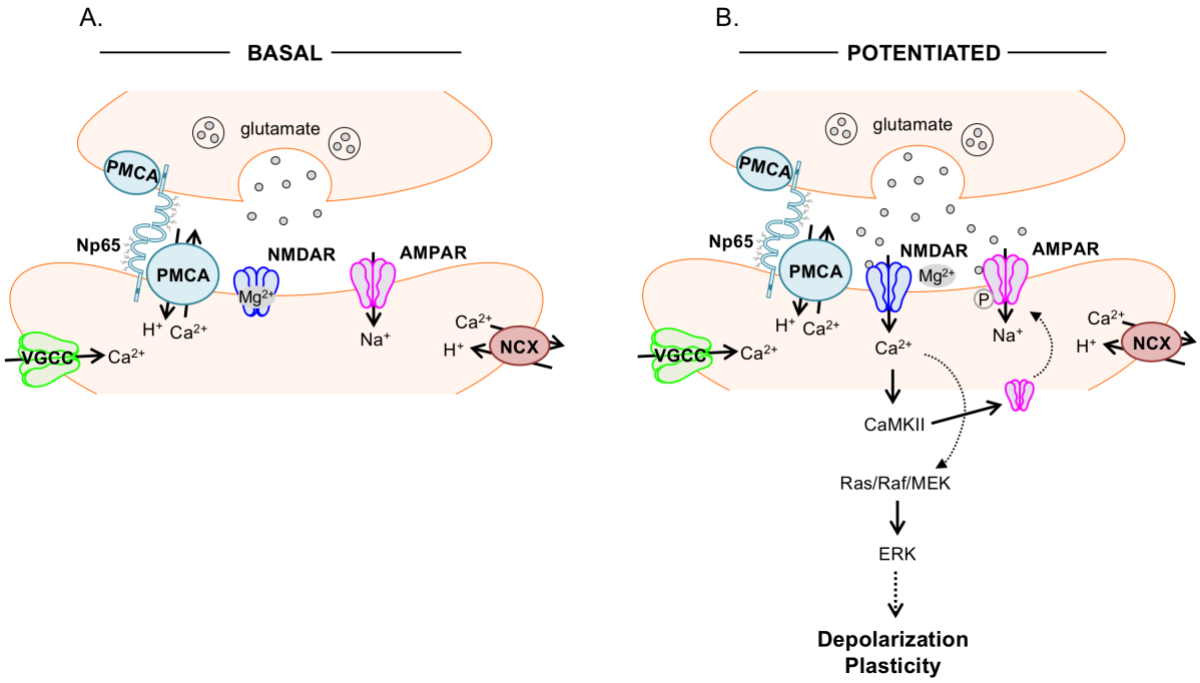

Figure 4. Hypothetical model of PMCA involvement in synaptic plasticity and signaling at excitatory synapses. A) During basal synaptic transmission, glutamate release from presynaptic terminals binds both the NMDAR and AMPARs. Na^+ flows through the AMPAR but not through the NMDAR due to the existence of Mg^{2+} block. **B)** Depolarization of the postsynaptic cell removes the Mg^{2+} block of the NMDAR channel and allows both Na^+ and Ca^{2+} to flow into the dendritic spine. Activity-dependent elevations in Ca^{2+} in the spine trigger Ca^{2+}-dependent signaling cascades including several kinases that orchestrate synaptic plasticity. Abbreviations: Np65 (Neuroplastin65), the voltage-gated Ca^{2+} channels (VGCCs), N-methyl-D-aspartate

receptor (NMDAR), α-amino-3-hydroxy-5-methyl-4-isoxazolepropionic acid receptor (AMPAR), plasma membrane Ca^{2+} ATPase (PMCA), Na^{+}/Ca^{2+} exchangers (NCX). The diagram was created using Neuroscience-PPT-Toolkit-Suite (Copyright © motifolio.com).

1.8. Neuroinflammation and plasticity

Cytokines are small signaling molecules in the central nervous system secreted by neurons, microglia and astrocytes. They include interleukins, chemokines, tumor-necrosis factor, interferons, growth and cell stimulating factors. These cytokines and their receptors are constitutively expressed in various brain regions under physiological and/or pathophysiological conditions (Khairova et al., 2009). There is a growing interest on the role of cytokines in plasticity such as LTP and homeostatic plasticity e.g. synaptic scaling (Bourgognon & Cavanagh, 2020; Stellwagen & Malenka, 2006).

Tumor-necrosis factor-alpha (TNF-α) is primarily localized in neurons of the hypothalamus and caudal raphe nuclei (Breder et al., 1993; Churchill et al., 2008), also in astrocytes (Chung & Benveniste, 1990; Lieberman et al., 1989). Primary localization of cytokine receptors TNFR1 and TNFR2 was observed on neurons and glia in the cortex, hippocampus, thalamus (Boka et al., 1994; Tchelingerian et al., 1993). Mice lacking TNF-α display severe impairment in spatial memory and learning (Baune et al., 2008) whereas rats injected with TNF-α better performed better in learning and memory-related behavioral tasks (Brennan et al., 2004). TNF-α released from glial cells increases the insertion of AMPAR in the plasma membrane of synapses via PI3K signaling and in turn synaptic strength increases. On the contrary, removal of TNF-α from brain slices weakens synaptic activity (Beattie et al., 2002). Not only excitatory signaling, but also inhibitory signaling including $GABA_A$ receptors internalization is regulated by TNF-α (Stellwagen et al., 2005; Stuck et al., 2012). However, the role of TNF-α in LTP and LTD is not entirely understood yet. Some early studies reported that LTP induction or maintenance did not affected in TNF-α KO mice (Albensi & Mattson, 2000; Stellwagen & Malenka, 2006). However, a later study showed an inhibition of LTP in CA1 neurons upon treatment with TNF-α (1.8 nM) (Singh et al., 2019). Although TNF-α was reported to be required for the induction of LTD via NF-κB activation in the hippocampus (Albensi & Mattson, 2000), this was not confirmed by other studies (Stellwagen & Malenka, 2006). Therefore, it still remains to be elucidated whether and how precisely TNF-α levels control the balance between physiological and/or pathophysiological conditions.

Under inflammatory conditions including neurodegeneration and mood disorders, TNF-α levels rise from picomolar to millimolar levels and this drastic change in TNF-α levels brings along various alterations in cellular physiology (Fig. 5). Pathophysiological levels of TNF-α were found to inhibit LTP in the CA1 region and the DG region of the rat hippocampus (Butler

et al., 2004; Cunningham et al., 1996; Tancredi et al., 1992). Phosphorylation of MAPKs including p38-MAPK, ERK and the c-Jun N-terminal kinase (JNK) was seen upon TNF-α treatment leading to inhibition of LTP (Singh et al., 2019). Moreover, increased levels of TNF-α led to NF-κB activation and potentiation of NMDAR and AMPAR. This is further suggested to cause glutamate excitotoxicity (Bernardino et al., 2005; Zou & Crews, 2005) and cell death (Li et al., 2004). Along the same line, synaptic insertion of Ca^{2+}-permeable AMPAR lacking GluR2 subunit is fostered by TNF-α what may increase the risk of excitotoxicity (Leonoudakis et al., 2004; Stellwagen et al., 2005). The maintenance of TNF-α levels seems to be a crucial line between physiology and pathophysiology. Indeed, it was shown that TNF-α modulates synaptic plasticity in a concentration dependent manner (Maggio & Vlachos, 2018). Electrophysiological recordings in acute brain slices treated with high concentrations of TNF-α (1 µg/ml) showed impaired LTP. Interestingly, in the same study, low concentrations of TNF-α (100 ng/ml) even improved LTP. The molecular mechanism modulating plasticity effects of TNF-α was suggested as intraneuronal Ca^{2+} signaling via the IP_3R (Park et al., 2008) and the ryanodine receptor-mediated Ca^{2+} release from intracellular Ca^{2+} stores (Maggio & Vlachos, 2018). Therefore, it is plausible to think of TNF-α as a modulator of intracellular Ca^{2+} homeostasis and alterations during the establishment and stability of neuronal plasticity under physiological and pathophysiological conditions.

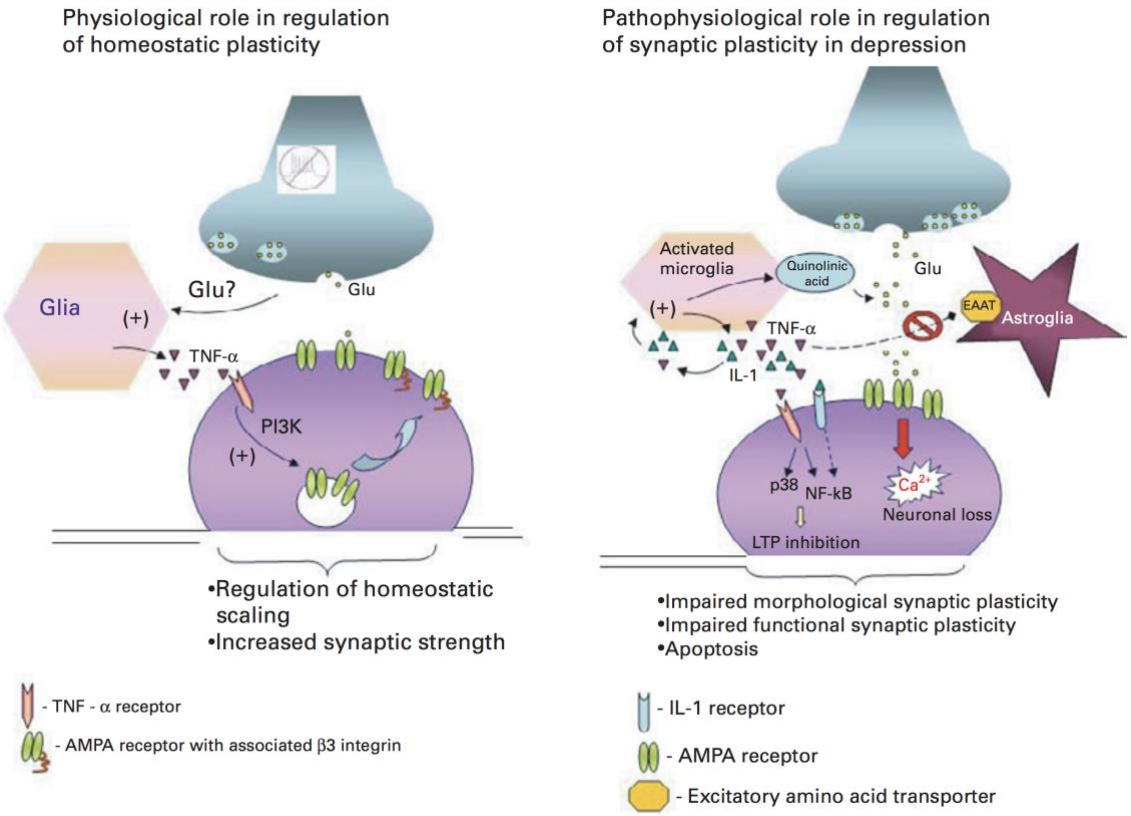

Figure 5. The role of pro-inflammatory cytokines in synaptic plasticity. The illustration on the left represents the role of constitutively expressed TNF-α in regulation of homeostatic synaptic plasticity under physiological conditions. The release of TNF-α by glia is triggered upon decreased neuronal activity. TNF-α binds and activates neuronal TNF-α receptors type I (TNFR1). This further activates the phosphoinositide-3 kinase (PI3K) pathway and up-regulates specific adhesion molecule-beta 3 integrin, which in turn triggers insertion of AMPAR into the plasma membrane and increases synaptic strength. The various signaling cascades initiated by high levels of pro-inflammatory cytokines under pathophysiological conditions such as depression is illustrated on the right. First, high levels of cytokines such as TNF-α and interleukin-1 (IL-1) activate the production of quinolinic acid and release of glutamate by microglia. Second, TNF-α and IL-1 also inhibit glutamate removal by astrocytes and result in an excess of extracellular glutamate and neurotoxicity. Third, TNF-α binds to TNFR1 and up-regulates the recruitment of Ca^{2+}-permeable AMPA receptor subunits to plasma membrane, thus foster Ca^{2+} entry and neurotoxicity-related cell death. Fourth, TNFR1 activation further activates p38-MAPK and NF-kB signaling and inhibits LTP. These effects of high levels of pro-inflammatory cytokines on synaptic plasticity might explain signaling mechanisms underlying the cognitive deficits and memory impairments found in patients with depression. Illustration was taken from Khairova *et al*. (2009).

2. Hypothesis and aims of the thesis

The main hypothesis of my doctoral thesis is: PMCA-Neuroplastin complexes promote Ca^{2+} clearance to regulate Ca^{2+}-dependent signaling associated to plastic changes in spines of mature hippocampal neurons. To relate mechanistically this proposition with the Ca^{2+} handling machinery, I investigated whether the localization and/or function of PMCA-Neuroplastin complexes are functionally linked to the activity of ionotropic glutamate receptors at the synapse. In addition, I tend to study whether pathophysiological conditions emulated by pro-inflammatory cytokine TNF-α may be linked to altered PMCA-Neuroplastin expression and/or their function in Ca^{2+} clearance.

To test this hypothesis, I aimed at:

a) Characterizing structural changes in dendritic spine morphology induced by high-frequency stimulation and the presence of PMCA-Neuroplastin complexes in the dendrites and spines using immunocytochemistry and confocal microscopy in cultured rat hippocampal neurons.
b) Investigating the role of PMCA-Neuroplastin complexes in Ca^{2+} clearance by performing fast Ca^{2+} imaging and using the genetically encoded Ca^{2+} sensor GCaMP5 or the chemical Ca^{2+} indicator OGB-1. I aimed to study the participation of PMCA-Neuroplastin complexes in Ca^{2+} handling during the wide range of neuronal activity combining Neuroplastin65 overexpression and several pharmacological reagents with various stimulation protocols.
c) Investigating a potential crosstalk between PMCA-Neuroplastin complexes and ionotropic glutamate receptors (Chen & Chesler, 2015; Garside et al., 2009; Lisek et al., 2017; Scheuss et al., 2006). First, I aimed to check whether protein levels of PMCA and NMDARs are affected by Neuroplastin elimination in samples from wild-type and Neuroplastin-deficient mice. Second, I aimed to investigate activity-regulated synaptic localization of these transmembrane proteins by using super resolution STED microscopy in cultured neurons. Third, to explore the functional link between PMCA-Neuroplastin complexes and ionotropic glutamate receptors, I evaluated PMCA-Neuroplastin-mediated Ca^{2+} clearance by combining live-cell Ca^{2+} imaging with pharmacological blockage of glutamate receptors activity, PMCA activity, and others.
d) Investigating the phosphorylation of downstream signaling molecules i.e., ERK1/2 and CaMKIIα and whether their phosphorylation is modulated by PMCA-Neuroplastin complexes, by using Western blotting, confocal microscopy and super resolution STED microscopy.

e) Studying neuronal Ca^{2+} regulation during not only physiological but also pathophysiological conditions like neuroinflammation. Therefore, I aimed to test whether pro-inflammatory cytokine TNF-α has an impact on Ca^{2+} restoration and PMCA-Neuroplastin protein levels.

3. Materials and methods

3.1. Commonly used materials

Table 1. List of primary antibodies

Antibody	Species	Dilution	Company/CAS
anti-pERK1/2 (pT202/pY204.22A)	mouse	IF: 1:200 IB: 1:1,000	Santa Cruz Biotechnology sc-136521
anti-ERK1 (G-8)	mouse	IB: 1:1,000	Santa Cruz Biotechnology sc-271269
phospho-p44/42 MAPK (ERK1/2) (Thr202/TYR204)	rabbit	IB: 1:2,000	Cell Signaling Technology 4370
p44/42 MAPK (ERK1/2)	rabbit	IB: 1:2,000	Cell Signaling Technology 4695
anti-beta Tubulin	rabbit	IB: 1:5,000	Abcam ab6046
anti-CaMKII alpha (phospho T286)	rabbit	IF: 1:200	Abcam ab5683
anti-Neuroplastin	sheep	IF: 1:500 IB: 1:5,000	RD systems (AF5174)
anti-Calcium pump panPMCA (5F10)	mouse	IF: 1:500 IB: 1:10,000	Abcam ab2825
anti-Neuroplastin65	goat	IF: 1:500 IB: 1:5,000	RD systems (AF5360)
anti-Shank2	guinea pig	IF: 1:500-1:1,000	Synaptic Systems 162 204
anti-NMDA receptor, subunit 2A	rabbit	IF: 1:200	ThermoFisher Scientific A-6473
NMDAR2A antibody	rabbit	IB: 1:1,000	Cell Signaling Technology 4205S

Secondary antibodies used in this study for confocal microscopy were alexa Fluor®-488-, Cy3- or Cy5-conjugated and produced in donkey (Jackson ImmunoResearch). For STED microscopy, anti-mouse-IgG-Atto 647N (#50185) and anti-rabbit-IgG-Atto 594 (#77671) produced in goat (Sigma-Aldrich).

Table 2. Commonly used buffers and kits

Material	Composition/Company
10x PBS	1.34 M NaCl, 2.7 M KCl, 14 mM KH_2PO_4, 43 mM Na_2HPO_4, ddH_2O, pH 7.3-7.4
10x TBS	0.2 M Tris-base, 1.37 M NaCl, ddH_2O, pH 7.6
NucleoBond Xtra Midi EF Kit	Macherey-Nagel
Tyrodes Buffer	119 mM NaCl, 2.5 mM KCl, 25 mM HEPES, 30 mM Glucose, 2 mM $MgCl_2$, 2 mM $CaCl_2$, ddH_2O
1x hypotonic lysis buffer	10 mM HEPES, 1.5 mM $MgCl_2$, 10 mM KCl, pH 7.9, with protease and phosphatase inhibitors

Table 3. List of pharmacological inhibitors

Inhibitors	Concentration	Company/CAS
Caloxin2A1	20 µM	Eurogentec, AS-62604
Caloxin3A1	20 µM	Eurogentec, AS-62606
Caloxin1B1	20 µM	Eurogentec, AS-64236
Tetrodotoxin citrate	0.1 µM	Tocris, 1069
ORM-10103	5 µM	Sigma, SML0972
Nifedipine	10 µM	Sigma, N7634
Carboxyeosin	5 µM	Marker Gene Technology, M1300
D-AP5	50 µM	Tocris, 0106
CNQX disodium salt	10 µM	Tocris, 1045

3.2. Molecular biology

Table 4. Plasmids used in this study

Plasmids	Company/CAS
GCaMP5	TagRFPT and GCaMP5 were cloned into FUGW vector, Xiao Lin's submitted doctoral thesis
Np65-GCaMP5	Np65-TagRFPT and GCaMP5 were cloned into FUGW vector, Xiao Lin's submitted doctoral thesis
RFPT	TagRFPT was cloned into FUGW vector, Xiao Lin's submitted doctoral thesis

3.2.1. Transformation

The purchased plasmid DNA was transformed into XL10 GOLD *E.coli* competent cells (bacteria) by heat shock method at 42°C for 45 seconds followed by 2 minutes of incubation on ice. The transformed bacteria were grown on agar plate and incubated at 37°C for overnight.

3.2.2. Bacterial inoculation

Single colonies from the agar plate were cultured overnight in 2.5 ml LB-medium with Ampicillin at 37°C. Next day, 1ml of culture was transferred into 250 ml LB-medium with antibiotic and cultures were grown at 37°C.

3.2.3. Plasmid purification

For mammalian cells transfection, cDNA plasmids were purified by NucleoBond® Xtra Midi EF Kit (Machery-Nagel) following manufacturer's instructions. The plasmid concentration was measured by using NanoDrop1000 (peQLab).

3.3. Cell culture

3.3.1. Hippocampal neurons

Rat primary hippocampal neurons were obtained from embryonic day 18 (E18) of embryos of pregnant rats and dissected tissue was trypsinized, and washed out with 1X horse serum in DMEM solution. The hippocampi were then mechanically dissociated into a single-cell suspension using a flame-polished glass pipette. The cell density was determined by counting on a Neubauer chamber. 50,000 neurons were plated on 12-well cell culture plates. After 1.5 h, the media was replaced with Neurobasal media containing 2% of B27

supplement and 1% of L-glutamine and 1% of penicillin/streptomycin. The media was replaced with fresh media after 24 h and half of the media was replaced with fresh media every 5 days. Cultures were maintained at 37ºC and 5% CO_2.

3.3.2. Transfection

In this study, the primary rat neurons were transiently transfected with plasmid DNA by Lipofectamine 2000 (#11668-019, Invitrogen) in Neurobasal media (GIBCO) with 1% of L-glutamine. Transfection was performed at day *in vitro* (DIV) 11 for calcium imaging experiments.

3.4. Biochemical experiments

3.4.1. Harvesting of cells and protein determination

The cells were harvested in 1x hypotonic lysis buffer and lysates were kept on ice. For immunoblots from brain homogenates, hippocampi were stored at −80°C until sample preparation. Tissues were unfrozen in ice-cold 1x hypotonic lysis buffer, and homogenized with tissue homogenizer. Proteins in lysates were stained with Amido Black. After washing off the excess dye, bound Amido Black was solubilized in 0.1% NaOH. Protein concentration was determined photometrically at 620 nm.

Table 5. Solutions used for protein determination

Buffer	Composition
Amido Black	14.4 g amido black in 1 L washing solution
Washing solution	900 ml methanol, 100 ml acetic acid

3.4.2. Immunoblotting

The cell/tissue lysates were collected as mentioned above. The SDS sample buffer was added to supernatant and boiled for 10 min at 95ºC. Proteins were separated by sodium dodecyl sulfate–polyacrylamide gel electrophoresis (SDS-PAGE) on 10% gels and transferred to a nitrocellulose membrane (Whatman). After blocking with 5% non-fat milk in Tris-buffered saline (TBS) containing 0.1% of Tween 20 for 1 h at room temperature, the membranes were incubated with indicated antibodies overnight at 4ºC., washed with TBS three times, and then incubated with corresponding secondary antibody conjugated to horseradish peroxidase enzyme for 1 h at room temperature. Immunodetection was

performed with the following antibodies: anti-pERK1/2 (pT202/pY204.22A) mouse, anti-ERK1 (G-8) mouse, anti-pERK1/2 (pT202/pY204) rabbit, anti-ERK1/2 rabbit, anti-beta Tubulin rabbit, anti-neuroplastin sheep, anti-calcium pump panPMCA mouse, NMDAR2A rabbit, horseradish peroxidase-conjugated anti-mouse (Dako, #P0447; 1:4,000), anti-rabbit (gamma-chain specific, Sigma, #A1949-1VL; 1:4,000) or anti-sheep IgG (H+L, Jackson ImmunoResearch, #313-035-003 1:5,000) antibodies. The secondary antibodies were visualized by ECL solution using Intas ECL system (Intas Chemocan ECL Imaging).

Table 6. Buffers and solutions used for immunoblotting

Buffer	Composition
2x SDS buffer	125 mM Tris-HCl, pH6.8, 4% SDS, 20% glycerin, 0.2% bromophenol blue, 10% β-mercaptoethanol, double distilled water (dd H_2O)
1x TBS	10x TBS, dd H_2O
1x TBS-T	10x TBS, Tween-20, dd H_2O
10x TGS buffer	Bio-Rad (161-0772)
10x Blot buffer	0.25 M Tris-base, 1.92 M glycine, 0.2% SDS, dd H_2O
1x Blot buffer	10x blot buffer, methanol, dd H_2O
Western blot stripping buffer	62.5 mM Tris-HCl pH 6.8, 2% SDS, 0.7% β-mercaptoethanol
Ponceau S	0.5% Ponceau S, 3% TCA, dd H_2O

3.5. Cell biology experiments

3.5.1. Pharmacological treatment of neurons

Before immunocytochemistry assay, neurons were treated with 20 µM of Caloxins for 30 min in 1x Tyrodes buffer at 37°C. Electrical stimulation was delivered in a 12-well plate together with electrodes 1x Tyrodes buffer at 37°C. High frequency stimulation protocol was taken from Harvey *et al*., 2008 (40 APs at 80 Hz, repeated 8 times at 0.2 Hz).

Before calcium imaging experiments (see later), neurons were treated with 1 ng/ml TNF-alpha (RD Systems, #10291-TA) for 24 h in neuronal media at 37°C. For western blotting, 1 ng/ml TNF-alpha was added for 1, 6, 12, 24 and 48 h.

3.5.2. Immunocytochemistry

Hippocampal neurons were fixed at day *in vitro* 15-16 with 4% paraformaldehyde (PFA) for 10 min at 37°C, permeabilized and blocked with PBS containing 10% horse serum in 0.1% Triton X-100 for 40 min at room temperature. The neurons were incubated with anti-calcium pump panPMCA mouse, anti-NMDA receptor subunit 2A rabbit, anti-Neuroplastin sheep, anti-pERK1/2 (pT202/pY204.22A) mouse, anti-CaMKIIα (phospho T286) rabbit and anti-Shank2 guinea pig antibodies for overnight at 4°C. For confocal microscopy, the primary antibodies were visualized with fluorescent Alexa Fluor-488, Cy3 and Cy5 conjugated secondary antibodies produced in donkey for 1 h. For STED microscopy, anti-mouse-IgG-Atto 647N and anti-rabbit-IgG-Atto 594 produced in goat were used. The coverslips were mounted with Mowiol.

Table 7. Solutions used for immunocytochemistry

Buffer/Solution	Composition
Blocking buffer	10% horse serum, 0.1% Triton X-100 in 1x PBS
4% Paraformaldehyde (PFA)	Paraformaldehyde powder, HCl (dilute), 1N NaOH, 1x PBS, dd H_2O
Mowiol	2.4 g Mowiol, 0.2 M Tris pH 8.5, 0.02% Sodium Azide

3.6. Microscopy and image analysis

3.6.1. Confocal microscopy

Images were acquired using HCX APO 63/1.40 NA objective coupled to a TCS SP5 confocal microscope under sequential scanning mode with 6.0-fold digital magnification. Morphology of fixed neurons expressing RFPT-GCaMP5 was followed by using green and red channels together. For excitation of the respective channels, the Argon laser was set to 488 nm for GFP (GCaMP5) and the 561 was set to 561 nm for RFPT. Z-stacks (41.01 x 41.01 x 5 µm physical lengths) were digitalized in a 1024 x 512 pixels format file. Spines were detected manually using maximum intensity and z-projection method of ImageJ software. Spines were counted as minimum 0.5 µm length. Spine length and width were measured and shape parameter (length/width) was calculated. Spine density was calculated by normalizing the number of spines to the length of dendritic shaft (10 µm).

3.6.2. Super resolution stimulated emission depletion (STED) microscopy

STED images were acquired with a Leica TCS SP8-3X STED system (Leica Microsystems). A pulsed white light laser (WLL) was used for excitation ranging from 470 to 670 nm. A 775 nm pulsed depletion laser was used to achieve STED. Images were scanned with a 100x objective (Leica, HC APO CS2 100x/1.40 oil). Excitation was done using the WLL at 650 nm for Atto647N (p-ERK1/2 or panPMCA; STED and confocal), 561 nm for Atto594 (p-CaMKIIα or Neuroplastins or NMDAR2A; STED and confocal), and 488 nm for Alexa Fluor 488-conjugated secondary antibody (Shank2; confocal mode). Emission spectra were detected at 660–710 nm for Atto647N, 590-620 nm for Atto594, and 500-530 nm for Alexa Fluor 488. Images were digitalized in a 1024 x 1024 pixels format file, 5 optical zoom factor, 22.73 nm x/y image size, 8x line averaging and as z-stacks. The number of steps was 10-12 and z-step size was 0.16 nm. The same settings as STED channels were set for corresponding confocal channels, only the excitation power was reduced in half.

Deconvolution of STED and confocal images was done with Huygens Professional 19.10 software (Scientific Volume Imaging). Within the deconvolution wizard, images were auto-stabilized and were subjected to a background correction. The signal-to-noise ratio was set to 15 for STED and 30-40 for confocal images. The optimized iteration mode of the CMLE was set as a threshold of 0.01 for STED and 0.05 for confocal images as described before (van Bommel et al., 2019).

Puncta analysis of p-ERK1/2 and p-CaMKIIα immunofluorescence was performed using Fiji. Z-stacks of STED images were projected as “Max Intensity”. Shank2 puncta threshold was adjusted with a limit from 50 to 255 (for 8-bit images) to obtain binary images as region of interest. Shank2 binary images were processed with watershed segmentation to refine the shapes of Shank2-positive objects. Shank2 clusters were measured by filtering the cluster size as minimum 0.01 μm^2. Image calculator option of Fiji was used to select p-ERK1/2 and p-CaMKIIα clusters overlapping with Shank2 puncta. The cluster size which was smaller than 0.001 μm^2 was eliminated. Among selected clusters, the number, intensity and area of p-ERK1/2 and p-CaMKIIα clusters were quantified.

Analysis of PMCA and Neuroplastin or NMDAR2A fluorescence signal was carried out in depth by using three different softwares. First, the intensity and area of clusters were quantified by using Fiji. Z-stacks were displayed as maximum intensity and Shank2 binary images were created by adjusting threshold (lower limit was 50 and upper limit was 255 for 8-bit images). Shank2 binary images were processed with watershed segmentation to refine the shapes of Shank2-positive objects. Shank2 clusters were measured by filtering the cluster size as minimum 0.01 μm^2. Obtained region of interests (ROIs) were applied to

PMCA and Neuroplastin or NMDAR2A images to measure the intensity (mean gray values) and area. The numbers of PMCA and Neuroplastin or NMDAR2A clusters were normalized to total area of Shank2-positive objects (N° of clusters/μm^2).

Colocalization analysis was performed by using Huygens Professional 19.10 software after images were deconvolved as described above. Colocalization analyzer tool in Huygens was used and STED channels of PMCA and Neuroplastin or NMDAR2A were selected. Threshold was estimated as Gaussian minimum defined by software. Shank2 binary images were applied as ROI. Colocalization coefficients were obtained and the Pearson coefficients were plotted.

The shortest distance between PMCA and Neuroplastin or NMDAR2A was measured by using Imaris software (Imaris x64 9.5.1, Oxford Instruments). Deconvolved Shank2 images were used to create surfaces (Shank2 area above 0.25 μm^2). Deconvolved PMCA and Neuroplastin or NMDAR2A images were used to create spots (PMCA XY-estimation was measured as 0.070 µm, Neuroplastin XY-estimation was measured 0.100 µm and NMDAR2A XY-estimation was measured 0.100 µm). PMCA and NMDAR spots were further filtered in a 0.300 µm distance to Shank2 surfaces in order to focus on spots around the synapse. The shortest distance of Neuroplastin spots to PMCA or NMDAR2A spots to PMCA spots were computed by using a “Shortest Distance To Spots” statistics tool.

3.6.3. Live cell calcium imaging

Rat hippocampal neurons were transfected with RFPT-GCaMP5 or Np65-RFPT-GCaMP5 at day *in vitro* 11. Live cell imaging was performed at day *in vitro* 15-16. During the imaging session, coverslips were maintained in a RC-49MFSH magnetic imaging/recording chamber with removable electrodes (Warner Instruments, Hamden, CT, USA) and imaged at 32^{o}C. An inverted microscope (Observer. D1; Zeiss) together with an EMCCD camera (Evolve 512; Delta Photometrics) controlled by VisiView® Software (Visitron Systems GmbH) was used. A 63x objective and GFP/RFP single band exciters ET filter set (excitation 470/40, excitation 572/35, emission 59022m, dichroic 59022BS) were used. Transfected neurons were selected with both RFP and GFP expression.

For PMCA inhibition experiments, a cocktail of extracellularly binding PMCA inhibitors, Caloxins 2A1+3A1+1B1 (20 µM each) (Pande et al., 2005; Pande et al., 2008; Szewczyk et al., 2010) was added in the recording chamber. A pre-incubation with Carboxyeosin (5 µM) was alternatively used to inhibit PMCA action intracellularly (Roome & Empson, 2010). To minimize its intrinsic fluorescence of this inhibitor, a fast wash-out was done right before imaging initiation. To avoid interference of spontaneous action potentials, intrinsic neuronal activity was silenced using TTX (0.1 µM) in the recording chamber in experiments shown in Figures 9, 16 and 18 (also mentioned in the figure legends). For glutamate receptors

experiments in Figures 19, 20, 21, and 22, D-APV (50 µM) and CNQX (10 µM) were added in the recording chamber (without TTX). In order to avoid potential contribution of the Na^+/Ca^{2+} exchanger (NCX) to calcium clearance, ORM-10103 (5 µM) was added in some experiments shown in Figures 18 and 22. To avoid Ca^{2+} entry via L-type voltage-gated Ca^{2+} channels, Nifedipine (10 µM) was used in Figure 22.

Calcium transients were evoked with low-frequency stimulation (5-10 pulses at 10 Hz) or high-frequency stimulation (HFS; 8 trains of 40 pulses at 80 Hz) protocols using a S48 stimulator unit (GRASS Technologies). Calcium transients were acquired at 20 Hz during 40 s. Five seconds of the baseline was recorded before each stimulation.

Calcium transient analysis was performed initially using Fiji. RFPT channel was used to select region of interest (ROI). Dendrites and spines of each neuron were selected individually. Selected ROIs were applied to GCaMP5 channel and gray values of each ROI were obtained by “Multi measure” function of Fiji. The calcium kinetics were quantified using AxonTM pCLAMPTM 10.7.0 Electrophysiology Data Acquisition and Analysis Software (Molecular Devices) as shown in Figure 6. Result files obtained with Fiji were applied to this software. Baseline and signal region for each result were kept the same throughout the experiment with cursors given in the pCLAMP software. Decay time (ms), half-width (ms), peak amplitude (F-F0), baseline and rise time (ms) were quantified for each spines and dendrites as described in the Clampfit batch analysis user guide from AxonTM pCLAMPTM 10.7.0 Electrophysiology Data Acquisition and Analysis Software (Molecular Devices). Values were normalized for the final data presentation. Baseline values were further normalized to RFPT intensity to control the fluctuations of the expression level of RFPT-GCaMP5 from one to the other transfected neuron.

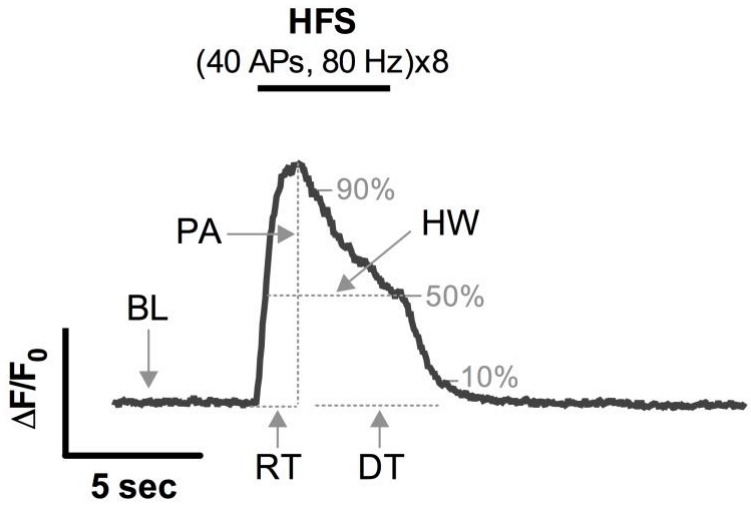

Figure 6. The representation of data analysis for calcium kinetics. The illustration represents how calcium kinetics were quantified using Axon™ pCLAMP™ 10.7.0 Electrophysiology Data

Acquisition and Analysis Software (Molecular Devices). Baseline and signal region for each result were kept the same throughout the experiment with cursors given in the pCLAMP software. Decay time (DT; ms), half-width (HW; ms), peak amplitude (PA), baseline (BL) and rise time (RT; ms) were quantified for each spines and dendrites as described in the Clampfit batch analysis user guide from Axon™ pCLAMP™ 10.7.0 Electrophysiology Data Acquisition and Analysis Software (Molecular Devices). Values were normalized for the final data presentation. The average baseline was detected using "baseline cursors" given by software. "Signal cursors" were placed to where stimulation was applied and the peak amplitude (F-F_0) was found by the software relative to the baseline. Half-width was automatically set by the software using 50% of peak amplitude. Decay time was calculated between the associated "from 90%" and "to 10%" of the signal. Rise time was set as the time between the associated "from 10%" and "to 90%" of the signal. Baseline values were further normalized to RFPT intensity to control the fluctuations of the expression level of RFPT-GCaMP5 from one to the other transfected neuron.

Table 8. Solutions used for live cell imaging

Buffer/Solution	Composition
2xTyrodes buffer	5 mM KCl, 50 mM HEPES, 60 mM Glucose
Recording solution	119 mM NaCl, 1x Tyrodes buffer, 2 mM $MgCl_2$ and $CaCl_2$, ddH_2O

3.7. Statistical analysis

The results were presented as mean ± SEM (standard error of the mean) or violin plots with median accompanied by the number of cells or the number of dendrites or spines in the figure legends. For statistical analysis, Prism 5 software (GraphPad) was used. Statistical difference between two groups was compared with the unpaired t test or Mann Whitney test for non-parametric data. For calcium imaging data, paired test within the same group was used if recording was continued on the same cell. Statistical significance was indicated as following: *p<0.05, **p<0.01, ***p<0.001 vs control; $^{\#}$p<0.05, $^{\#\#}$p<0.01, $^{\#\#\#}$p<0.001 between conditions. All experiments were repeated from at least two-three (or more) independent cultures.

4. Results

4.1. Characterization of the HFS-induced structural plasticity and Neuroplastin-promoted PMCA levels in dendrites and spines of hippocampal neurons.

In order to trigger plastic changes in spines, I have used high-frequency stimulation (HFS) protocol defined as eight trains of 40 APs at 80 Hz ((40APs, 80 Hz) x8) which have been shown by Harvey *et al*., to induce plastic changes in the spines of cultured neurons (Harvey, Ehrhardt, et al., 2008). The HFS is delivered as field stimulation by platine electrodes immersed into Tyrodes buffer in the recording chamber. Similar HFS protocols have been previously used by other authors to trigger various synaptic plastic responses at the synapse for instance synaptic potentiation in CA1 hippocampal synapses (Papatheodoropoulos & Kouvaros, 2016), ryanodine receptor-mediated Ca^{2+} release and morphological plasticity of spines (Riquelme et al., 2011) and activation of CaMKIV and ERK2 (Kasahara et al., 2001). First, I started with the characterization of the HFS-induced structural changes in spines of cultured hippocampal neurons. For this, neurons were transfected with a plasmid encoding RFPT-GCaMP5 at DIV11 and were allowed to mature until use at DIV15. The expression of RFPT served to monitor with detail the complete morphology of the transfected neurons, whereas GCaMP5 expression was used later to monitor Ca^{2+} changes in them (see Fig. 9). After 30 min of HFS and following fixation, I was able to observe and quantify the spine morphology and size in non-stimulated control and HFS-exposed neurons using confocal microscopy (Fig. 7A). Compared to control, increased length (Fig. 7B; Control: 1.739 ± 0.05698 vs HFS: 1.937 ± 0.05599) and increased width of spines (Fig. 7C; Control: 0.5689 ± 0.01239 vs HFS: 0.6220 ± 0.01702) were observed upon HFS. Shape parameter was unchanged (Fig. 7D, length/width; Control: 3.328 ± 0.1216 vs HFS: 3.471 ± 0.1109) but spine density was increased upon HFS (Fig. 7E; Control: 2.851 ± 0.1053 vs HFS: 3.312 ± 0.1010). These results show that the used HFS protocol is indeed capable to promote morphological changes in spines, which are very similar with those occurring in structural synaptic plasticity as indicated in the literature (Harvey, Ehrhardt, et al., 2008; Kasahara et al., 2001; Papatheodoropoulos & Kouvaros, 2016; Riquelme et al., 2011). Therefore, I used this HFS protocol in the following experiments with the purpose to study the role of Neuroplastin-PMCA in signaling and morphological plasticity in spines.

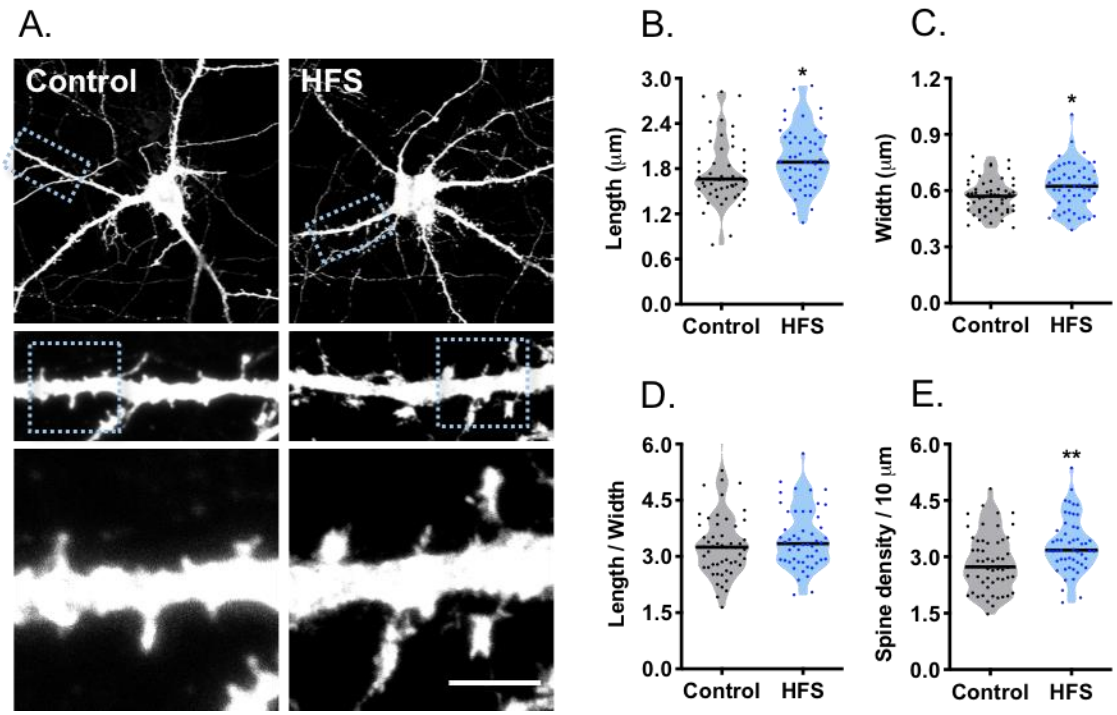

Figure 7. High-frequency stimulation induces structural changes in dendritic spine morphology. A) Hippocampal neurons were transfected at DIV11 with RFPT-GCaMP5. At DIV 15, neurons were stimulated with a high-frequency-stimulation (HFS) and neurons were fixed 30 min after. Scale bar is 5 µm. **B-E)** The data display violin plots with medians of spine length (**B**), spine width (**C**), shape parameter (**D**, length/width) and spine density (**E**, per 10 µm) n= 54 dendrites from 26 neurons for control and n= 52 dendrites from 30 neurons for HFS condition (three independent cultures). Unpaired t-test *p<0.05, ** p<0.01.

Our laboratory (Bhattacharya et al., 2017; Herrera-Molina et al., 2017; Lin et al., 2021) and other colleagues (Gong et al., 2018; Schmidt et al., 2017) have shown that PMCAs form protein complexes with Neuroplastin and that elimination of Neuroplastin expression results in loss of PMCAs in Neuroplastin-deficient brains. Next, I checked whether Neuroplastin65 overexpression is capable of promoting PMCA levels in neurons, particularly in dendrites and spines. Neurons were transfected with RFPT-GCaMP5 or Np65-RFPT-GCaMP5 at DIV 11. Following fixation and co-staining with RFPT and panPMCA antibodies at DIV14, confocal microscopy was used to scan neurons including soma and their dendritic segments (Fig. 8A). PMCA intensity was quantified and normalized to RFPT or Np65-RFPT intensity to control the expression of the constructs from one to the other transfected neuron. Compared to control neurons expressing RFPT, PMCA levels were increased upon Neuroplastin65 overexpression in dendrites and spines (Fig. 8B; RFPT: 0.8594 ± 0.06169 vs Np65-RFPT: 2.437 ± 0.1806 in dendrites and RFPT: 0.9216 ± 0.08013 vs Np65-RFPT: 2.198 ± 0.1662 in

spines). These results indicate that Neuroplastin65 is capable of increasing PMCA levels in dendrites and spines.

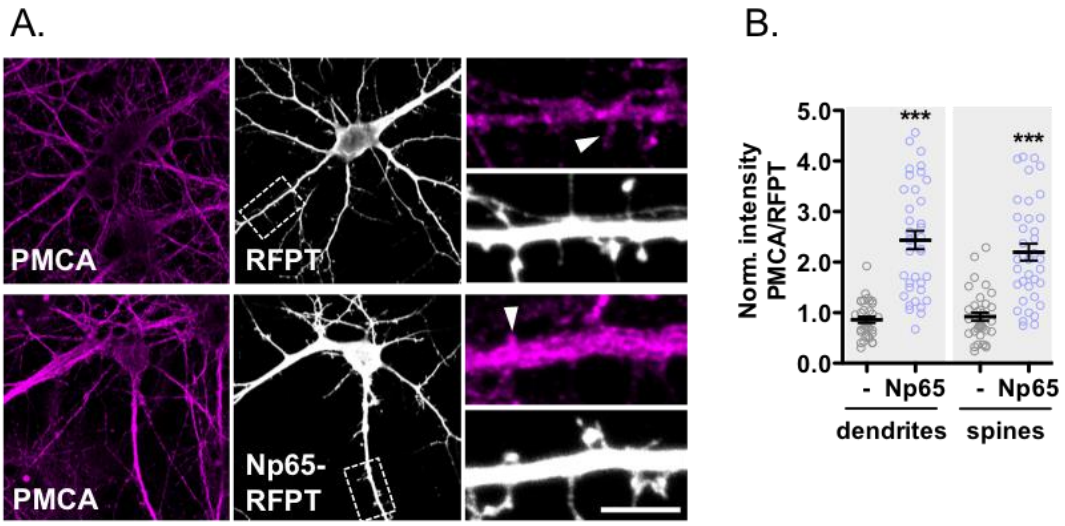

Figure 8. PMCA levels are increased in dendrites and spines upon Neuroplastin65 overexpression. A) Hippocampal neurons were transfected at DIV 11 with RFPT-GCaMP5 or Np65-RFPT-GCaMP5. At DIV 14, neurons were fixed, stained with panPMCA and RFPT antibody, and later scanned using confocal microscopy. Scale bar is 5 µm. **B)** The graph shows endogenous PMCA intensity normalized to RFPT intensity in dendrites and spines. n= 34 dendritic segments from 30 neurons for control and n= 37 dendritic segments from 31 neurons for Np65 (three independent cultures). Mann Whitney U test for normalized data ***p<0.001.

4.2. Neuroplastin-promoted PMCA activity regulates Ca^{2+} clearance in neurons

PMCA-Neuroplastin complexes are proposed to be important regulators of intracellular Ca^{2+} levels in different cell types. Herrera-Molina *et al*., showed reduced PMCA levels lead to altered [iCa^{2+}] by monitoring Ca^{2+} dynamics with Fluo-4 and FuraRed in the cell somata of Neuroplastin-deficient neurons during KCl stimulation (Herrera-Molina et al., 2017). PMCA expression was found to be required for Ca^{2+} clearance in T cells by using Fluo-3 and FuraRed in Neuroplastin-deficient T cells (Korthals et al., 2017). Intracellular Ca^{2+} was shown to be altered by Neuroplastin in neurons by using Fluo-5F and evoked by a single AP or a train of APs (10APs at 30 Hz) in Neuroplastin-knockdown neurons (Schmidt et al., 2017). However, these results did not clarify whether PMCA-Neuroplastin complexes contribute to Ca^{2+} clearance distinctively in dendrites and spines. Also, the potential contribution to Ca^{2+} clearance regulated by PMCA-Neuroplastin complexes during high neuronal activity is unknown. Therefore, I took the advantage of live-cell calcium imaging to monitor rapid calcium dynamics in cultured neurons transfected with RFPT-GCaMP5 or with NP65-RFPT-GCaMP5 (Fig. 9A). For this, calcium imaging was performed in Tyrodes buffer in the

presence of TTX to avoid network activity and Carboxyeosin a potent PMCA activity inhibitor (Chen & Chesler, 2015; Empson et al., 2007; Jones et al., 2010) as described in Figure 9B. To evoke Ca^{2+} changes reported by the GCaMP5 sensor, neurons were stimulated with HFS and recorded during 40 seconds (Fig. 9C-D). Spines and dendritic shafts were identified by using RFPT signals as previously described (Winnubst et al., 2015). In dendrites of RFPT-GCaMP5 neurons, treatment with PMCA inhibitor (Carboxyeosin, CE) slowed down Ca^{2+} restoration by increasing decay time and half-width (Fig. 9E-F; Table 9 in Appendix). Also, inhibition of PMCA increased peak amplitude (Fig. 9J) and decreased rise time (Fig. 9K; Table 9 in Appendix). Importantly, the overexpression of Neuroplastin65 accelerated Ca^{2+} restoration by decreasing decay time and half-width (Fig. 9E-F). Interestingly, peak amplitude (Fig. J) was decreased and rise time did not change (Fig. 9K) in the dendrites of Neuroplastin65-RFPT-GCaMP5 neurons. This is visualized with example traces in Figure 9C-D. Treatment of Np65 overexpressing neurons with PMCA inhibitor slowed down Ca^{2+} restoration by increasing decay time and half-width (Fig. 9E-F) compared to untreated Np65 overexpressing neurons. While peak amplitude was reduced upon PMCA inhibition in Neuroplastin65 overexpressing neurons (Fig. 9J) and not affecting rise time (Fig. 9K). In spines, treatment with PMCA inhibitor or overexpression of Neuroplastin65 showed similar effect with dendrites on decay time, half-width and peak amplitude (Fig. 9G, H and L; Table 9 in Appendix). Therefore, these results showed that Neuroplastin-PMCA complexes are important player in the Ca^{2+} clearance in dendrites and spines during high neuronal activity. As a particularity of the spines, upon Neuroplastin65 overexpression, treatment with the PMCA inhibitor significantly increased rise time pointing to alteration of the Ca^{2+} influx machinery located at the synapses (Fig. 9M; Table 9 in Appendix).

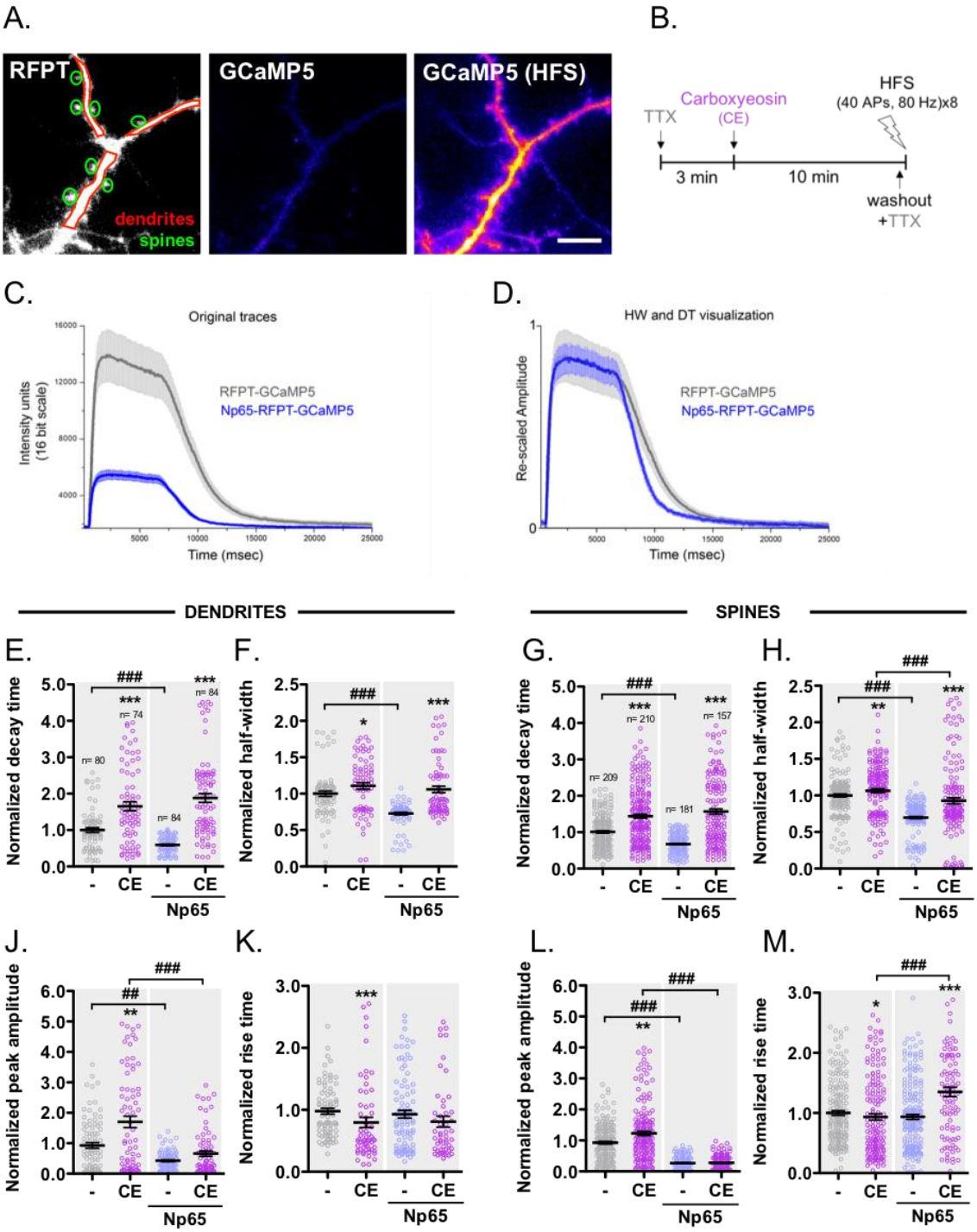

Figure 9. Basal and Neuroplastin overexpression-promoted PMCA complexes regulate Ca^{2+} clearance in neurons. A-B) Hippocampal neurons were transfected at DIV 11 with RFPT-GCaMP5 or Np65-RFPT-GCaMP5. Calcium imaging was performed at DIV 15-16 in Tyrodes buffer with TTX (0.1 µM). The experimental procedure including pharmacological treatment and electrical stimulation is shown. TTX was added to inhibit the network activity. Three minutes after TTX, PMCA inhibitor (Carboxyeosin, CE, 5 µM) was applied for 10 min before recording. After washout with Tyrodes buffer and adding TTX again, high-frequency-stimulation (HFS, 8 trains of

40 APs at 80 Hz) was applied as a field stimulation. Scale bar is 5 µm. **C-D)** Representative traces of Ca^{2+} transients from neurons expressing RFPT-GCaMP5 and Np65-RFPT-GCaMP5 are shown. Original traces show faster Ca^{2+} clearance and slower peak amplitude in Neuroplastin65 overexpressing neurons (**C**). Then, peak amplitude was rescaled for a better visualization of half-width (HW) and decay time (DT) (**D**). **E-M)** Calcium kinetics upon HFS were quantified. Normalized decay time (**E** and **G**), half-width (**F** and **H**), peak amplitude (**J** and **L**) and rise time (**K** and **M**) are presented as graphs in dendrites and spines. Data is shown as the mean±SEM (n values indicate the number of dendrites and spines that were analyzed). n= 19 neurons for control (gray circles), n= 18 neurons for CE-treated neurons (magenta circles), n= 14 neurons for Np65 overexpression (blue circles) and n=12 neurons for Np65+CE (magenta circles). (three independent cultures per condition). Mann-Whitney U test *p<0.05, **p<0.01, ***p<0.001 between with vs. without CE; $^{\#}$p<0.05, $^{\#\#}$p<0.01, $^{\#\#\#}$p<0.001 between RFPT-GCaMP5 vs. Np65-RFPT-GCaMP5.

Spontaneous network activity is an early and fundamental process initiating neuronal connectivity and maturation (Ivenshitz & Segal, 2010; Khazipov et al., 2001; Minlebaev et al., 2007; Opitz et al., 2002). Moreover, synchronized spontaneous activity is known to be required for stabilization and successful transmission to establish local synaptic plasticity (Winnubst et al., 2015). To support the physiological role of PMCA-Neuroplastin complexes in Ca^{2+} clearance, Ca^{2+} transients were monitored in dendrites and spines of spontaneously active hippocampal neurons. For this, neurons were transfected with RFPT-GCaMP5 or Np65-RFPT-GCaMP5 at DIV 11 and then, run-free recorded at DIV 15 while Ca^{2+} changes occurred naturally due to synaptically driven spontaneous network activity. Representative traces of Ca^{2+} transients from neurons expressing RFPT-GCaMP5 and Np65-RFPT-GCaMP5 are shown in Figures 10A-B. Compared to the dendrites and spines of RFPT-GCaMP5 neurons, overexpression of Neuroplastin65 accelerated Ca^{2+} restoration by decreasing decay time in dendrites and spines (Fig. 10C and E; Table 10 in Appendix) whereas half-width remained unchanged (Fig. 10D and F; Table 10 in Appendix). Interestingly, peak amplitude was significantly smaller in dendrites and spines of Neuroplastin65 overexpressing neurons (Fig. 10G and I; Table 10 in Appendix). Rise time increased in Np65 overexpressing neurons compared to RFPT-GCaMP5 neurons (Fig. 10H and J; Table 10 in Appendix). All these four parameters were visualized with representative traces showing the acceleration of Ca^{2+} clearance in Neuroplastin65 overexpressing neurons (Fig. 10B) compared to endogenous Neuroplastin65 expression (Fig. 10A). These data confirm that the overexpression of Neuroplastin65, which leads to increased PMCA levels (Fig. 8), fosters the capacity of neurons to restore the increases of Ca^{2+} levels occurring due to spontaneous intrinsic activity in neurons.

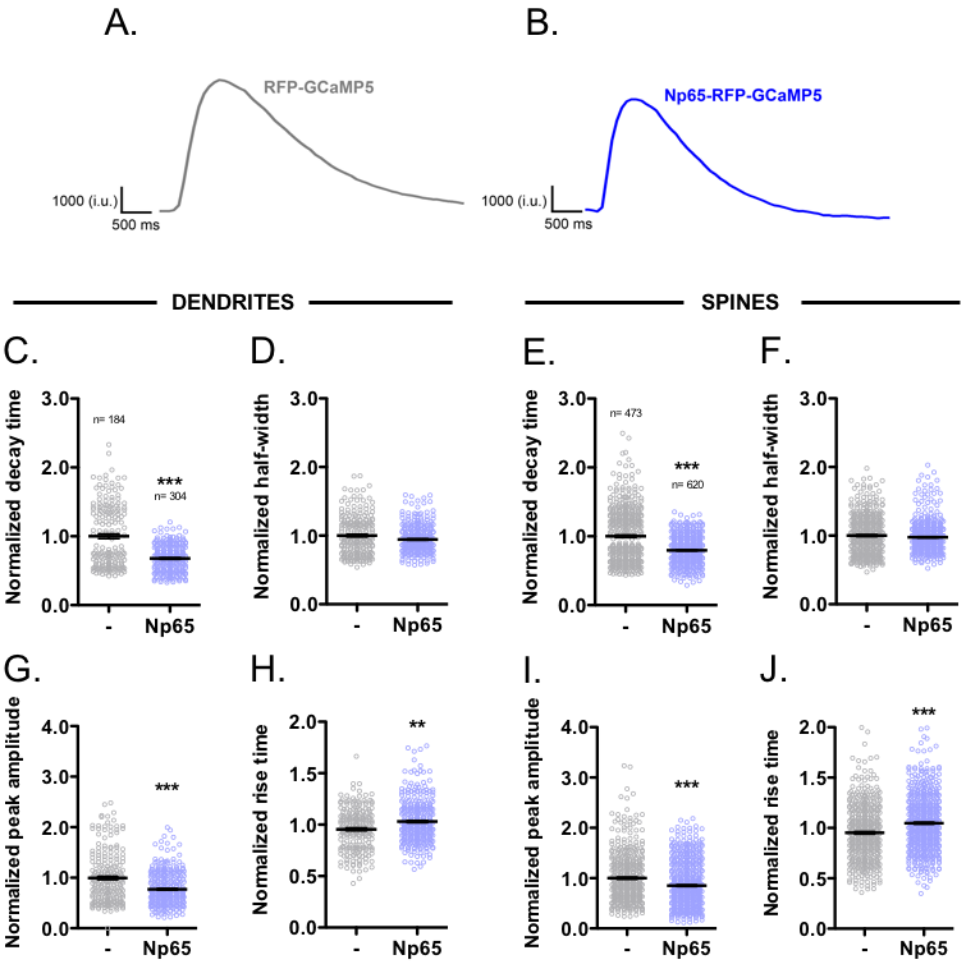

Figure 10. Overexpression of Neuroplastin alters spontaneous activity by increasing Ca^{2+} extruding capacity of neurons. Hippocampal neurons were transfected at DIV 11 with RFPT-GCaMP5 and Np65-RFPT-GCaMP5. Representative traces of Ca^{2+} transients from neurons expressing RFPT-GCaMP5 and Np65-RFPT-GCaMP5 are shown. Calcium imaging was performed at DIV 15 in Tyrodes buffer. Calcium kinetics as spontaneous activity were quantified. Normalized decay time (**C** and **E**), half-width (**D** and **F**), peak amplitude (**G** and **I**) and rise time (**H** and **J**) are presented as graphs. Data is shown as the mean±SEM (n values indicate the number of events that were analyzed). n= 4 neurons for RFPT-GCaMP5, n= 5 neurons for Np65-RFPT-GCaMP5 (two independent cultures) Mann-Whitney U test *p<0.05, **p<0.01, ***p<0.001 compared to RFPT-GCaMP5 (gray circles).

4.3. A potential crosstalk between PMCA-Neuroplastin complexes and ionotropic glutamate receptors

Considering the crucial importance of proper Ca^{2+} homeostasis for the cell physiology, it is expected that major molecular players of Ca^{2+} influx and Ca^{2+} clearance are tightly co-regulated and/or in close functional communication with each other. The N-methyl-D-aspartate receptors (NMDARs) are ionotropic glutamate receptors and one of the main

sources of Ca^{2+} influx at the synapse (see Fig. 1; Fig. 4). Given the reported association between NMDAR and PMCA2 via PSD95 at macromolecular level in rat brain homogenates (Garside et al., 2009), the reduced PMCA activity in neurons treated with the NMDAR antagonist ketamine (Lisek et al., 2018; Lisek et al., 2017), and the major role of PMCA-mediated extracellular pH shift to boost NMDAR-dependent synaptic currents (Chen & Chesler, 2015; Makani & Chesler, 2010; Stawarski et al., 2020), I became interested in the crosstalk between PMCA-Neuroplastin complexes and NMDAR. First, I performed quantitative Western blot analyses to determine the total amount of PMCAs, NMDAR2A and NMDAR2B in total homogenates from the hippocampi of Neuroplastin-deficient mice (*Nptn*$^{-/-}$) and wild-type mice (*Nptn*$^{+/+}$, Fig. 11A). The Neuroplastin65 and 55 were probed with an anti-sheep neuroplastin antibody detecting both isoforms (Np65 and Np55). In the hippocampus of Neuroplastin-deficient animals, PMCA levels were significantly reduced compared to wild-type animals (Fig. 11B; PMCA levels: *Nptn*$^{+/+}$: 100.0 ± 16.05 vs *Nptn*$^{-/-}$: 46.37 ± 2.139). Interestingly, I also found reduced levels of GluN2A subunit and unchanged levels of GluN2B subunit of NMDAR (Fig. 11B; NMDAR2A levels: *Nptn*$^{+/+}$: 100.0 ± 10.29 vs *Nptn*$^{-/-}$: 71.01 ± 4.303; NMDAR2B levels: *Nptn*$^{+/+}$: 100.0 ± 1.099 vs *Nptn*$^{-/-}$: 119.6 ± 12.49).

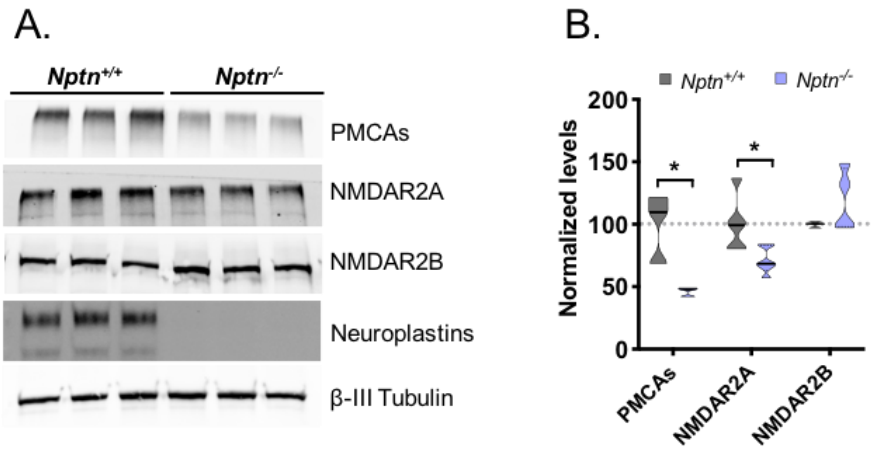

Figure 11. PMCA and NMDAR2A levels are altered in *Nptn*$^{-/-}$ hippocampus. Wild-type and Neuroplastin-deficient hippocampi were collected and homogenized in buffer A (0.32 M sucrose, 5 mM HEPES, pH 7.4 with protease inhibitor cocktail and PhosSTOP). Proteins were immunoblotted with panPMCA, NMDAR2A, NMDAR2B, Neuroplastins and β-III tubulin antibodies as shown. The graph shows the mean±SEM from 4-6 animals per genotype (student t test compared to wild-type (*Nptn*$^{+/+}$) *p<0.05.

The presence of different PMCA isoforms has been demonstrated at pre- and post-synaptic sites of neurons in different brain regions (Burette et al., 2003; Burette et al., 2009; Garside et al., 2009; Ono et al., 2019). While both Neuroplastin65 and 55 are present at the synapse (Hill et al., 1988; Smalla et al., 2000; Willmott et al., 1992), only Neuroplastin65 is tightly

attached to the post synaptic density (PSD) and its levels are increased after NMDA-dependent Hebbian-like induced plasticity (Langnaese et al., 1997; Smalla et al., 2000). However, PMCAs and Neuroplastins have not been shown together as interaction partners at the synapse yet. Here, I assessed their synaptic localization together with GluN2A-containing NMDAR (NMDAR2A) using super-resolution STED microscopy in hippocampal neurons immunostained with anti-pan-PMCA, anti-pan-neuroplastin or anti-NMDAR2A antibodies (Fig. 12A; Table 11 in Appendix). To assess the presence of these proteins in the post-synaptic area, the number, total puncta signal (intensity x area), intensity and area of the PMCA (Fig. 12B-E; Table 11 in Appendix), Neuroplastin (Fig. 12F-I; Table 11 in Appendix) and NMDAR2A (Fig. 12J-M; Table 11 in Appendix) clusters were quantified within Shank2-positive puncta as the region of interest. In addition to unstimulated control, HFS was applied to the neurons which were fixed one minute after and immunostained as described before. Importantly, HFS did not modify the area of Shank2-puncta (Table 12 in Appendix). The number of puncta (Fig. 12B), total puncta signal (intensity x area, Fig. 12C) and area (Fig. 12E) of PMCA clusters were significantly increased upon HFS compared to control whereas the intensity (Fig. 12D) of PMCA clusters remained unchanged. HFS results in significantly increased number (Fig. 12F) of Neuroplastin clusters. The total puncta signal (intensity x area, Fig. 12G), intensity (Fig. 12H) and area (Fig. 12I) of Neuroplastin clusters did not change upon HFS. The number (Fig. 12J), total puncta signal (intensity x area, Fig. 12K), intensity (Fig. 12L) and area (Fig. 12M) of NMDAR2A clusters were not altered one minute after HFS. Altogether these data suggest that PMCA-Neuroplastin complexes are rapidly recruited into Shank2-positive post-synapses whereas synaptic localization of NMDAR2A is not affected in response to HFS.

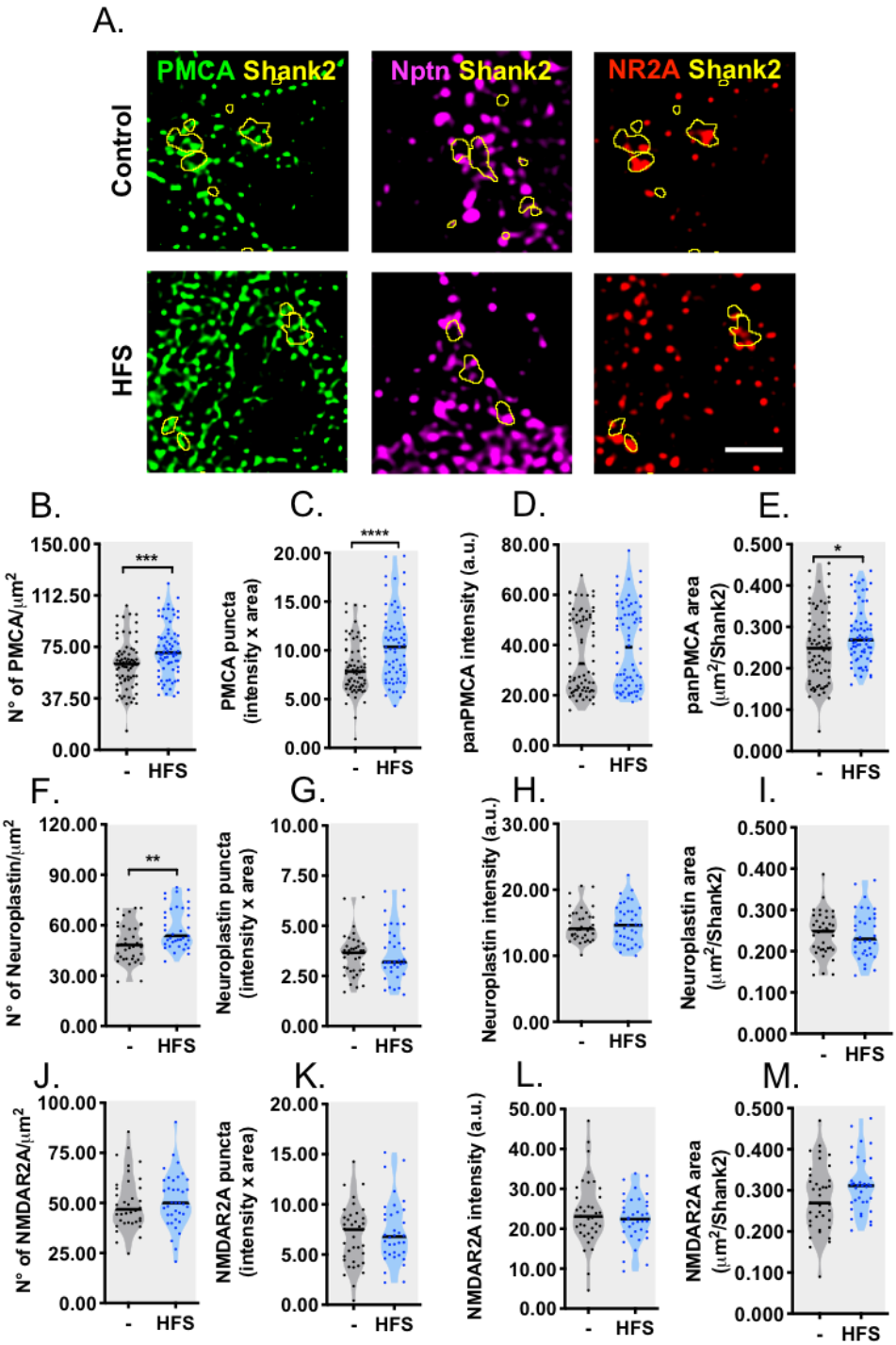

Figure 12. Synaptic localization of PMCA, Neuroplastin and NMDAR2A after high-frequency stimulation. A) Hippocampal neurons (DIV 16-17) were exposed to HFS and one minute after, fixed and then stained with antibodies against panPMCA and neuroplastin or against GluN2A-containing NMDAR (NMDAR2A) and anti-Shank2 antibodies. For increased resolution, STED images were deconvolved with Huygens Professional 19.10 software. Shank2-positive puncta were used as region of interest for analysis. Scale bar is 1 µm. **B-M)** The number of clusters (**B**, **F** and **J**), total puncta signal (intensity x area; **C**, **G** and **K**), intensity (**D**, **H** and **L**) and area (**E**, **I** and **M**). The data are displayed using violin plots with medians. PMCA staining: n=

74 neurons for control and n= 70 neurons for HFS (six independent cultures). Neuroplastin staining: n= 38 neurons for control and n= 36 neurons for HFS (three independent cultures). NMDAR2A staining: n= 37 neurons for control and n= 36 neurons for HFS (three independent cultures). Unpaired t-test *p<0.05, **p<0.01 vs. control.

I have further studied synaptic localization of PMCA, Neuroplastin and GluN2A-containing NMDAR (NMDAR2A) by quantifying the colocalization of clusters of two of these proteins into Shank2-positive areas using Pearson colocalization coefficient (Fig. 13). The Pearson colocalization coefficient between PMCA and Neuroplastin clusters into Shank2-positive areas was notably high in non-stimulated control neurons and remained unchanged one minute after HFS (Fig. 13B; control: 0.8215 ± 0.009731 vs HFS: 0.8281 ± 0.008761). The distance between PMCA and Neuroplastin clusters, defined as the statistically shortest distance between clusters of two proteins and localized at a maximal distance of 300 nm from the periphery of Shank2-positive areas, was rather short in control neurons and remained also unchanged one minute after HFS (Fig. 13C; control: 0.1109 ± 0.009557 vs HFS: 0.1347 ± 0.01705). The Pearson colocalization coefficient between PMCA and NMDAR2A clusters within Shank2-positive area was very low in control condition and remained unchanged upon HFS (Fig. 13E; control: 0.1828 ± 0.01015 vs HFS: 0.1871 ± 0.007362). The shortest distance between PMCA and NMDAR2A clusters was not affected by HFS (Fig. 13F; control: 0.2332 ± 0.008412 vs HFS: 0.2259 ± 0.006278). Altogether, these data show that 1) PMCA and Neuroplastin are in tight proximity with each other (beyond resolution of STED microscopy + deconvolution, ≤50 nm), 2) PMCA-Neuroplastin complexes exist both within and also around Shank2-positive areas, 3) PMCA-Neuroplastin closeness is unaltered after HFS and 4) NMDAR2A clusters are relatively less close to PMCA, a feature that is not changed by HFS.

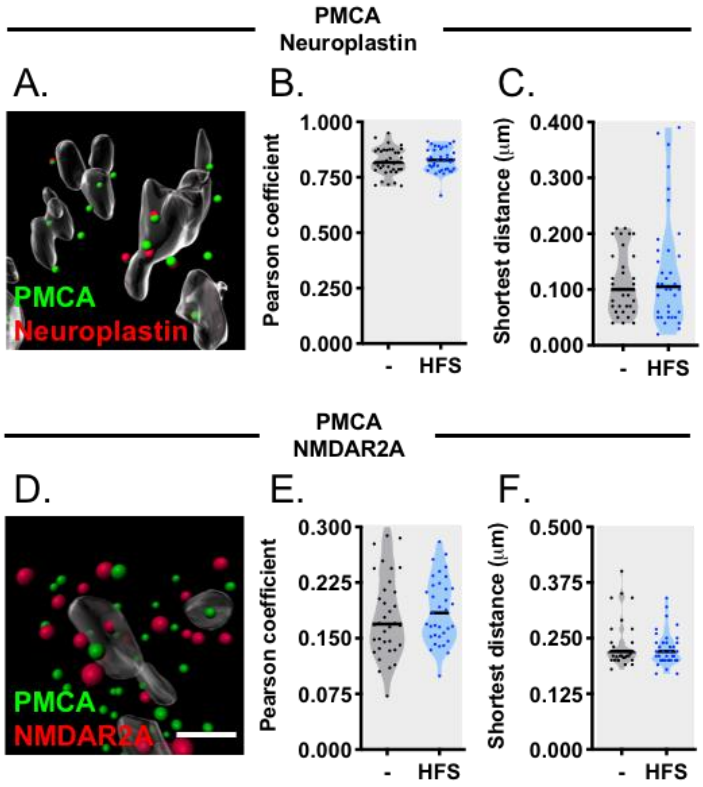

Figure 13. Co-localization and distance of PMCA with Neuroplastin or NMDAR2A. Hippocampal neurons were stimulated at DIV 16-17 with high-frequency-stimulation (HFS). One minute after, they were fixed and then stained with antibodies against PMCAs and Shank2 and neuroplastin or GluN2A-containing NMDAR (NMDAR2A). For increased resolution, STED images were deconvolved with Huygens Professional 19.10 software. 3D reconstructions were created by using Imaris x64 9.5.1 software (**A** and **D**). Scale bar is 0.5 µm. Shank2-positive puncta were used as region of interest. Pearson colocalization coefficient was quantified by using colocalization analyzer tool of Huygens software and ImageJ (**B** and **E**). The shortest distance between PMCA and Neuroplastin (**C**) or PMCA and NMDAR2A (**F**) spots around 0.300 µm distance from Shank2 surfaces were quantified by using Imaris x64 9.5.1 software. The data display violin plots with medians. PMCA-Neuroplastin co-stainings include n= 38 neurons for control and n= 36 neurons for HFS (three independent cultures). PMCA-NMDAR2A co-stainings include n= 37 neurons for control and n= 36 neurons for HFS (three independent cultures). No statistically significant difference between two groups.

To further elaborate on the crosstalk between PMCA-Neuroplastin complexes and NMDAR, I tested whether the synaptic localization of the three transmembrane proteins is regulated by inhibitors of glutamate receptor activity or PMCA activity. To this end, hippocampal neurons were pre-treated with well characterized glutamate receptor antagonists, APV and CNQX. In order to inhibit all four PMCA, a cocktail of the selective PMCA inhibitors Caloxin2A1, Caloxin3A1 and Caloxin1B1 was used (Pande et al., 2005; Pande et al., 2008; Szewczyk et

al., 2010). When neuronal cultures were exposed to HFS, the neurons were also fixed one minute after and immunostained as described above (Fig. 14A). The previously described recruitment of PMCA and Neuroplastin into the Shank2-positive areas upon HFS (Fig. 12) was not observed in the presence of APV and CNQX or Caloxins. Upon pharmacological treatments, the numbers (Fig. 14B; Table 13 in Appendix), total puncta signals (Fig. 14C; Table 13 in Appendix), intensities (Fig. 14D; Table 13 in Appendix) and areas (Fig. 14E; Table 13 in Appendix) of PMCA clusters were only slightly changed following HFS. Likewise, the numbers (Fig. 14F; Table 13 in Appendix), total puncta signals (Fig. 14G; Table 13 in Appendix), intensities (Fig. 14H; Table 13 in Appendix) and areas (Fig. 14I; Table 13 in Appendix) of Neuroplastin clusters were almost not changed by HFS in the presence of APV and CNQX or Caloxins cocktail. In the presence of any pharmacological treatment, no significant changes were observed in the number (Fig. 14J; Table 13 in Appendix), total puncta signal (Fig. 14K; Table 13 in Appendix), intensity (Fig. 14L; Table 13 in Appendix) or area (Fig. 14M; Table 13 in Appendix) of NMDAR2A clusters nor in control condition neither upon HFS. Furthermore, only slight alterations were observed in the presence of either inhibitor compared to untreated control (indicated as a dashed line) being overall very modest when compared to Figure 12. HFS did not modify the area of Shank2-puncta in the presence of inhibitors (Table 12 in Appendix). Taken together the results from Figures 12-14, it is possible to conclude that 1) the synaptic localization and abundance of PMCA and Neuroplastin is dynamic and similar, 2) the synaptic localization of PMCA and Neuroplastin is modified by HFS, 3) Neuroplastin-PMCA complexes are in a close proximity to but not directly contacting NMDAR2A; and 4) HFS fails to modify PMCA-Neuroplastin synaptic location when the glutamate receptor activity is inhibited.

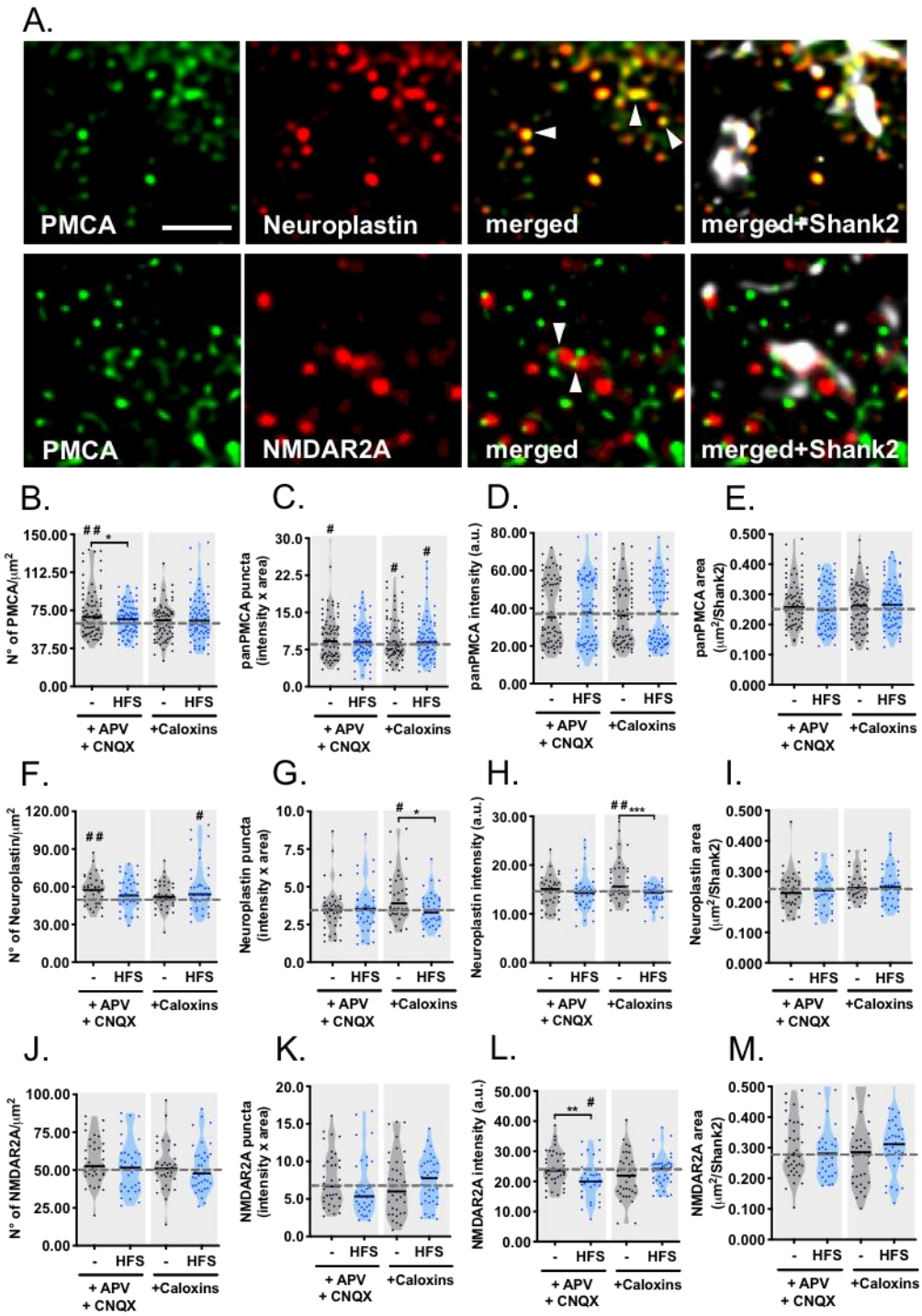

Figure 14. Synaptic localization of PMCA, Neuroplastin and NMDAR2A seems to be modulated by glutamate receptor and PMCA activity. A) Hippocampal neurons were pre-incubated at DIV 16-17 with APV (50 µM) and CNQX (10 µM) or Caloxins (20 µM) for 5 min and then stimulated with high-frequency-stimulation (HFS). One minute after HFS, neurons were fixed and stained with anti-panPMCA, anti-neuroplastin or anti-NMDAR2A and anti-Shank2 antibodies. For increased resolution, STED images were deconvolved with Huygens Professional 19.10 software. Scale bar is 1 µm. **B-M)** The graphs show the number (**B**, **F**, **J**), total puncta signal (**C**, **G**, **K**; intensity x area), intensity (**D**, **H**, **L**) and area (**E**, **I**, **M**) of PMCA, Neuroplastin and

NMDAR2A clusters upon drug treatment. Shank2-positive puncta were used as region of interest. The data display violin plots with medians. PMCA stainings include n= 77 neurons for APV+CNQX, n= 72 neurons for APV+CNQX+HFS, n= 74 neurons for Caloxins and n= 75 neurons for Caloxins+HFS (six independent cultures). Neuroplastin stainings include n= 39 neurons for APV+CNQX, n= 39 neurons for APV+CNQX+HFS, n= 37 neurons for Caloxins and n= 38 neurons for Caloxins+HFS (three independent cultures). NMDAR2A stainings include n= 38 neurons for APV+CNQX, n= 35 neurons for APV+CNQX+HFS, n= 37 neurons for Caloxins and n= 37 neurons for Caloxins+HFS (three independent cultures). Unpaired t-test *$p<0.05$, **$p<0.01$, **$p<0.001$ within the drug treated group; $^{\#}p<0.05$, $^{\#\#}p<0.01$ compared to control from Figure 12 (dashed line).

I also checked whether the colocalization of PMCA with Neuroplastin in Shank2-positive areas is affected by the presence of inhibitors for glutamate receptors or PMCAs. The Pearson colocalization coefficient between PMCA and Neuroplastin was unchanged in the presence of APV-CNQX or Caloxins compared to control from Figure 13 indicated as a gray dashed line (Fig. 15A-B; Table 14 in Appendix). The Pearson colocalization coefficient between PMCA and Neuroplastin was significantly increased upon HFS in the presence of the glutamate receptor antagonists APV and CNQX. This was also the case when PMCA was inhibited with Caloxins (Fig. 15A; Table 14 in Appendix). However, the shortest distance between PMCA and Neuroplastin was slightly increased upon HFS in the presence of APV and CNQX compared control indicated as a dashed line (Fig. 15B; Table 14 in Appendix). Caloxins significantly increased the distance between PMCA and Neuroplastin compared to control, effect that was prevented by HFS (Fig. 15B; Table 14 in Appendix). Although these results showed statistically significant differences (Fig. 15A-B), the biological relevance of them requires further investigation and they need to be confirmed using independent techniques for instance single molecule tracking. On the other hand, the Pearson colocalization coefficient between PMCA and NMDAR2A was unchanged in the presence of APV and CNQX or Caloxins (Fig. 15C; Table 14 in Appendix). The shortest distance between PMCA and NMDAR2A was mainly unaffected by pharmacological pre-treatment and HFS (Fig. 15D; Table 14 in Appendix) suggesting that PMCA do not associate abundantly and/or directly to NMDAR2A. Therefore, the results from Figures 14 and 15 support that glutamate receptor activity modulates HFS-induced synaptic recruitment of PMCA and Neuroplastin. The synaptic localization of NMDAR2A is largely unaffected by blocking glutamate receptor activity or PMCA activity in the evaluated experimental conditions.

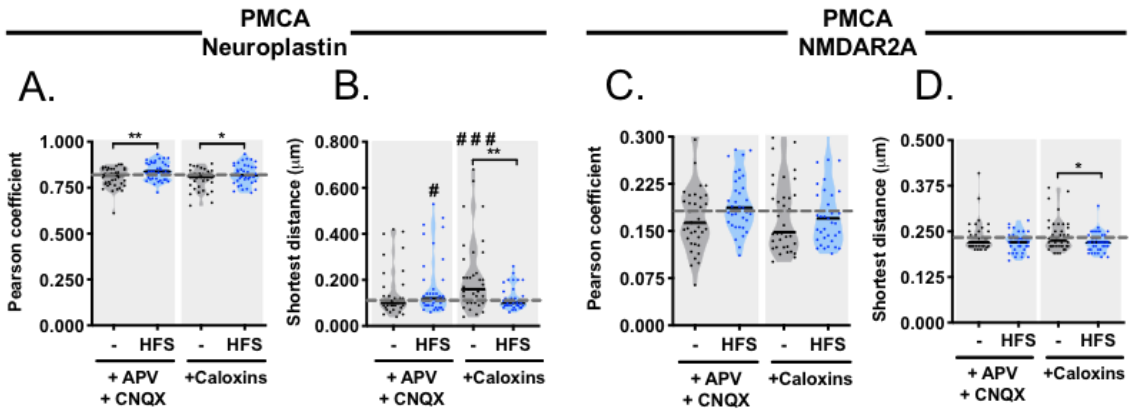

Figure 15. Co-localization and distance of PMCA with Neuroplastin or NMDAR2A in synapses treated with glutamate receptor and PMCA inhibitors. Hippocampal neurons were pre-incubated at DIV 16-17 with APV (50 µM) and CNQX (10 µM) or Caloxins (20 µM) for 5 min and then stimulated with high-frequency-stimulation (HFS). One minute after, neurons were fixed and stained with anti-panPMCA and anti-Shank2 and anti-neuroplastin or anti-NMDAR2A antibodies. **A-D)** STED images were deconvolved with Huygens Professional 19.10 software. Pearson colocalization coefficient was quantified by using colocalization analyzer tool of Huygens software and ImageJ (**A** and **C**). The shortest distance between PMCA and Neuroplastin (**B**) or PMCA and NMDAR2A (**D**) spots around 0.300 µm distance from Shank2 surfaces were quantified by using Imaris x64 9.5.1 software. Shank2-positive puncta were used as region of interest. The data display violin plots with medians. PMCA-neuroplastin co-stainings include n= 39 neurons for APV+CNQX, n= 38 neurons for APV+CNQX+HFS, n= 36 neurons for Caloxins and n= 38 neurons for Caloxins+HFS (three independent cultures). PMCA-NMDAR2A co-stainings include n= 38 neurons for APV+CNQX, n= 35 neurons for APV+CNQX+HFS, n= 37 neurons for Caloxins and n= 37 neurons for Caloxins+HFS (three independent cultures). Unpaired t-test *p<0.05, **p<0.01, **p<0.001 within the drug treated group; $^{\#}$p<0.05, $^{\#\#}$p<0.01 compared to control in Figure 13 (dashed line).

Prior to address functionally the crosstalk between PMCA-Neuroplastin complexes and glutamate receptors, I further characterized the role of endogenous PMCA in Ca^{2+} clearance in dendrites and spines as well as further controlled my experimental approach and set-up. For this, I performed live-cell calcium imaging in RFPT-GCaMP5 transfected neurons silenced with TTX (0.5 µM) and pre-treated with Caloxin cocktail (20 µM). Representative traces of Ca^{2+} transients from neurons treated or untreated with Caloxins are shown (Fig. 10A-C). Control experiments were performed with the addition to the recording chamber of saline vehicle, meaning Tyrodes buffer without Caloxins. As expected (Fig. 9 and 10), quantification of calcium kinetics upon stimulation with 5 APs at 10 Hz revealed that PMCA inhibition with Caloxins slows down Ca^{2+} clearance by increasing decay time in dendrites and

spines (Fig. 16D; Table 15 in Appendix). Half-width, rise time and baseline were not affected by PMCA inhibition (Fig. 16E, F and G; Table 15 in Appendix). Control experiment (saline without Caloxins) showed no difference in decay time, half-width, rise time or baseline (Fig. 16H, I, J and K; Table 15 in Appendix). These experiments confirm that endogenous PMCA activity is important for Ca^{2+} clearance in dendrites and spines. This function of endogenous PMCA is robust and evidenced by using completely different PMCA inhibitors and stimulation protocols (Fig. 9 vs. Fig. 16).

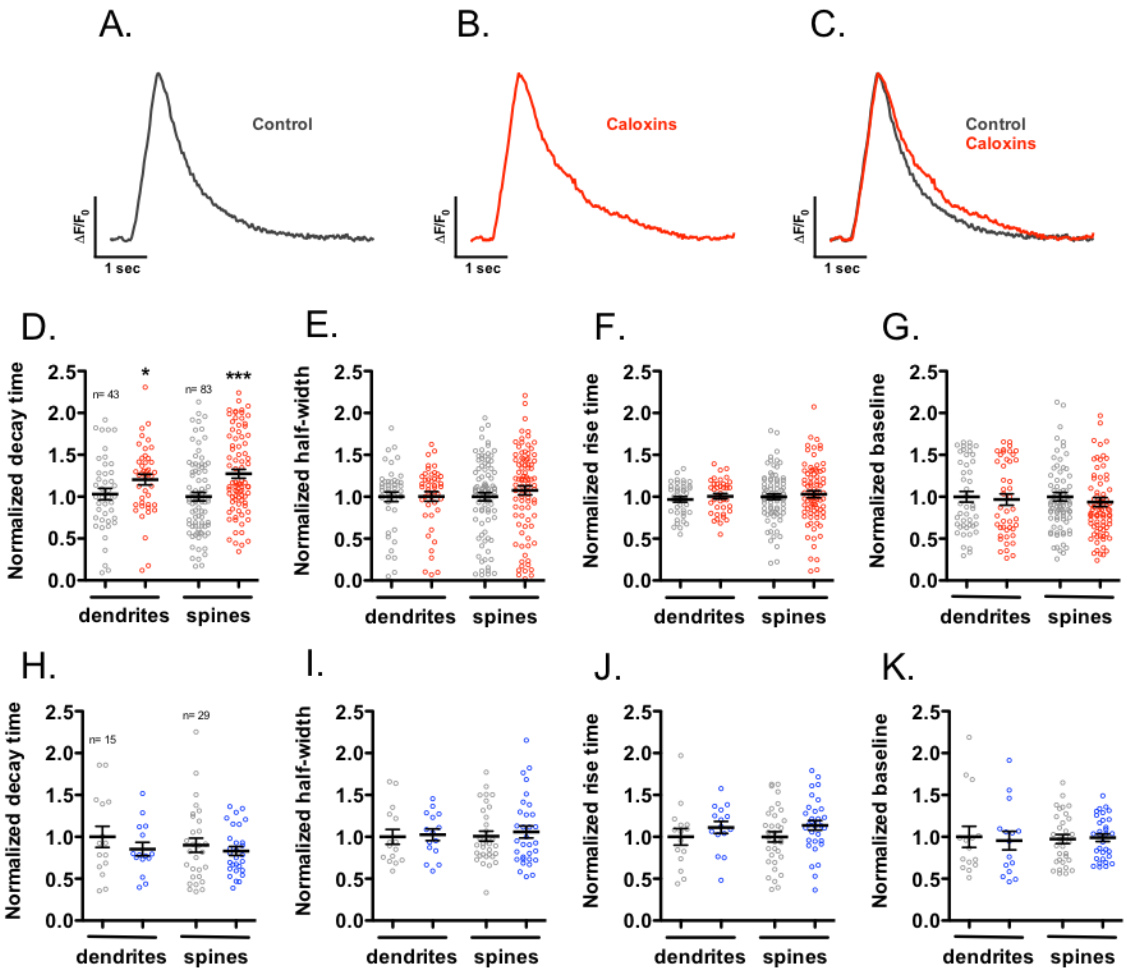

Figure 16. PMCA inhibition by Caloxins slows down Ca^{2+} clearance in dendrites and spines. Hippocampal neurons were transfected at DIV 11 with RFPT-GCaMP5. Calcium imaging was performed at DIV 15 in Tyrodes buffer with TTX (0.5 µM). Gray colour represents basal condition and red colour represents 5 min after PMCA inhibitor (Caloxins, 20 µM). Control experiment with saline (no Caloxins) is represented in blue colour. Representative traces of Ca^{2+} transients from neurons treated or untreated with Caloxins are shown (**A-C**). Calcium kinetics upon stimulation with 5 APs at 10 Hz were quantified. Normalized decay time (**D** and **H**)**,** half-width (**E** and **I**)**,** rise time (**F** and **J**) and baseline (**G** and **K**) are presented as graphs. Data is shown as the mean±SEM (n values indicate the number of dendrites and spines that were

analyzed). n= 12 neurons for control and n= 12 neurons for Caloxins (three independent cultures). Mann Whitney test *p<0.05, **p<0.01, ***p<0.001 compared to control (gray circles).

GCaMPs as genetically encoded fluorescent Ca^{2+} indicators (GECIs) are widely used for the measurement of intracellular calcium dynamics. GCaMPs have many advantages such as allowing *in vivo* monitoring of neuronal activity, dispensing with the need for loading with calcium indicator or targeting specific neuronal populations (Lock et al., 2015). Nevertheless, monitoring subcellular Ca^{2+} transients or local Ca^{2+} signals in microdomains with GCaMPs can be limited by their slow speed to release bound Ca^{2+} as well as by the binding of more than one ion per sensor molecule. To confirm my findings from GCaMP5-based live-cell calcium imaging, I have used Oregon Green BAPTA-1 (OGB-1) which has a 1:1 and fast binding and dissociation kinetics for Ca^{2+}, allowing the detection and quantification of rapid Ca^{2+} transients (Badura et al., 2014). Hippocampal neurons were transfected with RFPT to be able to monitor neuronal morphology (Fig. 17A). Then, neurons were loaded with OGB-1 (2 µM) 30 min, treated or not with Caloxins cocktail (20 µM) and then stimulated with HFS. Compared to control, PMCA inhibition with Caloxins slowed down Ca^{2+} restoration by increasing decay time in dendrites and spines (Fig. 17B; Control: 1.000 ± 0.02758 vs Caloxins: 1.166 ± 0.03151 and Fig. 17D; Control: 1.000 ± 0.01656 vs Caloxins: 1.127 ± 0.02390). Half-width did not change in dendrites (Fig. 17C; Control: 1.000 ± 0.03411 vs Caloxins: 0.9895 ± 0.03641) whereas it was reduced following Caloxins in spines (Fig. 17E; Control: 1.000 ± 0.03032 vs Caloxins: 0.9282 ± 0.02379). Rise time was increased with Caloxins in dendrites (Fig. 17F; Control: 1.000 ± 0.1081 vs Caloxins: 1.836 ± 0.1847) and remained unchanged in spines (Fig. 17H; Control: 1.000 ± 0.06475 vs Caloxins: 1.078 ± 0.05424). This change in rise time was not observed when GCaMP5 was used (Fig. 16C). This difference may be explained due to the facts that OGB-1 and GCaMPs have different sensitivity to intracellular Ca^{2+} levels, dynamic range and kinetics (Chen et al., 2013). Also, OGB-1 diffuses into organelles which may explain why the effect is more evident in dendrites (Fig. 17F). Importantly, peak amplitude was not affected by Caloxins in dendrites and spines (Fig. 17G; Control: 0.9422 ± 0.07304 vs Caloxins: 0.8599 ± 0.04047 and Fig. 17I; Control: 0.9731 ± 0.05754 vs Caloxins: 0.8968 ± 0.03534). Therefore, these data generated using OGB-1 fit and confirm to the previous results using GCaMP5 in Figures 9, 16 and 18 (see later).

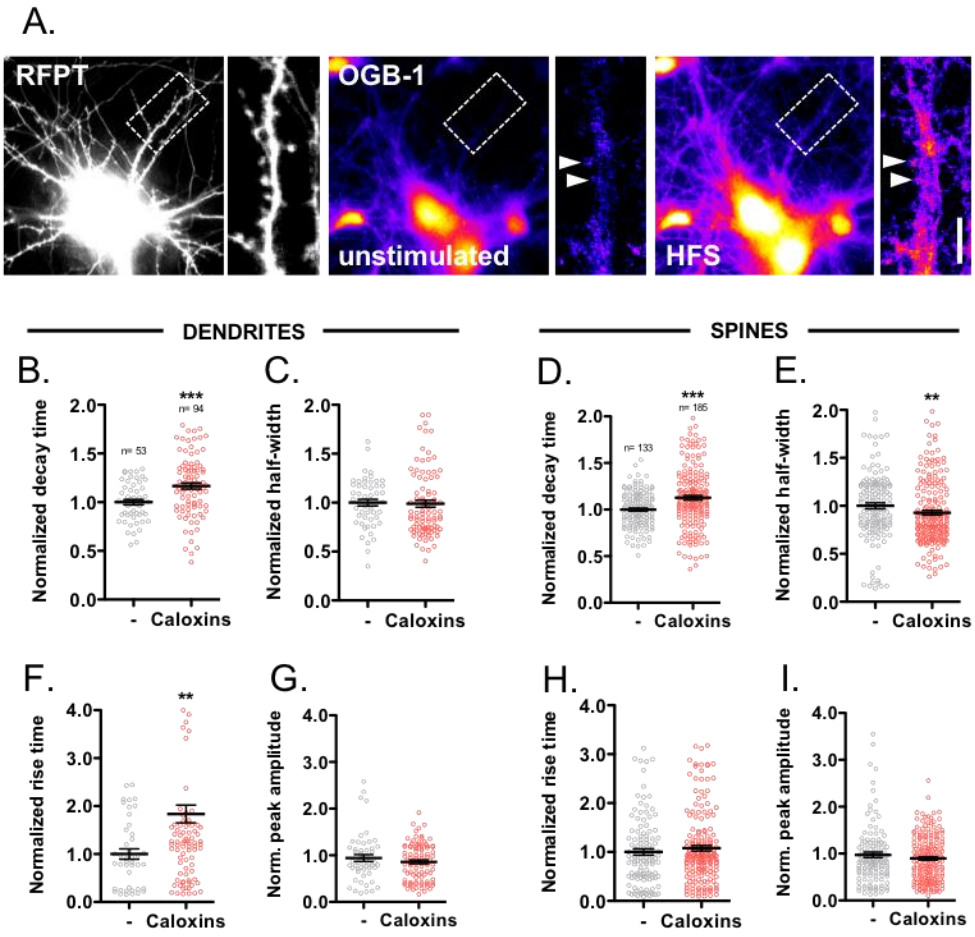

Figure 17. Calcium clearance by PMCA in OGB-1-loaded neurons. A) Hippocampal neurons were transfected at DIV 11 with RFPT carrying plasmid. Then, neurons were loaded at DIV 15-16 with Oregon Green 488 BAPTA-1, AM (OGB-1, 2 µM) for 30 min. Calcium imaging was performed in Tyrodes buffer. Caloxins (20 µM) were added 3 min before HFS. Scale bar is 10 µm. **B-I)** Calcium kinetics upon HFS ((40 APs, 80 Hz)x8) were quantified. Normalized decay time (**B** and **D**)**,** half-width (**C** and **E**)**,** rise time (**F** and **H**) and peak amplitude (**G** and **I**) are presented as graphs. Data is shown as the mean±SEM (n values indicate the number of dendrites and spines that were analyzed). n= 10 neurons for control and n= 14 neurons for Caloxins (three independent cultures). Mann Whitney test *p<0.05, **p<0.01, ***p<0.001 vs control (gray circles).

By knowing both PMCA and Na^+/Ca^{2+} exchangers (NCX) contribute to Ca^{2+} extrusion in dendrites and spines (Scheuss et al., 2006), I wondered whether PMCA-mediated Ca^{2+} clearance (reported by decay time, see Fig. 9, 16, 17) can be dissociated from the activity of NCX in dendrites and spines in my experimental conditions (see Fig. 1). In order to test this, RFPT-GCaMP5 neurons were treated with a specific inhibitor of NCX ORM-10103 (5 µM) (Jost et al., 2013) together with TTX (0.5 µM) and stimulated using 5-10 APs at 10 Hz. Following this recording, the cocktail of Caloxins were added on top and neurons were stimulated again after 5 and 10 minutes. Therefore, calcium kinetics quantified from TTX and

ORM-10103 treated neurons were used to normalize these experiments (gray circles, Fig. 18). In the presence of the NCX inhibitor ORM-10103, PMCA inhibition with Caloxins was affective to slow down Ca^{2+} clearance by increasing decay time in dendrites and spines (Fig. 18A and C; Table 16 in Appendix) whereas the half-width (Fig. 18B and D; Table 16 in Appendix) and the rise time (Fig. 18E and G; Table 16 in Appendix) were largely unaffected by the presence of Caloxins. Interestingly, in the presence of ORM-10103, addition of Caloxins resulted in a reduced baseline signal in dendrites and spines (Fig. 18F and H; Table 16 in Appendix) pointing to the initiation of auxiliary compensatory mechanism(s) to decrease baseline Ca^{2+} levels when both NCX and PMCA are inhibited together. Altogether PMCA activity clearly plays a role in Ca^{2+} clearance in neurons and it can be distinguished from the activity of the Na^{+}/Ca^{2+} exchanger in my experimental conditions.

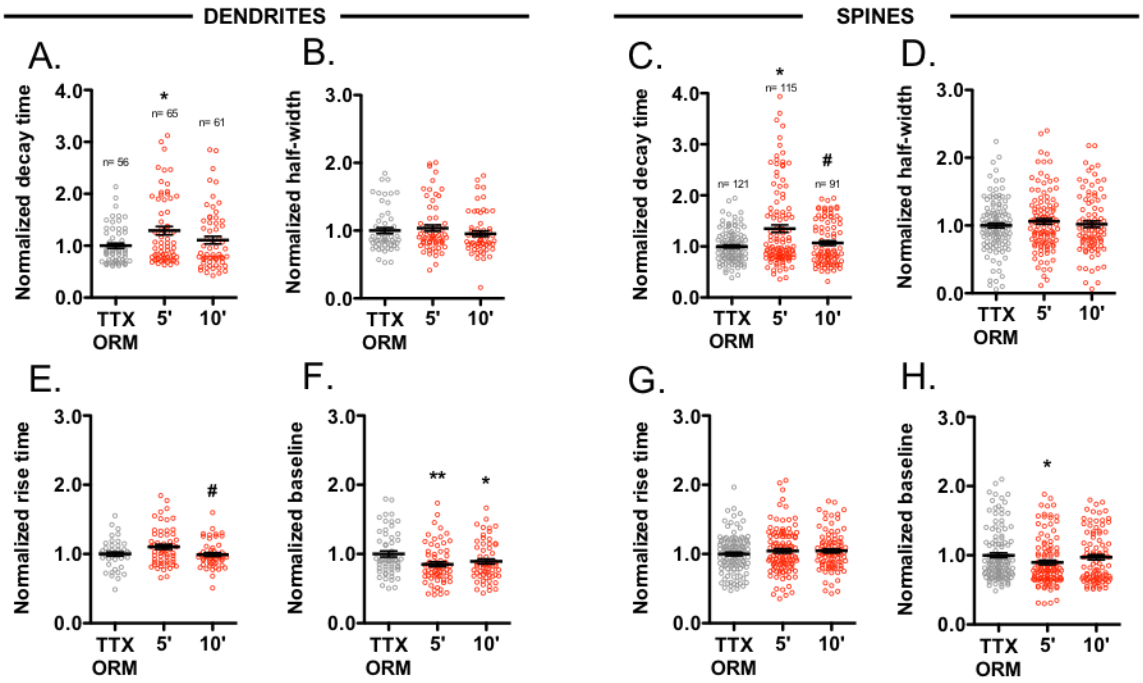

Figure 18. PMCA-mediated Ca^{2+} clearance is independent from Na^{+}/Ca^{2+} exchanger in neurons. Hippocampal neurons were transfected at DIV 11 with RFPT-GCaMP5. Calcium imaging was performed at DIV 16 in Tyrodes buffer with TTX (0.1 µM) and ORM-10103 (5 µM). Following baseline recording, neurons were treated with PMCA inhibitor Caloxins (20 µM). Calcium kinetics upon stimulation with 5-10 APs at 10 Hz were presented as graphs (basal condition is in gray and 5 and 10 min after Caloxins are in red colour). Normalized decay time (**A** and **C**)**,** half-width (**B** and **D**)**,** rise time (**E** and **G**) and baseline (**F** and **H**) are presented as graphs. Data is shown as the mean±SEM (n values indicate the number of dendrites and spines that were analyzed). n= 16 neurons for all conditions (three independent cultures). Mann Whitney test, *p<0.05 compared to control (gray circles); #p<0.05 between Caloxins-treated groups.

After further confirming the specificity and capacity of the experimental approach to evaluate PMCA activity on Ca^{2+} clearance (Figures 9, 16, 17 and 18), I tested the impact of the crosstalk between PMCA-Neuroplastin complexes and glutamate receptors on Ca^{2+} regulation of hippocampal neurons transfected with RFPT-GCaMP5. Glutamate receptor activity was blocked with APV and CNQX 3 min before applying 5-10 APs at 10 Hz during live cell calcium imaging. Continuing, PMCA was inhibited with Caloxins and neurons were stimulated again with 5-10 APs at 10 Hz after 2, 5 and 10 minutes as shown (Fig. 19A-B). Compared to the first stimulation of neurons exposed only to APV and CNQX, PMCA inhibition with Caloxins did not necessarily alter the decay time (Fig. 19C and E; Table 17 in Appendix), the half-width (Fig. 19D and F; Table 17 in Appendix) or the rise time (Fig. 19G and H; Table 17 in Appendix) in the dendrites and spines. Interestingly, the slowing down effect of PMCA inhibition on Ca^{2+} clearance observed in Figures 16, 17 and 18 did not take place when glutamate receptors were blocked (Fig. 19). These data indicate that PMCA requires the activation of NMDA-type and/or AMPA-type glutamate receptors to contribute to the Ca^{2+} restoration in dendrites and spines.

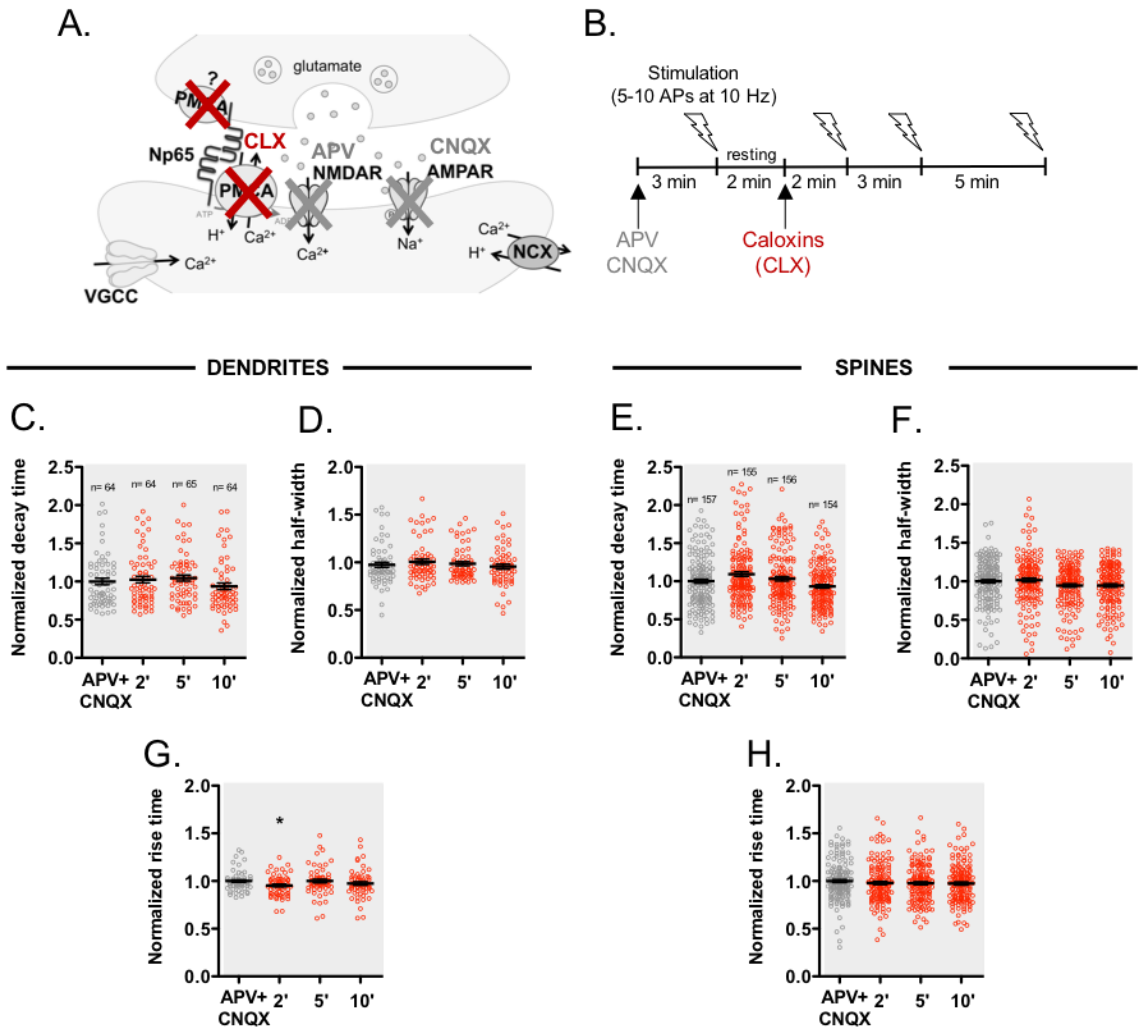

Figure 19. PMCA-mediated Ca^{2+} clearance is sensitive to glutamate receptor activity. A-B) Hippocampal neurons were transfected at DIV 11 with RFPT-GCaMP5. Calcium imaging was performed at DIV 15-16 in Tyrodes buffer with APV (50 µM) and CNQX (10 µM). The experimental procedure including pharmacological treatment and electrical stimulation is shown. Calcium kinetics upon stimulation with 5-10 APs at 10 Hz were presented as graphs (basal condition is in gray and 2, 5 and 10 min after PMCA inhibitor - 20 µM Caloxins are in red colour). **C-H)** Normalized decay time (**C** and **E**), half-width (**D** and **F**) and rise time (**G** and **H**) are presented as graphs. Data is shown as the mean±SEM (n values indicate the number of dendrites and spines that were analyzed). n= 16 neurons for all conditions (three independent cultures). Mann Whitney test *p<0.05 compared to control (gray circles).

The requirement of glutamate receptor activity for Neuroplastin-PMCA-mediated Ca^{2+} clearance was also investigated using the HFS protocol in hippocampal neurons transfected with RFPT-GCaMP5 or Np65-RFPT-GCaMP5. As indicated in Figures 20A and B, neurons were pre-treated with APV and CNQX for 3 min to block glutamate receptor activity and then, Carboxyeosin was added to inhibit PMCA. Therefore, this experimental protocol is complementary to the one used in Figure 19 and directly comparable to the one used in Figure 9. PMCA inhibition with Carboxyeosin resulted in a slower Ca^{2+} clearance by increasing decay time in dendrites and spines (Fig. 20C and E; Table 18 in Appendix). Interestingly, this increase in the decay time by Carboxyeosin in the background of glutamate receptor inhibition, was however smaller than the one occurring in the present of Carboxyeosin only (Figure 9). More interestingly, in the background of glutamate receptor inhibition (Fig. 20C and E; Table 18 in Appendix), Neuroplastin65 overexpression did not foster Ca^{2+} restoration by PMCA as also shown before (Figure 9). Ca^{2+} restoration was even slower in Neuroplastin65 overexpressing neurons in the presence of APV and CNQX (Fig. 20C-E). Carboxyeosin was effective to increase decay time in Neuroplastin65 overexpressing neurons pre-treated with APV and CNQX (Fig. 20C and E; Table 18 in Appendix) but again, not as effectively as shown before when glutamate receptors were available for activation (Figure 9). Half-width nearly did not change except a significant increase following Carboxyeosin treatment in Neuroplastin65 overexpressing neurons compared to RFPT-GCaMP5 expressing neurons (Fig. 20D and F; Table 18 in Appendix). How PMCA inhibition became more apparent in Neuroplastin65 overexpressing neurons could be explained with increased levels of PMCA which was shown in Figure 8. Interestingly, in dendrites, peak amplitude was unaltered under all conditions when glutamate receptors were blocked compared to control (Fig. 20G). In spines, only PMCA inhibition increased peak amplitude in Neuroplastin65 overexpressing neurons (Fig. 20I). Peak amplitude was significantly affected by PMCA inhibition and/or Neuroplastin overexpression when glutamate receptors were operating (Fig. 9J and L). While rise time was decreased

upon Carboxyeosin treatment in the background of APV and CNQX, this was unchanged in Neuroplastin65 overexpressing neurons (Fig. 20H and J; Table 18 in Appendix). Therefore, as mentioned about decay time, the presence of APV and CNQX resulted in a dissimilar effect of Carboxyeosin on half-width, peak amplitude and rise time to what was shown in Figure 9. These results indicate that the blockage of NMDA- and/or AMPA-type glutamate receptors impairs the capacity of Neuroplastin-PMCA complexes to restore Ca^{2+} transients during HFS-evoked high neuronal activity (Figure 20) or low frequency stimulation (Figure 19).

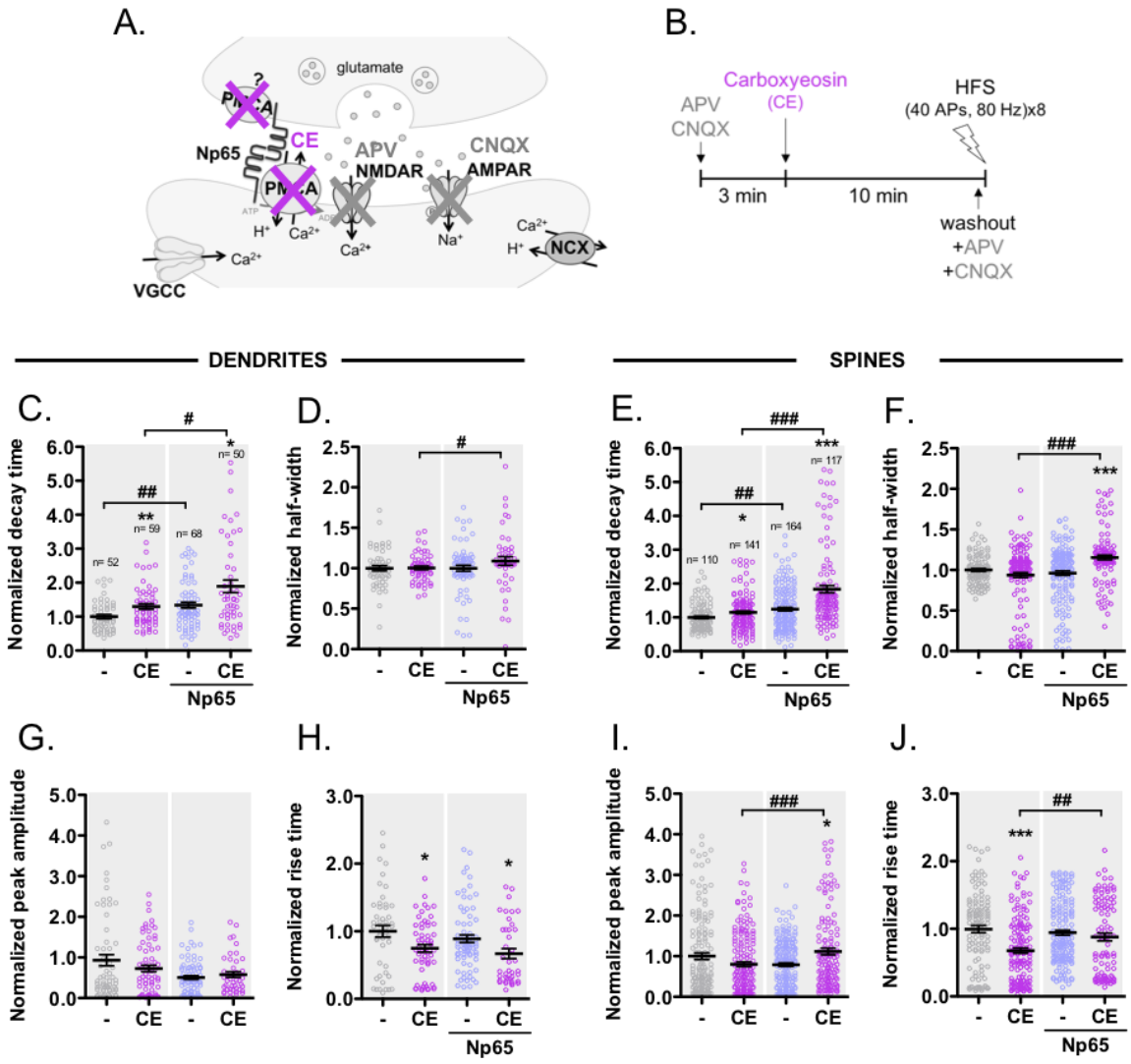

Figure 20. HFS-induced Neuroplastin-PMCA-mediated Ca^{2+} clearance under conditions of NMDA and AMPA receptor blocking. A-B) Hippocampal neurons were transfected at DIV 11 with RFPT-GCaMP5 and Np65-RFPT-GCaMP5. Calcium imaging was performed at DIV 15-16 in Tyrodes buffer with APV (50 µM) and CNQX (10 µM). The experimental procedure including pharmacological treatment and electrical stimulation is shown. APV and CNQX were added to

block glutamate receptor activity. Three minutes after APV and CNQX, PMCA inhibitor (Carboxyeosin, CE, 0.5 µM) was applied for 10 min before recording. After washout with Tyrodes buffer and adding APV and CNQX again, high-frequency stimulation (HFS, 8 trains of 40 APs at 80 Hz) was applied as a field stimulation. **C-J)** Calcium kinetics upon HFS were quantified. Normalized decay time (**C** and **E**), half-width (**D** and **F**), peak amplitude (**G** and **I**) and rise time (**H** and **J**) are presented as graphs in dendrites and spines. Data is shown as the mean±SEM (n values indicate the number of dendrites and spines that were analyzed). n= 13 neurons for control, n= 14 neurons for CE, n=14 neurons for Np65 and n= 11 neurons for Np65+CE (three independent cultures). Mann-Whitney U test *p<0.05, **p<0.01, ***p<0.001 between with vs. without CE; $^{\#}$p<0.05, $^{\#\#}$p<0.01, $^{\#\#\#}$p<0.001 between RFPT-GCaMP5 vs. Np65-RFPT-GCaMP5.

I also evaluated the effect of glutamate receptor inhibition on Ca^{2+} transients evoked by low-frequency stimulation using live-cell calcium imaging. For this, either RFPT-GCaMP5- or Np65-RFPT-GCaMP5-expressing hippocampal neurons were stimulated with low-frequency stimulation (10 APs at 10 Hz) and then, after a resting period, exposed to APV (50 µM) and CNQX (10 µM) and stimulated again. As expected, treatment with APV and CNQX resulted in a faster Ca^{2+} clearance evidenced by a decreasing decay time and half-width in dendrites and spines (Fig. 21A-D; Table 19 in Appendix). Peak amplitude was decreased upon APV and CNQX treatment in dendrites and spines of RFPT-GCaMP5 and Np65-RFPT-GCaMP5 neurons (Fig. 21E and G). An increased rise time was found in dendrites (Fig. 21F) while this was not significant in spines of APV and CNQX-treated neurons (Fig. 21H; Table 19 in Appendix). Overexpression of Neuroplastin65 accelerated Ca^{2+} clearance by reducing decay time and half-width which is consistent with results in Figure 9 and Figure 10 (Fig. 21A-D; Table 19 in Appendix). Also consistent with the results in Figure 9, peak amplitude was decreased (Fig. 21E and G) and the rise time was not influenced in the dendrites and spines of Neuroplastin65 overexpressing neurons compared to control (Fig. 21F and H; Table 19 in Appendix). Treatment of Neuroplastin65 overexpressing neurons with APV and CNQX further accelerated Ca^{2+} clearance with a much significant reduction in decay time and half-width (Fig. 21A-D; Table 19 in Appendix). While peak amplitude was reduced (Fig. 21 E and G), rise time remained unchanged following APV and CNQX treatment in dendrites and spines of Neuroplastin65 overexpressing neurons compared to control (Fig. 21F and H; Table 19 in Appendix). PMCA-Neuroplastin65-gain-of-function was not observed in dendrites and only partially in spines in the presence of APV and CNQX. Interestingly, rise time was faster in dendrites and spines of APV and CNQX-treated Np65-RFPT-GCaMP5 neurons pointing to further alteration(s) in the Ca^{2+} influx machinery located at the synapses.

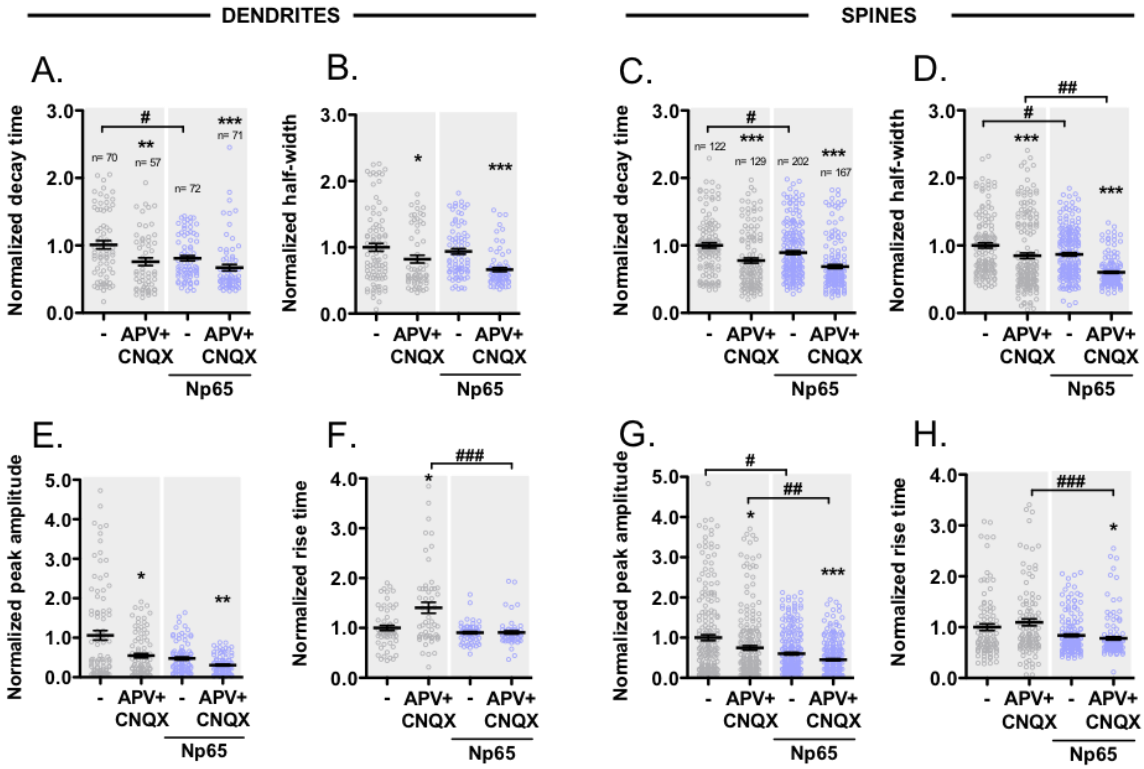

Figure 21. Low-frequency stimulation-induced Ca^{2+} dynamics in control RFP- and Neuroplastin65-RFP- neurons treated with glutamate receptor blockers. Hippocampal neurons were transfected at DIV 11 with RFPT-GCaMP5 or Np65-RFPT-GCaMP5. Calcium imaging was performed at DIV 15-16 in Tyrodes buffer. Glutamate receptor antagonists (APV and CNQX) were applied for 4-5 min before recording. Calcium kinetics upon stimulation with 10 APs at 10 Hz were quantified. Normalized decay time (**A** and **C**), half-width (**B** and **D**), peak amplitude (**E** and **G**) and rise time (**F** and **H**) are presented as graphs Data is shown as the mean±SEM (n values indicate the number of dendrites and spines that were analyzed). n= 10 neurons for control, n= 10 neurons for APV+CNQX, n= 11 neurons for Np65 and n= 11 neurons for Np65+APV+CNQX (three independent cultures per condition). Mann-Whitney U test *p<0.05, **p<0.01, ***p<0.001 between with vs. without APV+CNQX; $^{\#}$p<0.05, $^{\#\#}$p<0.01, $^{\#\#\#}$p<0.001 between RFPT-GCaMP5 vs. Np65-RFPT-GCaMP5.

Calcium homeostasis is finely orchestrated by several players influencing Ca^{2+} influx and Ca^{2+} clearance. In order to better focus on Ca^{2+} influx via glutamate receptors and Ca^{2+} clearance via PMCA, next I aimed to avoid the additional contribution of the L-type voltage-gated Ca^{2+} channels (VGCC) and the Na^{+}/Ca^{2+} exchanger (NCX). For this, RFPT-GCaMP5 transfected neurons were treated with the selective L-type VGCC blocker Nifedipine (10 µM) (Kiryushko et al., 2006) and the NCX inhibitor ORM-10103 (5 µM) (Jost et al., 2013). To test PMCA-mediated Ca^{2+} clearance, Caloxins (20 µM) were added as described in Figure 22 A-B. APV (50 µM) and CNQX (10 µM) were also added when required for blocking glutamate

receptors activity. Calcium responses upon HFS were quantified. Compared to control, PMCA inhibition with Caloxins in the presence of Nifedipine and ORM-10103 did not affect decay time (Fig. 22C; Table 20 in Appendix), half-width (Fig. 22D; Table 20 in Appendix), peak amplitude (Fig. 22G; Table 20 in Appendix) and rise time (Fig. 22H; Table 20 in Appendix) in dendrites. However, treatment with Caloxins resulted in a decreased decay time (Fig. 22E; Table 20 in Appendix), unchanged half-width (Fig. 22F; Table 20 in Appendix), increased peak amplitude (Fig. 22I; Table 20 in Appendix) and decreased rise time (Fig. 22J; Table 20 in Appendix) in spines. Blocking glutamate receptors with APV and CNQX in the presence of Nifedipine and ORM-10103 caused a decreased decay time in dendrites and spines (Fig. 22C and E; Table 20 in Appendix), unchanged half-width in dendrites (Fig. 22D; Table 20 in Appendix) and decreased half-width in spines (Fig. 22F; Table 20 in Appendix), decreased peak amplitude in dendrites and spines (Fig. 22G, I; Table 20 in Appendix) and increased rise time (Fig. 22H, J; Table 20 in Appendix). Compared to APV and CNQX, adding Caloxins together with APV and CNQX decelerated Ca^{2+} extrusion by increasing decay time in dendrites and spine (Fig. 22C and E; Table 20 in Appendix) and increasing half-width in spines (Fig. 22F; Table 20 in Appendix) while not affecting half-width in dendrites (Fig. 22D; Table 20 in Appendix). Peak amplitude was increased in dendrites and spines when Caloxins were added together with APV and CNQX (Fig. 22G and I; Table 20 in Appendix) and rise time was decreased (Fig. 22H and J; Table 20 in Appendix). These data indicate that PMCA carries out Ca^{2+} clearance during HFS-induced neuronal activity and requires glutamate receptors activity. However, the contribution of intracellular stores, i.e. the endoplasmic reticulum should be investigated since calcium entry via glutamate receptors and L-type VGCC were pharmacologically blocked in this experiment. The absence of glutamate receptors activity alters Ca^{2+} handling (including Ca^{2+} influx and clearance) and reverses the effect of PMCA inhibition with Caloxins. Also, Nifedipine and ORM-10103 treatment revealed some distinct differences in calcium kinetics between dendrites and spines.

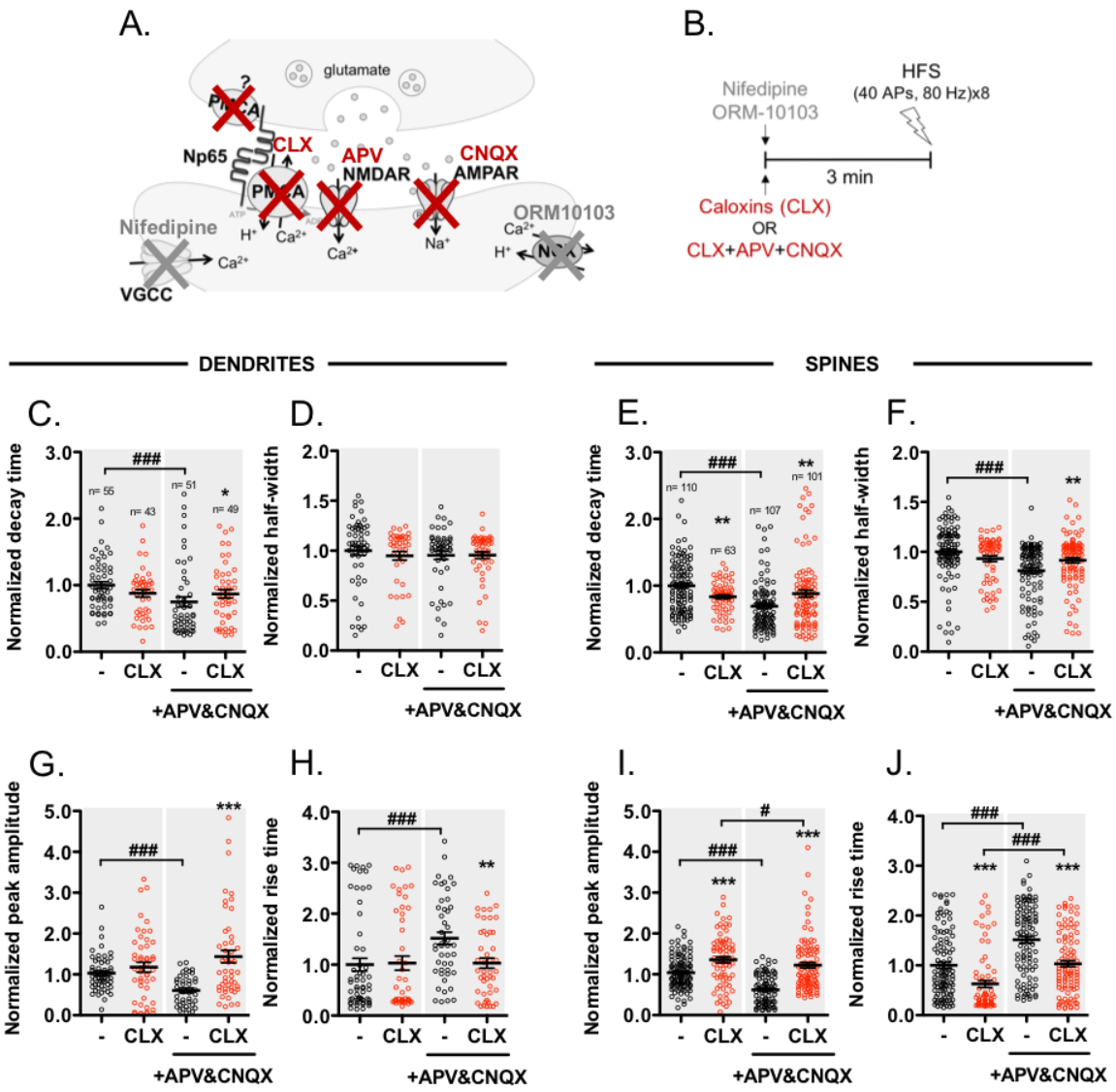

Figure 22. PMCA-mediated Ca^{2+} clearance requires glutamate receptor activity. A-B) RFPT-GCaMP5 expressing hippocampal neurons (DIV 15-16) were treated with Nifedipine (10 µM) and ORM-10103 (5 µM) and then further pharmacological treatment and electrical stimulation is shown. PMCA inhibitor (Caloxins, CLX, 20 µM) was applied for 3 min before recording together with Nifedipine and ORM-10103. Glutamate receptor antagonists (APV and CNQX) were also added for indicated conditions. High-frequency-stimulation (HFS) was applied as a field stimulation. **C-J)** Calcium kinetics upon HFS were quantified. Normalized decay time (**C** and **E**), half-width (**D** and **F**), peak amplitude (**G** and **I**) and rise time (**H** and **J**) are presented as graphs. Data is shown as the mean±SEM (n values indicate the number of dendrites and spines that were analyzed). n= 10 neurons for control, n= 9 neurons for CLX, n= 9 neurons for APV+CNQX and n= 8 neurons for CLX+APV+CNQX (three independent cultures). Mann-Whitney U test *p<0.05, **p<0.01, ***p<0.001 between with vs. without CLX; $^{\#}$p<0.05, $^{\#\#}$p<0.01, $^{\#\#\#}$p<0.001 between with vs. without APV+CNQX.

4.4. PMCA and Neuroplastin modulate phosphorylation of downstream signaling molecules.

Neuroplastin modulates the activation of several downstream signaling molecules. Neuroplastin55-induced signaling involves extracellular signal-regulated kinase 1/2 (ERK1/2) and p38 mitogen activated protein kinase (MAPK) (Owczarek et al., 2010). Extracellular engagement of Neuroplastin was also reported to activate ERK1/2 and PI3 kinase (Owczarek et al., 2011). However, how endogenous Neuroplastin expression modulates activation of kinases such as ERK1/2 remains unsolved. ERK1/2 phosphorylation is known to be essential for neuronal transcriptional events and regulates several forms of plasticity (Thomas & Huganir, 2004). ERK1/2 activity was shown to be required for structural plasticity of synapses (Wu et al., 2001) and also synaptic plasticity (Davis et al., 2000; Dudek & Fields, 2001). Considering that increased ERK1/2 phosphorylation was found in the forebrain of another strain of Neuroplastin65 KO mice (Amuti et al., 2016), I wondered whether ERK1/2 phosphorylation is also altered in in the hippocampus of Neuroplastin-deficient mutant mice, with reduced levels of PMCA and NMDAR2A (Fig. 11A) and impaired capacity to elicit synaptic plasticity (Bhattacharya et al., 2017). To approach this idea, quantitative Western blot analyses by using a p-ERK1/2 (T202/Y204) and ERK1/2 antibodies in a total of six biological replicates per genotype was performed. The total protein homogenates from the hippocampi of Neuroplastin-deficient mice (*Nptn*$^{-/-}$) were compared with wild-type mice (*Nptn*$^{+/+}$) side-by-side (Fig. 23A). The β-III tubulin antibody was used as a neuron-specific loading control. In the hippocampus of Neuroplastin-deficient animals, p-ERK1/2 levels were strongly increased compared to wild-type animal (Fig. 23B; *Nptn*$^{+/+}$: 100.0 ± 6.456 vs *Nptn*$^{-/-}$: 404.9 ± 88.95). The ERK1/2 levels did change in the absence of Neuroplastin (Fig. 23B; *Nptn*$^{+/+}$: 100.0 ± 9.599 vs *Nptn*$^{-/-}$: 134.0 ± 21.82). These data indicate that ERK1/2 activation is clearly altered in the hippocampi of Neuroplastin-deficient mice.

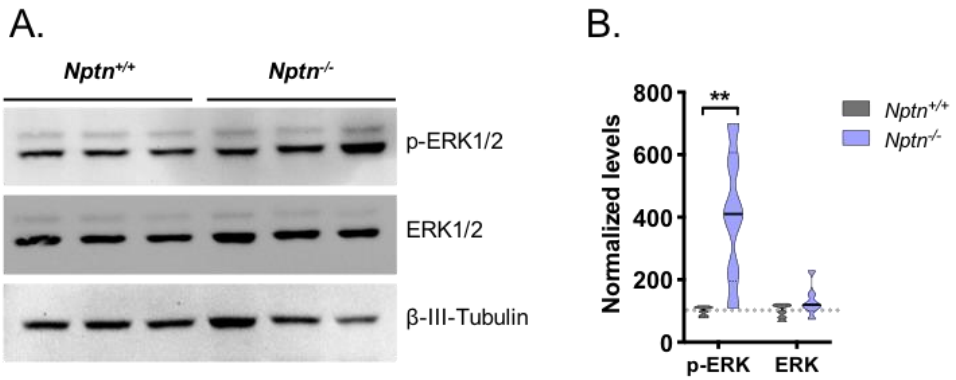

Figure 23. Increased phosphorylation level of ERK1/2 in the hippocampus of *Nptn*$^{-/-}$ mice. A) Wild-type and Neuroplastin-deficient hippocampi were collected and homogenized in buffer A (with protease inhibitor cocktail and PhosSTOP). Proteins were immunoblotted with p-ERK1/2

(T202/Y204), ERK1/2 and β-III tubulin antibodies as indicated. **B)** The graph represents the normalized levels of p-ERK1/2 and ERK1/2. Data is shown as mean±SEM from 6 animals (*Nptn*$^{+/+}$ *and Nptn*$^{-/-}$) per genotype. Student's t test, ***p* < 0.05, ****p* < 0.001.

By knowing the existence of a potential link between Neuroplastin-PMCA expression and ERK1/2 phosphorylation levels (Fig. 23), I aimed to establish a causal relationship between Neuroplastin-PMCA-regulated Ca^{2+} clearance and ERK1/2 activation in the context of morphological plasticity of spines. For this, morphological plasticity of spines in hippocampal neurons was triggered with the HFS protocol (Harvey, Ehrhardt, et al., 2008). To show that HFS is effective to activate ERK1/2 activation, neurons were harvested 10, 20 and 30 min after HFS and the homogenate was submitted to quantitative Western blot analysis by using p-ERK1/2 (T202/Y204) and ERK1/2 antibodies (Fig. 24A). In agreement with the literature, compared to the control condition (no stimulation), there was an increase in p-ERK1/2 levels upon HFS (Fig. 24B; control: 1.000 ± 0.000; HFS 10': 1.118 ± 0.09985; HFS 20': 1.575 ± 0.1865 and HFS 30': 2.494 ± 1.029).

To monitor HFS-triggered ERK1/2 phosphorylation in more detail, I used RFPT-GCaMP5 expressing neurons. RFPT and GCaMP5 signals made it possible to tightly control the experimental progress by monitoring cellular morphology and confirming the proper delivery of the electrical field stimulation, respectively. After 30 min of the HFS, neurons were fixed and immunostained with a p-ERK1/2 (T202/Y204) antibody. The p-ERK1/2 immunoreactivity was low in non-stimulated neurons, but clearly increased upon HFS in both dendritic and somatic regions of both non-transfected and transfected neurons (Fig. 24C).

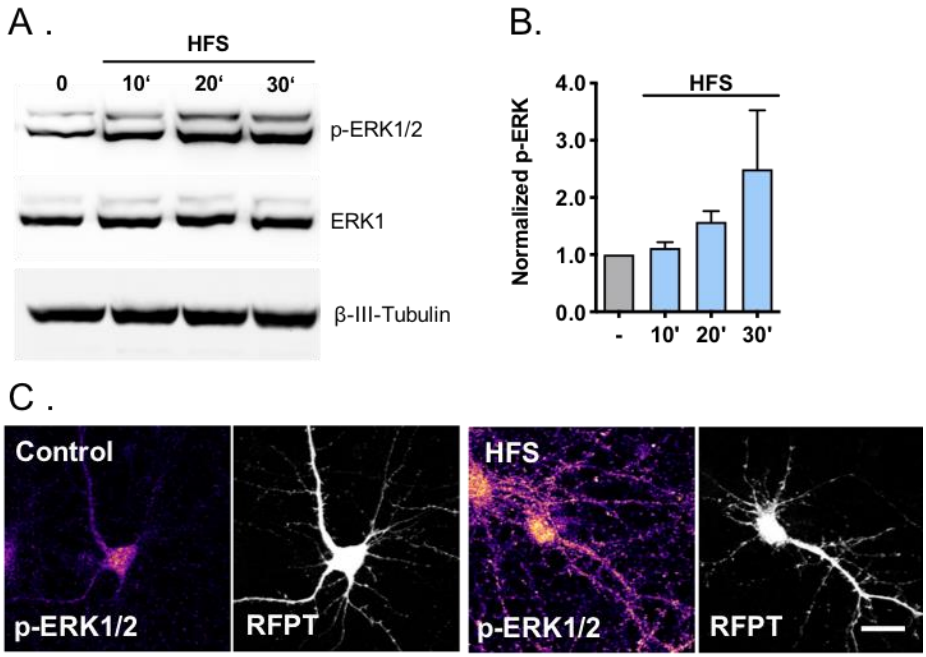

Figure 24. HFS-induced ERK1/2 activation in hippocampal neurons. A) Neurons were stimulated at DIV 14 with HFS protocol and harvested after 10, 20 or 30 minutes. Immunoblotting was performed with p-ERK1/2 (T202/Y204), ERK1 and β-III tubulin antibodies as shown. **B)** Normalized values correspond to mean±SEM from four-five independent cultures. **C)** Neurons were transfected at DIV 11 with RFPT-GCaMP5 and then, stimulated at DIV 16-17 with HFS. After 30 min, neurons were fixed and stained with p-ERK1/2 (T202/Y204) antibody. Scale bar is 20 µm.

Together with ERK1/2, CaMKII serves as crucial molecular hub for cell signaling involved in synaptic transmission (Opazo et al., 2010), synaptic plasticity and memory (Shonesy et al., 2014). Therefore, I investigated HFS-induced CaMKII and ERK1/2 phosphorylation in the dendritic spines and whether their activation is modulated by Neuroplastin-PMCA activity as accounted by the use of Caloxins (20 µM). Hippocampal neurons were silenced with TTX (0.1 µM) to avoid the interference of intrinsic network activity-induced signaling and to establish a low basal phosphorylation level. Neurons were stimulated with HFS and fixed after 5 min, and immunostained with p-CaMKIIα (T286) and p-ERK1/2 (T202/Y204) antibodies. To identify postsynaptic density area in the dendritic spines, Shank2 was immunolabelled with a specific antibody. Shank2-positive areas were selected as a region of interest to monitor synaptic localization of p-CaMKIIα and p-ERK1/2 using two-channel super-resolution STED microscopy (Fig. 25A). In Shank2-positive areas, HFS enhanced CaMKIIα and ERK phosphorylation by increasing the number of clusters (Fig. 25B and F; Table 21 in Appendix) and their total puncta signal (Fig. 25C and G; Table 21 in Appendix). Although, the intensity of p-CaMKIIα and p-ERK1/2 signal did not change upon HFS (Fig. 25D and H; Table 21 in Appendix), the area of p-CaMKIIα was increased upon HFS (Fig. 25E; Table 21 in Appendix) and the area of p-ERK1/2 did not change (Fig. 25I; Table 21 in Appendix). Interestingly, PMCA inhibition with Caloxins by itself did not alter importantly any measured parameter with the exception of the increased number (Fig. 25F; Table 21 in Appendix) and area (Fig. 25I; Table 21 in Appendix) of p-ERK1/2 compared to untreated control. More interestingly, in the presence of Caloxins, HFS failed to increase CaMKIIα and ERK phosphorylation (Fig. 25B-H, except Fig. 25I; Table 21 in Appendix). Altogether, these data indicate that the HFS-induced CaMKIIα and ERK1/2 phosphorylation in Shank2-positive postsynaptic area requires PMCA activity.

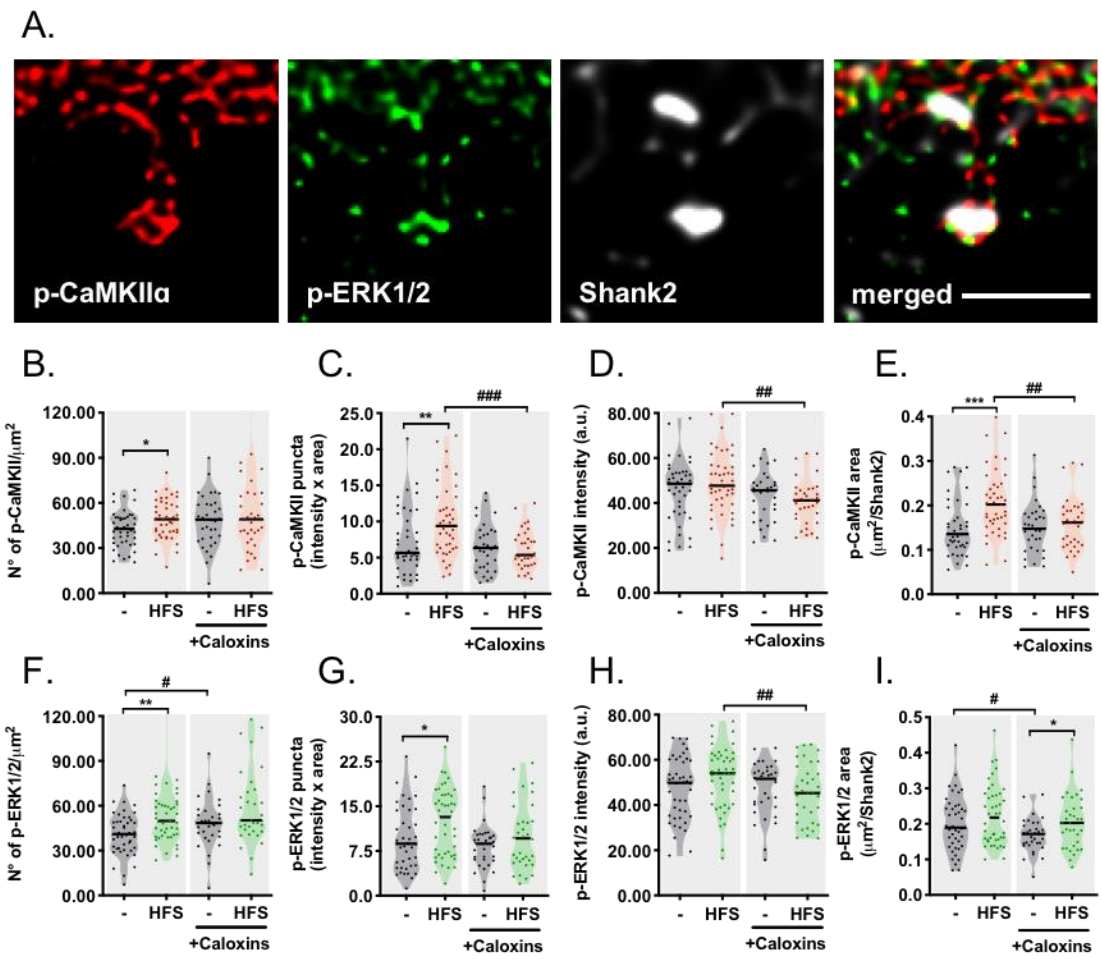

Figure 25. Failed synaptic activation of p-CaMKII and p-ERK1/2 in Caloxin-treated neurons. **A)** Hippocampal neurons (DIV 15-16) were silenced with TTX (0.1 μM) for 20 min and then pre-incubated with a cocktail of PMCA inhibitors (Caloxins, 20 μM) for another 10 min. Then, neurons were stimulated with HFS and five minutes after were fixed and stained with anti-pCaMKIIα (T286), anti-pERK1/2 (T202/Y204) and anti-Shank2 antibodies. For increased resolution, STED images were deconvolved with Huygens Professional 19.10 software. Scale bar is 1 μm. **B-I)** The graphs show the number of p-CaMKIIα and p-ERK1/2 clusters (**B** and **F**), puncta (intensity x area; **C** and **G**), intensity (**D** and **H**), and area (**E** and **I**). Shank2-positive puncta were used as region of interest. The data display violin plots with medians. n= 42 neurons for control, n= 43 neurons for HFS, n= 33 neurons for Caloxins and n= 33 neurons for Caloxins+HFS (three-four independent cultures). Unpaired t test *p<0.05, **p<0.01, ***p<0.001 between control vs HFS; $^{\#}$p<0.05, $^{\#\#}$p<0.01, $^{\#\#\#}$p<0.001 between with vs. without Caloxins.

4.5. Assessment of the effect of tumor necrosis factor on Ca^{2+} clearance.

Tumor-necrosis factor-alpha (TNF-α) is a pro-inflammatory cytokine shown to modulate synaptic scaling by increasing surface localization of AMPARs (Leonoudakis et al., 2004; Stellwagen et al., 2005) and synaptic plasticity through intracellular Ca^{2+} stores (Maggio &

Vlachos, 2018; Park et al., 2008). How exactly TNF-α modulates Ca^{2+} handling and plasticity under physiological and pathophysiological conditions is not fully understood yet. The potential effect of TNF-α on Ca^{2+} clearance was so far studied in neuronal soma upon Caffeine-mediated Ca^{2+} release from the endoplasmic reticulum (Park et al., 2008). However, neuronal soma differs from dendrites and spines in terms of Ca^{2+} handling (which will be further discussed in chapter 5.2.). Since TNF-α treatment alters network activity in neuronal cultures (Clarkson et al., 2017), I wondered whether TNF-α modulates Ca^{2+} clearance in dendrites and spines during different neuronal activity. RFPT-GCaMP5-transfected hippocampal neurons were treated with TNF-α (1ng/ml) for 24 h and then the GCaMP5-reported Ca^{2+} transients occurring due to synaptically driven intrinsic spontaneous network activity were recorded in a free-run mode. Offline quantification of decay time, half-width, peak amplitude and rise time in dendrites and spines served as a read out of Ca^{2+} restoration (Fig. 26). Interestingly, TNF-α treatment led to a significant delay in decay time compared to control in both dendrites and spines (Fig. 26A; dendrites: control: 0.9667 ± 0.03229 vs TNF-α: 1.564 ± 0.07917 and Fig. 26C; spines: control: 0.9737 ± 0.02885 vs TNF-α: 1.283 ± 0.03974). Half-width was also increased in dendrites and spines of TNF-α-treated neurons compared to control (Fig. 26B; dendrites: control: 0.9685 ± 0.03816 vs TNF-α: 1.375 ± 0.08369 and Fig. 26D; spines: control: 0.9688 ± 0.02955 vs TNF-α: 1.351 ± 0.06053). More interestingly, TNF-α treatment led to a decrease in peak amplitude compared to control in both dendrites and spines (Fig. 26E; dendrites: control: 1,000 ± 0,05081 vs. TNF-α: 0,7949 ± 0,08005 and Fig. 26G; spines: control: 1,000 ± 0,03506 vs TNF-α: 0,9654 ± 0,06407). Rise time was also increased in dendrites and spines of TNF-α-treated neurons compared to control (Fig. 26F; dendrites: control: 0,9727 ± 0,06745 vs. TNF-α: 1,227 ± 0,1005 and Fig. 26H; spines: control: 1,000 ± 0,05200 vs TNF-α: 1,299 ± 0,06163). Thus, TNF-α treatment strongly alters Ca^{2+} transients in dendrites and spines of neurons ongoing spontaneous neuronal activity.

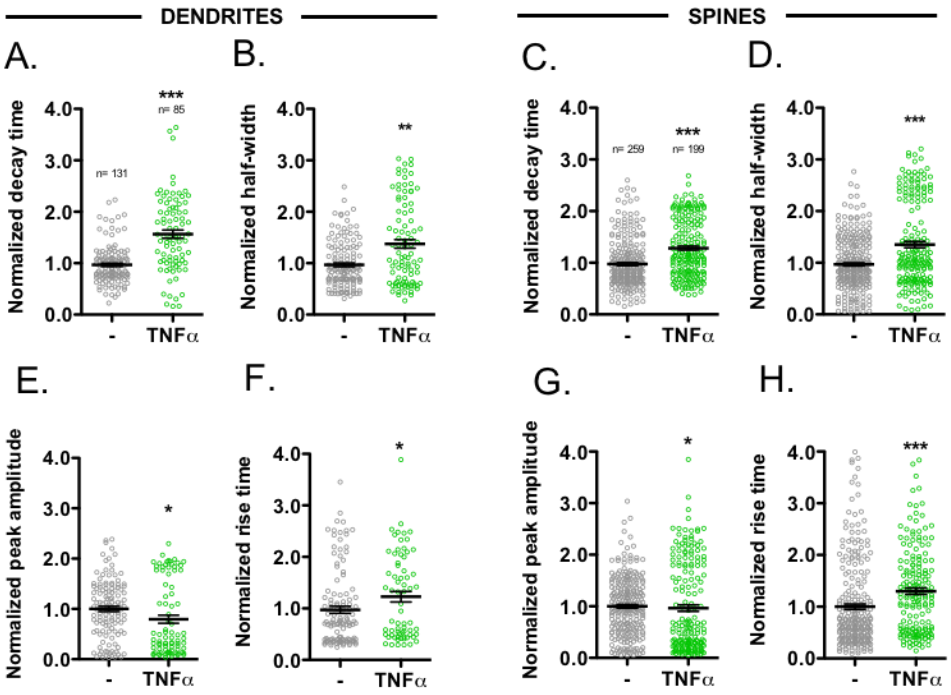

Figure 26. Tumor necrosis factor (TNF)-α alters the restoration of spontaneous Ca^{2+} transients in active neurons. A-B) Hippocampal neurons were transfected at DIV 11 with RFPT-GCaMP5. Transfected neurons were treated with TNF-α (1ng/ml) for 24 h before recording. Calcium imaging was performed at DIV 14-15 in Tyrodes buffer. Calcium kinetics as spontaneous activity were quantified. Normalized decay time (**A** and **C**), half-width (**B** and **D**), peak amplitude (**E** and **G**) and rise time (**F** and **H**) are presented as graphs. Data is shown as the mean±SEM (n values indicate the number of events that were analyzed). n= 9 neurons for control and n= 9 neurons for TNF-α (two independent cultures per condition). Mann-Whitney U test *p<0.05, **p<0.01, ***p<0.001 vs control (gray circles).

Next, I investigated the effect of TNF-α treatment on HFS-induced Ca^{2+} transients in dendrites and spines of RFPT-GCaMP5-transfected neurons. Representative fluorescent traces of neurons treated or untreated with TNFα are shown (Fig. 27A-C). Quantification of the Ca^{2+} transients triggered by HFS revealed that TNF-α treatment led to a slower Ca^{2+} restoration by increasing decay time in dendrites and spines (Fig. 27D; control: 1.000 ± 0.04280 vs TNF-α: 1.820 ± 0.1080 and Fig. 27F; control: 0.9800 ± 0.02823 vs TNF-α: 1.811 ± 0.06934). Half-width was also increased upon TNF-α treatment compared to control in dendrites and spines (Fig. 27E; control: 1.000 ± 0.02757 vs TNF-α: 1.342 ± 0.06229 and Fig. 27G; control: 1.000 ± 0.02091 vs TNF-α: 1.423 ± 0.04281). Interestingly, peak amplitude was not influenced by TNF-α treatment (Fig. 27H; control: 1.000 ± 0.1051 vs TNF-α: 1.001 ± 0.09201 and Fig. 27J; control: 1.000 ± 0.06757 vs TNF-α: 0.9719 ± 0.04726). Compared to control, TNF-α treatment resulted in a decreased rise time in dendrites and spines (Fig. 27I;

control: 0.9759 ± 0.06082 vs TNF-α: 0.6079 ± 0.04907 and Fig. 27K; control: 0.9630 ± 0.04768 vs TNF-α: 0.5258 ± 0.03121). Overall, treatment of neurons with TNF-α for 24 h altered the restoration of HFS-induced Ca^{2+} transients. As a comparison, TNF-α treatment resulted in a significant delay in Ca^{2+} clearance during spontaneous activity (Fig. 26A, B, C and D) and upon HFS (Fig. 27D, E, F and G). These results show that TNF-α modulates Ca^{2+} restoration during low and high neuronal activity. Considering the differences in peak amplitude and rise time upon TNF-α treatment during spontaneous activity (Fig. 26E, F, G and H) and high neuronal activity evoked by HFS (Fig. 27H, I, J and K), different Ca^{2+} sources seem to involve in TNF-α-mediated Ca^{2+} handling.

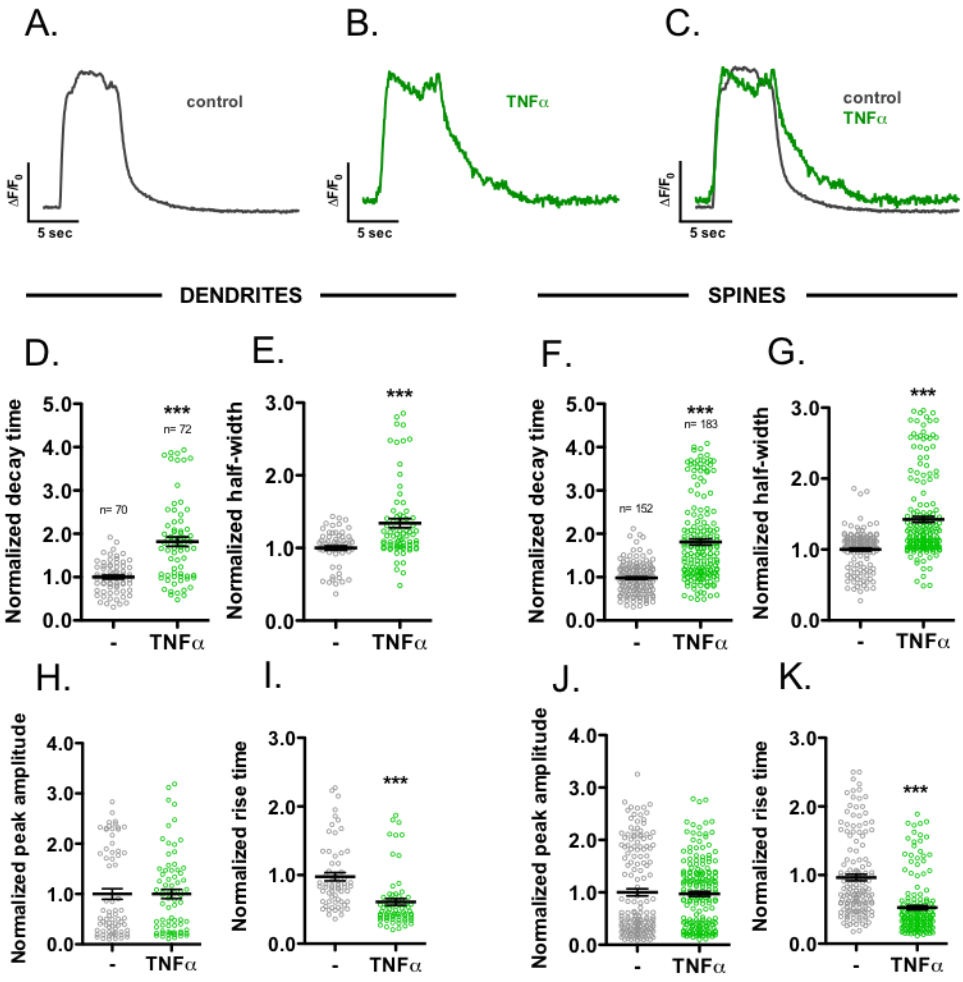

Figure 27. Tumor necrosis factor (TNF)-α alters the restoration of HFS-induced Ca^{2+} transients in neurons. Hippocampal neurons were transfected at DIV 11 with RFPT-GCaMP5 and were treated with TNF-α (1ng/ml) for 24 h before recording. Calcium imaging was performed at DIV 14-15 in Tyrodes buffer. Representative traces of Ca^{2+} transients from neurons treated or untreated with TNFα are shown (**A-C**). Calcium transients were triggered using HFS protocol ((40 AP, 80 Hz) x8). Normalized decay time (**D** and **F**), half-width (**E** and **G**), peak amplitude (**H** and **J**) and rise time (**I** and **K**) are presented as graphs. Data is shown as the mean±SEM (n values

indicate the number of dendrites and spines that were analyzed). n= 14 neurons for control and n= 14 neurons for TNF-α (three independent cultures). Mann-Whitney U test *p<0.05, **p<0.01, ***p<0.001 vs control (gray circles).

As TNF-α treatment led to a slower Ca^{2+} restoration, I wondered whether this delay is related to the altered levels of PMCA-Neuroplastin complexes and thus, the protein levels of PMCA and Neuroplastin following TNF-α treatment were evaluated. For this, cortical neurons were treated with TNF-α (1ng/ml) for 1 h, 6 h, 12 h, 24 h and 48 h and then, samples were harvested and immunoblotted with anti-panPMCA, anti-Neuroplastins and anti-β-III tubulin antibodies (Fig. 28A). Normalized PMCA and Neuroplastin levels revealed that TNF-α treatment did not affect their protein levels regardless of incubation time (Fig. 28B; PMCA levels: control: 1.000 ± 0.000; 1h: 1.160 ± 0.1356; 6h: 1.401 ± 0.2378; 12h: 1.262 ± 0.1618; 24h: 1.188 ± 0.2012; 48h: 1.260 ± 0.2145; Neuroplastin levels: control: 1.000 ± 0.000; 1h: 0.9161 ± 0.1199; 6h: 1.050 ± 0.2281; 12h: 0.9467 ± 0.1473; 24h: 0.9035 ± 0.1752; 48h: 0.7618 ± 0.1380). These data indicate that TNF-α treatment alters Ca^{2+} restoration without affecting the levels of Neuroplastin-PMCA complexes in neurons. TNF-α may be participating in Ca^{2+} restoration via intracellular Ca^{2+} stores as suggested by Maggio and Vlachos (2018).

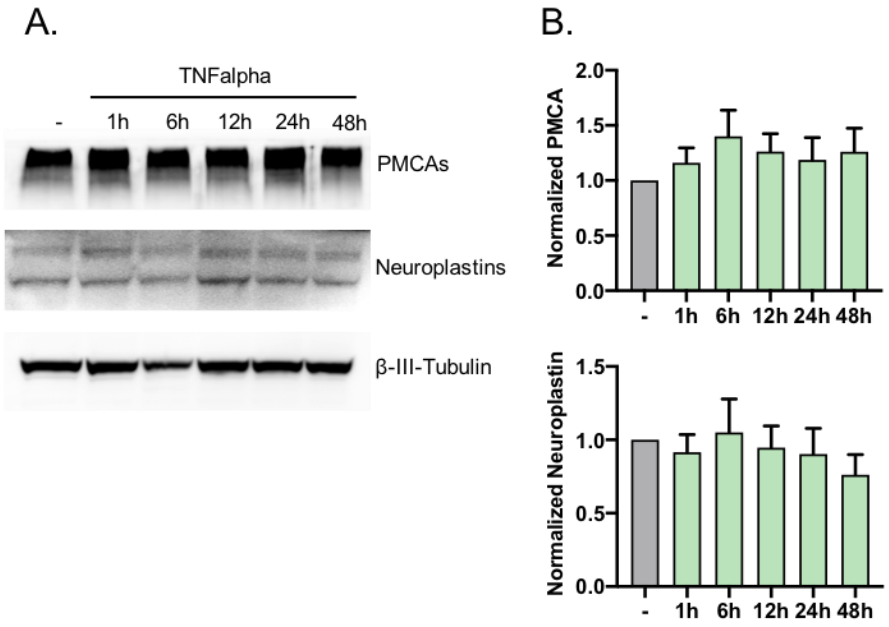

Figure 28. Tumor necrosis factor (TNF-α) does not alter PMCA nor Neuroplastin levels in neurons. A) Cortical neurons were treated at DIV 16 with TNFα (1ng/ml) for indicated time points and harvested. Immunoblotting was performed with panPMCA, neuroplastin and β-III tubulin antibodies as shown. **B)** The graphs display the normalized values correspond to mean±SEM from four independent cultures.

5. Discussion

In the present study, I have investigated the role of PMCA and Neuroplastin in Ca^{2+} clearance in dendrites and spines of primary hippocampal neurons *in vitro*. This function was characterized for Ca^{2+} transients evoked either by spontaneous intrinsic activity or upon electrical stimulation at different frequencies and dissected using pharmacological, genetic, and biochemical approaches. Of particular interest was the use of a high-frequency stimulation (HFS) protocol Harvey, Ehrhardt, et al. (2008) to trigger morphological changes of spines *in vitro* as shown here, recapitulating structural changes of spines associated to synaptic plasticity *ex vivo* and *in vivo* as shown by others (Kasahara et al., 2001; Papatheodoropoulos & Kouvaros, 2016; Riquelme et al., 2011).

A key finding of this thesis is that the function of PMCA-Neuroplastin complexes in Ca^{2+} extrusion is modulated by the activation of ionotropic glutamate receptors (NMDAR and/or AMPAR), constituting a novel functional link to regulate Ca^{2+} homeostasis in glutamatergic synapses. Another important finding is that NMDAR function is required to remodel the abundancy of PMCA-Neuroplastin complexes induced by HFS in postsynaptic areas. Furthermore, the activity of PMCA was found to fine-tune the activation of CaMKIIα and ERK1/2 induced by HFS. As PMCA was found significantly decreased, the ratio between GluN2A-containing NMDAR and GluN2B-containing NMDAR was altered and p-EKR1/2 was strongly elevated in the hippocampus of Neuroplastin-deficient mutant mice, it is very likely that the alterations of these regulatory mechanisms of Ca^{2+} clearance and signaling by these molecules contribute to the impaired hippocampal plasticity and the deficits in hippocampus-dependent learning and memory in the Neuroplastin-deficient mutant mice.

5.1. Use of HFS to study Ca^{2+} regulation, signaling and plasticity in cultured neurons

Synaptic plasticity includes modifications of the synaptic proteome and synaptic strength leading to flexibility and adaptivity of memory storage and its retrieval. Structural plasticity shows a wide range of pruning and generation of synapses and remodeling of axons and dendrites (Knoblauch & Sommer, 2016). Postsynaptic spines, small specializations growing on dendrites, are traditionally studied to understand structural dynamics of synapses. Their plasticity is known to be orchestrated by activity-dependent regulation of transcriptional and also translational organization of molecular organizers (Grutzendler et al., 2002; Holtmaat et al., 2005). LTP induction was shown to significantly increase spine volumes in hippocampal CA1 pyramidal neurons (Matsuzaki et al., 2004) whereas LTD causes spine retractions and shrinkage in CA1 pyramidal neurons from organotypic slice cultures (Nagerl et al., 2004). In this thesis, I used a previously published HFS protocol (Harvey, Ehrhardt, et al., 2008) to trigger structural modifications of spines in cultured neurons as similarly achieved by

comparable protocols (Papatheodoropoulos & Kouvaros, 2016; Riquelme et al., 2011; Smalla et al., 2000). In neurons, which were fixed 30 min after HFS, I found an increase in length, width, and the number of spines compared to unstimulated controls (Fig. 7). This result coincides with previous publications showing spine enlargement following various stimulation protocols such as chemically induced LTP (Kopec et al., 2006), tetanic stimulation (100 Hz for 1 s) (Lang et al., 2004) or two-photon glutamate uncaging (Matsuzaki et al., 2004). Molecular pathways, which are responsible for spine enlargement comprise synaptic insertion of additional AMPAR (Kopec et al., 2006), NMDAR-mediated Ca^{2+} influx, Calmodulin and CaMKIIα activation, as well as ERK1/2 activation, and enhanced actin polymerization (Alonso et al., 2004; Fischer et al., 2000; Fukazawa et al., 2003; Lang et al., 2004; Matsuzaki et al., 2004). Indeed, here I found that HFS is effective to promote a sustained and substantial activation of ERK1/2 in cultured hippocampal neurons (Fig. 24 and 25). An obvious limitation of my method was imaging of fixed samples. Monitoring spine enlargement in living neurons allows to follow rapid and dynamic changes simultaneously (Harvey, Yasuda, et al., 2008). In addition to my findings from fixed neurons, generation of new spines or growth of persisting spines in living neurons as shown by other studies could also be evaluated in the future (Nagerl et al., 2004). The second limitation was the application of an electrical field stimulation, which stimulates all neurons cultured together on the same coverslip. Besides numerous advantages of field stimulation, for instance, easy practical application, successful stimulation of neuronal populations and generation of network activity, the evident drawback is a lack of isolating post-synaptic stimulation. The use of an advanced imaging technique of two-photon microscopy coupled with glutamate uncaging could be a way to monitor structural plasticity of post-synaptic spines (Matsuzaki et al., 2004; Sun et al., 2019).

Neuroplastin is noted as an essential interaction partner of PMCA (Herrera-Molina et al., 2017; Korthals et al., 2017; Schmidt et al., 2017). Because we have recently shown that Neuroplastin does not depend on PMCA function to promote spine formation in young neurons (Vemula*, Malci* et al., 2020), I became interested in whether PMCA-Neuroplastin complexes play a more important role in mature neurons (DIV 14-16). In Neuroplastin65-overexpressing mature neurons, I found increased PMCA levels in dendrites and spines (Fig. 8). Likewise, Neuroplastin55 is also capable of increasing PMCA levels in neurons and HEK cells by forming stable plasma membrane-associated assemblies (Xiao Lin, submitted doctoral thesis). This is explained by the fact that the transmembrane domain of Neuroplastin is sufficient to bind and stabilize PMCA at the plasma membrane. Moreover, we have previously reported that Neuroplastin65-GFP overexpression increased PMCA levels in hippocampal neurons at DIV 9 and PMCA2 levels in HEK cells (Vemula*, Malci* et al., 2020). Apparently, Neuroplastin enables PMCA recruitment in both young and mature neurons, but

PMCA functions may differ during development and may become highly relevant for plasticity in later stages of development. In fact, mRNA transcripts of all PMCA isoforms (PMCA1-4) increase during the first two weeks of development in rat hippocampus, and the protein levels stay abundant thereafter (Kip et al., 2006). Similar to their protein expression, PMCA-mediated Ca^{2+}-ATPase activity also increases during the postnatal development in mouse brain (Marcos et al., 2009). Overall, Neuroplastin-mediated recruitment of PMCAs to the plasma membrane further supports their strong association and the functional relevance of this recruitment will be discussed in following chapters of this thesis.

5.2. PMCA-Neuroplastin complexes are essential regulators of Ca^{2+} extrusion in dendrites and spines

In the present study, I have investigated the role of PMCA-Neuroplastin complexes in Ca^{2+} clearance by focusing on dendrites and spines. A large number of molecular participants is involved in the fine-tuning of intracellular Ca^{2+} concentration in the post-synaptic area. While mechanisms of post-synaptic Ca^{2+} influx through activation of different Ca^{2+} sources have been well explored, the Ca^{2+} extrusion mechanisms were not elaborated over years. In the past, NCX was thought to remove most of the cytoplasmic Ca^{2+}, but PMCA has attracted attention with its remarkable capacity to pump the excess of Ca^{2+} out of the cell until full restoration of basal levels. Compared to NCX, PMCA as an ATPase pump has relatively higher affinity to Ca^{2+} but lower transport capacity (Carafoli et al., 2001). However, its high affinity to Ca^{2+} (Kd < 0.5 µM) gives PMCA an efficient pumping capacity even in the resting state during the level of free Ca^{2+} in the cytosol is in the range of 0.05-0.1 µM (Sibarov & Antonov, 2018). Indeed, reduced levels of PMCA in the absence of Neuroplastin results in a delay in Ca^{2+} clearance and an elevated intracellular Ca^{2+} levels in neurons and T cells (Herrera-Molina et al., 2017; Korthals et al., 2017; Schmidt et al., 2017). However, these recent findings are based on calcium imaging experiments in neuronal somata (Herrera-Molina et al., 2017; Schmidt et al., 2017). Most of excitatory signaling takes place at dendritic spines and they functionally differ from the soma. Compared to the soma, dendrites and spines are either lacking or having less intracellular structures like mitochondria and the ER. Spines, especially the classical mushroom-shaped dendritic spines, are considered as an isolated signaling compartment with a narrow neck, which creates a significant barrier against diffusion of ions. Therefore, spines operate their independent signaling machinery and maintain biochemical and electrical signals in the spine head (Bloodgood et al., 2009; Grunditz et al., 2008; Sabatini et al., 2002; Svoboda et al., 1996; Yuste & Denk, 1995). Specialized form of the ER called spine apparatus (SA) serves calcium deposits in the dendritic spines (Segal & Korkotian, 2014). SA is a dynamic subcellular structure, which enters and leaves spines spatiotemporally and existence of SA participates in synaptic

plasticity (Breit et al., 2018). Proteomics analysis revealed a significant reduction (46%) of synaptopodin, a marker for SA, in soluble protein fraction (with 0,5% Triton X-100) from Neuroplastin-deficient mice (unpublished data from Dr. Karl-Heinz Smalla). Therefore, investigating the role of PMCA-Neuroplastin complexes in Ca^{2+} clearance particularly in dendritic spines was important in my thesis.

I used the genetically encoded biosensor GCaMP5 and applied HFS which is known to generate high neuronal firing and to induce LTP. In TTX-silenced neurons, HFS increased fluorescence intensity of GCaMP5 in the cytoplasm, likely due to depolarization-induced Ca^{2+} influx and release from intracellular stores, and returned to baseline levels. Pharmacological inhibition of PMCA with Carboxyeosin (Choi & Eisner, 1999; Gatto & Milanick, 1993) resulted in a slower Ca^{2+} clearance in both dendrites and spines showing the importance of PMCA for dendritic and synaptic Ca^{2+} extrusion (Fig. 9). Along this line, Neuroplastin65 overexpression accelerated Ca^{2+} clearance (Fig. 9 and 10), which may be explained with an enhanced recruitment of PMCA to the plasma membrane by Neuroplastin65 shown in Figure 8. In the future, as an alternative strategy to pharmacology and overexpression, a knockdown approach of PMCA or Neuroplastin expression with siRNA or shRNA could be used to study the function of PMCA-Neuroplastin complexes.

Ca^{2+} extrusion mechanisms vary depending on different patterns of neuronal activity. PMCA was suggested to handle Ca^{2+} extrusion at a wide of range of cytosolic Ca^{2+} levels while others like NCX or Ca^{2+} uptake into intracellular stores via MCU and SERCA only contribute to removal of Ca^{2+} from the cytoplasm at relatively higher levels of activity (Chamberland et al., 2019). Here, I showed faster Ca^{2+} removal from the cytoplasm in Neuroplastin65-overexpressing neurons by recording spontaneous activity (Fig. 10). This indicates that the contribution of PMCA-Neuroplastin complexes to Ca^{2+} extrusion takes place not only during evoked activity by HFS but also upon spontaneous activity. Furthermore, PMCA activity triggered by 5-10 APs slows down Ca^{2+} clearance (Fig. 16) and this is independent from NCX (Fig. 18). Therefore, PMCA together with its interaction partner Neuroplastin seems to be an essential regulator of Ca^{2+} extrusion in dendrites and spines.

GCaMPs are calmodulin-based genetically encoded fluorescent calcium indicators (GECIs) and widely used for imaging calcium dynamics. While they have high Ca^{2+} affinity, some of them possess slow kinetics, what may make it complicated to follow fast kinetics. The development of ultrafast variants of GCaMP6f, GCaMP7f and recently GCaMP8f allows to monitor rapid intracellular Ca^{2+} dynamics (Chen et al., 2013; Dana et al., 2019). However, there is a debate on GECIs having a possibility to interfere with Ca^{2+} homeostasis and signaling pathways required for neuronal differentiation. Recently, several GCaMPs were

tested and some of them were shown to impair dendritic morphology after prolonged-expression (Gasterstadt et al., 2020). Compared to GCaMP3, GCaMP5G used in this study (Akerboom et al., 2012) was found to be relatively “neuron-friendly”. Additionally, I tested the synthetic Ca^{2+} dye Oregon Green BAPTA-1 (OGB-1) to compare with the use of GCaMP5G. Consistent with my CGaMP5G experiments, I found that PMCA contributes to HFS-induced neuronal activity when neurons were loaded with OGB-1 (Fig. 17). However, I observed that OGB-1 emits relatively dim fluorescence signal, which makes following Ca^{2+} transients in spines more difficult. In addition, OGB-1 shows slower kinetics compared to GCaMP5G suggesting use of GCaMPs is good tools for Ca^{2+} imaging performed in this study.

5.3. Functional link between PMCA-Neuroplastin complexes and NMDAR

In this thesis, I checked the expression of PMCA and NMDAR subunits in wild-type and Neuroplastin-deficient mice model focusing on the hippocampus (Fig. 11). In the constitutive Neuroplastin knockout mice (*Nptn*$^{-/-}$), I showed almost 54% less PMCA in agreement with literature (Bhattacharya et al., 2017; Herrera-Molina et al., 2017) and 30% less GluN2A-containing NMDAR, whereas GluN2B-containing NMDAR levels did not change. The decreased PMCA levels confirm the previous studies discovering the reduced PMCA expression in the absence of Neuroplastin (Bhattacharya et al., 2017; Herrera-Molina et al., 2017). Region-specific changes in PMCA isoform levels were shown in cortex and hippocampus of animals lacking Neuroplastin in glutamatergic neurons (Herrera-Molina et al., 2017). Moreover, transcript levels of PMCA isoforms were shown unaltered by the absence of Neuroplastin suggesting a complex post-transcriptional regulation of PMCA isoforms (Herrera-Molina et al., 2017). Overall, the altered level of GluN2A-containing NMDAR is an interesting finding. Most NMDARs contain two obligate GluN1 subunits and two GluN2 subunits and GluN2A takes the place of GluN2B during forebrain development (McKay et al., 2018). Since these homogenates were collected from the hippocampus of adult mice, GluN2A subunit is expected to be more abundant than GluN2B and likely to be influenced in the absence of Neuroplastin together with reduced levels of PMCA. Xiao Lin at the LIN has checked forebrain homogenates from wild-type and *Nptn*$^{-/-}$ mice and found no change in the levels of several synapse-associated proteins including PSD-95, vesicular glutamate transporter 1 and 2 (VGLUT1 and VGLUT2) and the synaptosomal-associated protein 25 (SNAP25) and others (Xiao Lin, submitted doctoral thesis). On the other hand, a study using another mouse model lacking Neuroplastin65 showed an increased level of GluN2A-containing NMDAR and unaltered level of GluN2B-containing NMDAR in the forebrain (Amuti et al., 2016). In fact, altered levels of GluN2A-containing NMDAR and no

change in GluN2B-containing NMDAR level in this study seems to be specific to Neuroplastin expression and consistent with their developmental switch.

Subcellular localization of PMCA2 and PMCA3 was found at highest levels within synaptic profiles of cerebellar cortex, PMCA2 was postsynaptic and PMCA3 was presynaptic (Burette & Weinberg, 2007). The presence of PMCA2 was shown at presynaptic active zones (Burette et al., 2009) and PSDs (Burette et al., 2010) by using immuno-electron microscopy. PMCA1 was also detected at presynaptic terminals of cultured hippocampal neurons (Ono et al., 2019). PMCA2a is selectively enriched in forebrain synaptosomes (Jensen et al., 2007). Earlier, by using cell fractionation and biochemistry, both Neuroplastins were shown in synaptic membrane protein fractions (Hill et al., 1988; Smalla et al., 2000), particularly Neuroplastin65 were found in the postsynaptic density preparation (Langnaese et al., 1997; Smalla et al., 2000). To my knowledge, there is no study showing PMCA and Neuroplastin together in intact synapses by using advanced microscopy and image processing techniques. Here, I used super resolution STED microscopy and image deconvolution, which provide a resolution around 60 nm to show synaptic localization of PMCA, Neuroplastin and GluN2A-containing NMDAR in Shank2-positive post-synaptic areas. Indeed, the three of them are present within Shank2-positive areas (Fig. 12). PMCA and Neuroplastin localize in a close proximity with a very high Pearson colocalization coefficient and in short distance (Fig. 13). These data support direct interaction between PMCA and Neuroplastin. PMCA and GluN2A-containing NMDAR localize at a distance with a very low Pearson colocalization coefficient and longer distance between them (Fig. 13). This is comprehensible and coherent as their interaction may happen indirectly via PSD-95 (Garside et al., 2009). Once synaptic localization of these three proteins was challenged by HFS, more PMCA and Neuroplastin were recruited to the synapse while the presence of GluN2A-containing NMDAR did not change upon HFS within the observed time window. Visualization of synaptic recruitment of PMCA-Neuroplastin complexes further contributes to explain why Neuroplastin65 overexpressing neurons accelerate Ca^{2+} clearance in spines. Immobility of GluN2A-containing NMDAR is consistent with a previous study showing that synaptic localization of GluN2A-containing NMDAR was unchanged upon chemical LTP, whereas GluN2B-containing NMDAR was dynamically removed and laterally diffused in immature neurons (Dupuis et al., 2014). The activity-dependent lateral diffusion of GluN2B-containing NMDAR is regulated by CaMKII and casein kinase II activity and required a direct binding of CaMKII to GluN2B (Dupuis et al., 2014; McKay et al., 2018). Immobility of GluN2A-containing NMDAR and high mobility of GluN2B-containing NMDAR may explain how glutamatergic synapses rapidly re-arrange their synaptic GluN2A/GluN2B ratio during activity-dependent metaplasticity. On the other hand, synaptic localization of PMCA and Neuroplastin, but not GluN2A-containing NMDAR, seems to be regulated by the activity of glutamate receptors

and PMCA itself. HFS-induced synaptic recruitment of PMCA-Neuroplastin complexes was not observed in the presence of APV and CNQX or Caloxins (Fig. 14). The mobility of PMCA-Neuroplastin complexes may require NMDAR-mediated synaptic transmission and/or Ca^{2+} signaling. For a better understanding of how synaptic localization of PMCA-Neuroplastin complexes is dynamically regulated by HFS or glutamate receptor activity, high-resolution and high-speed single nanoparticle imaging shall be used with luminescent nanoparticles like quantum dots instead of fixed cell imaging.

Here, I evidently showed a functional link between PMCA-Neuroplastin complexes and ionotropic glutamate receptors by using live-cell calcium imaging and monitoring Ca^{2+} changes evoked with 5-10 APs or HFS. In the presence of APV and CNQX, PMCA inhibition decelerated Ca^{2+} extrusion leastwise with a mild effect on decay time and no effect on half-width. When NMDAR and AMPAR were operating, PMCA inhibition caused a significantly increased decay time with 65% change in dendrites and 44% change in spines of TTX-silenced neurons (Fig. 9). However, this change was only 29% in dendrites and 14% in spines when APV and CNQX were added (Fig. 20, without TTX). Blocking glutamate receptor activity itself reduced decay time and half-width and this could be due to blocked Ca^{2+} entry via ionotropic glutamate receptors (Fig. 20). Interestingly, PMCA inhibition (Fig. 19) or Neuroplastin65 overexpression (Fig. 21) did not affect Ca^{2+} clearance in the presence of APV and CNQX when test pulses were applied. When neuronal activity was challenged with HFS, then the effect was even opposite to Figure 9 with a surprisingly increased decay time and unaltered half-width (Fig. 20). These data suggest that PMCA-Neuroplastin complexes require glutamate receptor activity to operate Ca^{2+} clearance fully and on time. Even though there are increased PMCA levels in Neuroplastin65 overexpressing neurons, the function of PMCA-Neuroplastin complexes seems to essentially demand on proper activity of glutamate receptors. In addition, HFS-induced rapid recruitment of PMCA-Neuroplastin complexes to the synapse was lacking when NMDAR and AMPAR were blocked in my STED experiments. Altogether not only localization but also function of PMCA-Neuroplastin complexes is sensitive to activity of NMDAR and AMPAR.

Particularly in experiments with APV and CNQX, the results in dendrites and spines behave quite similar, what might be due to the diffused distribution of VGCC overall in spines and dendrites. Therefore, I tested for a potential compensatory role of L-type VGCC and NCX in the link between PMCA-Neuroplastin complexes and glutamate receptors. While APV and CNQX resulted in faster Ca^{2+} clearance upon HFS as expected, interestingly PMCA inhibition also caused faster Ca^{2+} clearance (Fig. 22). First, it is plausible to think of the ER compensating cytosolic Ca^{2+} levels. While the ER has a heterogeneous distribution in CA1 dendritic spines, it was observed in approximately 50% of dendritic spines in cultured mouse

hippocampal neurons (Ng et al., 2014). The synaptic activation of NMDAR leads to rapid changes in the ER content of dendritic spines. Both ER dynamics and expansion are promoted by NMDAR activation (Ng et al., 2014). In their study, treatment of neurons with the NMDAR antagonist L689,560 resulted in smaller spines and decreased ER volume. The ER is known to rapidly and locally contribute to synaptic plasticity, supporting the microdomain hypothesis of Ca^{2+} handling. In spines containing ER, calcium influx through NMDARs was compensated by large calcium release events inducing plasticity (Holbro et al., 2009). According to Mahajan and Nadkarni, ER Ca^{2+} release via IP_3R modulates NMDAR-dependent plasticity by promoting synaptic depression (LTD) (Mahajan & Nadkarni, 2019). This must be important to counterbalance the Ca^{2+} homeostasis. And ER Ca^{2+} release via IP_3R is thought to be activated by metabotropic glutamate receptors (Mahajan & Nadkarni, 2019). Overall, interpreting the changes in decay time with or without APV and CNQX in Figure 21, in fact NMDAR activity-related ER content might be an explanation. For instance, how Caloxins alter decay time in the absence and presence of APV and CNQX can be explained with ER volume in the spine (Ng et al., 2014). However, whether the mechanism is an uptake or release of Ca^{2+} via ER has to be investigated. Second, there are also R-type VGCC in hippocampal spines responsible for Ca^{2+} entry. They are probably the least known class of VGCC. However, their local contribution to Ca^{2+} signaling strongly supports the hypothesis that the spine is compartmentalized into functionally independent Ca^{2+} microdomains (Bloodgood & Sabatini, 2007a, 2007b; Evans & Blackwell, 2015; Higley & Sabatini, 2012). Calcium microdomains near R-type VGCC were shown to activate calcium-activated potassium channels (SK channels) and regulate the induction of postsynaptic hippocampal LTP (Bloodgood & Sabatini, 2007b). Therefore, Ca^{2+} entry via R-type VGCC could be also involved in my experiments.

A potential mechanistic link between PMCA and NMDAR could be phospholipase Cγ (PLCγ) and phosphatidylinositol-4,5-bisphosphate (PIP_2). Proteomic analysis detected PLCγ and NMDAR complexes in synaptic preparations (Husi et al., 2000). PLCγ catalyzes the hydrolysis of PIP_2 into IP_3 and diacylglycerol (DAG). PIP_2 supports NMDAR activity by regulating the interaction with alpha-actinin (Michailidis et al., 2007). Via DAG, PKC activation enhances NMDAR currents in neurons (MacDonald et al., 2001) and in *Xenopus laevis* oocytes (Lan et al., 2001). Besides PMCA activation via Ca^{2+}-CaM, the activity of PMCA is also increased by acidic lipids, for instance PIP_2 are required for their activation (Choquette et al., 1984). PMCAs protect PIP_2 in the plasma membrane from hydrolysis by PLCγ and reduce levels of IP_3 (Penniston et al., 2014). Whether PLCγ-linked PIP_2 is the mechanism linking NMDAR and PMCA has to be investigated.

5.4. ERK1/2 and CaMKIIα are modulated by PMCA-Neuroplastin complexes

Many different protein kinases and phosphatases are essentially involved in LTP as protein phosphorylation and dephosphorylation are fundamentally required, for example, for the regulation of the function of neurotransmitter receptors. Activation of CaMKII and MAPK during LTP has been extensively investigated (Fukunaga et al., 2000; Liu et al., 1999; Selcher et al., 2003). In particular, ERK signaling seems to have a pivotal role in neuronal plasticity-regulated transcriptional events, regulation of synaptic plasticity (Selcher et al., 2003) and AMPAR insertion and transmission (Zhu et al., 2002). In addition to ERK, CaMKIIα also serves synaptic transmission as both AMPARs and NMDARs laterally relocate to the perisynaptic compartment via a CaMKII-dependent process shortly after induction of LTP (Dupuis et al., 2014; Groc & Choquet, 2020). AMPAR- and NMDAR-dependent hippocampal synaptic transmission requires CaMKIIα but not CaMKIIβ (Incontro et al., 2018). Also, CaMKII is required for synaptic recruitment of AMPAR during development (Opazo et al., 2010). To understand ERK function in synaptic plasticity, here I studied how ERK activity changes following application of HFS. I confirmed that HFS induces ERK1/2 activation in cultured hippocampal neurons (Fig. 24). This shows consistency with Kasahara *et al*., that shows activation of CaMKIV and ERK2 during LTP induction in the rat hippocampal CA1 region (Kasahara et al., 2001). Moreover, I showed that phosphorylation of ERK1/2 is dependent of Neuroplastin expression. In the hippocampus of Neuroplastin-deficient mice, I found an increased level of phosphorylated ERK1/2 whereas total levels of ERK1 did not change (Fig. 23). Elevated levels of p-ERK1/2 and p-CREB were also shown in the absence of Neuroplastin65 in mouse forebrain (Amuti et al., 2016). In order to extract phosphorylation events at the post-synapse, I showed synaptic localization of p-ERK1/2 and also p-CaMKIIα in Shank2-positive synaptic areas by using super resolution STED microscopy (Fig. 25). To do so, neurons were initially silenced with TTX to reduce high basal activity-dependent phosphorylation levels as previously shown with western blotting (Chandler et al., 2001). HFS increased phosphorylation levels of CaMKIIα and ERK1/2 at the synapse. Interestingly, this was not the case when PMCA was inhibited with Caloxins, suggesting that PMCA function is required for phosphorylation of CaMKIIα and ERK1/2. Moreover, PMCA inhibition itself increased the number and area or p-ERK1/2 clusters. This indicates that there may be a crosstalk between PMCA-controlled Ca^{2+} signaling and the ERK pathway. PMCA was shown to down-regulate ERK activation through interaction with RASSF1 and was suggested to modify the hypertrophic response in cardiomyopathy patients (Armesilla et al., 2004). However, the crosstalk between PMCA-mediated Ca^{2+} signaling and ERK pathway might be bidirectional. Expression of PMCA4 was down-regulated via MEK/ERK pathway in pulmonary arterial smooth muscle cells which is related to increased intracellular Ca^{2+}

concentrations in hypertension (Deng et al., 2021). A similar crosstalk was also shown in melanoma cells where PMCA4b expression was upregulated by the inhibition of the ERK pathway suggesting that ERK signaling is involved in regulation of PMCA expression (Hegedus et al., 2017). However, it is not known yet how PMCA-Neuroplastin complexes modulate downstream signaling and plasticity mechanisms. In order to monitor spatiotemporal dynamics of phosphorylation, biosensors for ERK or CaMKIIα activity shall be used to follow rapid activation upon Ca^{2+} oscillations in living cells (Ardestani et al., 2019; Harvey, Ehrhardt, et al., 2008; Tang & Yasuda, 2017). Upon phosphorylation, ERK is known to translocate into the nucleus where transcription is induced. In order to test whether PMCA-Neuroplastin-regulated Ca^{2+} signaling is associated with nuclear ERK activation, biosensors for nuclear ERK could be used (Zhai et al., 2013).

5.5. TNF-alpha treatment slows down Ca^{2+} clearance without altering levels of PMCA and Neuroplastin

In this study, I showed an effect of TNF-α treatment on Ca^{2+} restoration in dendrites and spines in cultured neurons. I found slower Ca^{2+} clearance in neurons treated with TNF-α (1ng/ml) for 24 h compared to control cells upon spontaneous activity (Fig. 26) and also evoked activity by HFS (Fig. 27). In addition to increased decay time and half-width, the reduced rise time indicates severely impaired intracellular Ca^{2+} rising affecting both dendrites and spines. Although there is a number of studies indicating TNF-α-induced AMPAR trafficking (Leonoudakis et al., 2004; Stellwagen et al., 2005), I found no change in the peak amplitude in TNF-α-treated neurons suggesting that TNF-α may modulate Ca^{2+} clearance without altering Ca^{2+} entry via glutamate receptors. Alternatively, intracellular store-mediated Ca^{2+} handling was previously suggested as a mechanism regulated by TNF-α (Park et al., 2008). However, it is not clear yet whether this is also the case upon HFS as the evidence from Park *et al.* was based on Caffeine-triggered Ca^{2+} release. HFS and Caffeine application are different stimuli from each other triggering various signaling pathways. On the other hand, whether TNF-α has an impact on PMCA-Neuroplastin complexes has to be elucidated. Whether Neuroplastin involves in neuroinflammation is not well explored yet. The interaction of Neuroplastin with the mesencephalic astrocyte-derived neurotrophic factor (MANF) was suggested to regulate suppression of inflammatory response via NF-κB signaling in HeLa and the glial C6 cells (Yagi et al., 2020). Neuroplastin was shown as S100A8/A9 receptor and necessary for cell proliferation and proinflammatory cytokine induction in skin lesions of chronic inflammation patients (Sakaguchi et al., 2016) and lung cancer cell lines (Sumardika et al., 2019). Here, I found that TNF-α treatment for varying time periods did not alter levels of PMCA and Neuroplastin in cultured neurons (Fig. 28). Previously PMCA and SERCA levels were shown as unchanged upon TNF-α treatment for 24 h (Park et al., 2008). Here, I

applied a treatment protocol ranging from 1 h up to 48 h and found no significant change in the expression levels of PMCA and Neuroplastin. Therefore, if TNF-α modulates Ca^{2+} clearance via PMCA-Neuroplastin complexes, this may rather be a functional impact without altering their expression levels. However, this hypothesis shall be experimentally proven by specifically focusing on PMCA function and using a direct experimental read-out such as measuring ATPase activity.

Could there be a link between Neuroplastin and TNF-α? TRAF6 is a prominent binding protein of TNF superfamily and involves in central nervous system diseases, such as stroke, neurodegenerative disease and neuropathic pain (Dou et al., 2018). In our previous work, we have shown that TRAF6 interacts with Neuroplastin during early neuronal developmental (Vemula*, Malci* et al., 2020). Could TRAF6 and Neuroplastin also be players in TNF-α-mediated Ca^{2+} signaling? We have previously detected high colocalization of TRAF6 and Neuroplastin in rat hippocampal neurons at DIV7 (Vemula*, Malci* et al., 2020). However, this interaction is restricted to an early time window and diminishes by DIV9. In mature neurons (DIV15-16), it is likely that TRAF6-Neuroplastin interaction is relatively weak under physiological conditions. Nevertheless, it needs to be investigated whether TRAF6 and Neuroplastin may be involved in TNF-α-related pathophysiological conditions.

5.6. Outlook

This study sheds new light on molecular mechanisms that contribute to PMCA-Neuroplastin-mediated synaptic plasticity in neurons. Considering the key findings in this thesis, I propose the following mechanism involving PMCA-Neuroplastin complexes during plasticity: Recently discovered PMCA-Neuroplastin complexes are present in dendrites and spines (Fig. 29A) and more Neuroplastin enables to recruit more PMCA to the plasma membrane (Fig. 29B). PMCA-Neuroplastin complexes are central players of Ca^{2+} clearance in dendrites and spines during basal and also potentiated synaptic transmission. Upon depolarization of the postsynaptic membrane, NMDAR are responsible for Ca^{2+} entry causing activity-dependent elevations in Ca^{2+} levels. At this point, PMCA-Neuroplastin complexes become even more important to counterbalance Ca^{2+} homeostasis. A key finding of this study is that PMCA-Neuroplastin complexes are in a close communication with NMDA- and/or AMPA-type glutamate receptors. However, this communication is possibly based on different levels of interactions and details such as whether it is NMDAR or AMPAR have to be further addressed. The crosstalk between PMCA-Neuroplastin complexes and ionotropic glutamate receptors serves a potential mechanism regulating synaptic plasticity via activation of Ca^{2+}-dependent signaling, namely ERK1/2 and CaMKIIα. However, the long-term outcome of PMCA-Neuroplastin-mediated activation of ERK1/2 and CaMKIIα needs to be studied in the

future. It will be interesting to investigate whether PMCA-Neuroplastin complexes not only regulate Ca^{2+} extrusion but also convey Ca^{2+} signals to modulate the nucleus for activity-dependent gene expression. Also, it would be interesting to evaluate how inflammatory conditions, for example promoted by TNF-α, affect Ca^{2+} restoration and to what extend this relates to PMCA-Neuroplastin function.

Overall, PMCA-Neuroplastin complexes act as moderators of Ca^{2+} levels, signaling and plasticity in neuronal dendrites and spines. Further studies will be needed to mechanistically explain the role of PMCA-Neuroplastin complexes in learning, memory and also disease-related cognitive or memory decline.

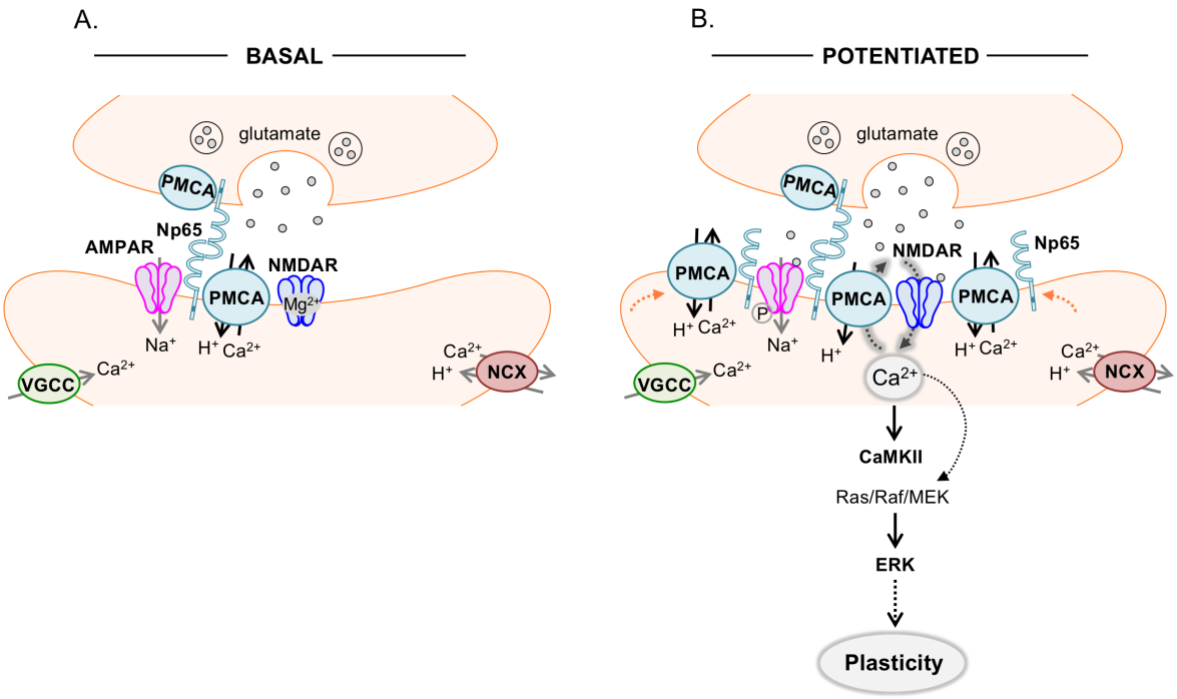

Figure 29. Proposed model for the role of PMCA-Neuroplastin complexes in Ca^{2+} clearance and signaling. A) During basal synaptic transmission, PMCA-Neuroplastin complexes are present in dendrites and spines and regulate Ca^{2+} clearance. Glutamate release from presynaptic terminals binds both the NMDAR and AMPARs and Na^{+} flows through only the AMPAR but not through the NMDAR due to the Mg^{2+} block. **B)** Upon depolarization of the postsynaptic membrane, the Mg^{2+} block of the NMDAR is removed and allows both Na^{+} and Ca^{2+} to flow into the dendritic spine. Upon potentiation, more Neuroplastin and PMCA recruits to the plasma membrane (indicated with orange dashed arrows). Then, PMCA-Neuroplastin complexes are in a close communication with NMDA- and AMPA-type glutamate receptors. Ca^{2+} clearance via PMCA requires NMDAR and AMPAR activity. The crosstalk between PMCA-Neuroplastin complexes and ionotropic glutamate receptors serves a potential mechanism regulating synaptic

plasticity via activation of downstream Ca^{2+}-dependent signaling cascades, namely ERK1/2 and CaMKIIα. Abbreviations: Np65 (Neuroplastin65), the voltage-gated Ca^{2+} channels (VGCCs), N-methyl-D-aspartate receptor (NMDAR), α-amino-3-hydroxy-5-methyl-4-isoxazolepropionic acid receptor (AMPAR), plasma membrane Ca^{2+} ATPase (PMCA), Na^{+}/Ca^{2+} exchangers (NCX). The diagram was created using Neuroscience-PPT-Toolkit-Suite (Copyright © motifolio.com).

6. Bibliography

Akerboom, J., Chen, T. W., Wardill, T. J., Tian, L., Marvin, J. S., Mutlu, S., Calderon, N. C., Esposti, F., Borghuis, B. G., Sun, X. R., Gordus, A., Orger, M. B., Portugues, R., Engert, F., Macklin, J. J., Filosa, A., Aggarwal, A., Kerr, R. A., Takagi, R., Kracun, S., Shigetomi, E., Khakh, B. S., Baier, H., Lagnado, L., Wang, S. S., Bargmann, C. I., Kimmel, B. E., Jayaraman, V., Svoboda, K., Kim, D. S., Schreiter, E. R., & Looger, L. L. (2012). Optimization of a GCaMP calcium indicator for neural activity imaging. *J Neurosci*, *32*(40), 13819-13840. https://doi.org/10.1523/JNEUROSCI.2601-12.2012

Albensi, B. C., & Mattson, M. P. (2000). Evidence for the involvement of TNF and NF-kappaB in hippocampal synaptic plasticity. *Synapse*, *35*(2), 151-159. https://doi.org/10.1002/(SICI)1098-2396(200002)35:2<151::AID-SYN8>3.0.CO;2-P

Alonso, M., Medina, J. H., & Pozzo-Miller, L. (2004). ERK1/2 activation is necessary for BDNF to increase dendritic spine density in hippocampal CA1 pyramidal neurons. *Learn Mem*, *11*(2), 172-178. https://doi.org/10.1101/lm.67804

Amuti, S., Tang, Y., Wu, S., Liu, L., Huang, L., Zhang, H., Li, H., Jiang, F., Wang, G., Liu, X., & Yuan, Q. (2016). Neuroplastin 65 mediates cognitive functions via excitatory/inhibitory synapse imbalance and ERK signal pathway. *Neurobiol Learn Mem*, *127*, 72-83. https://doi.org/10.1016/j.nlm.2015.11.020

Ardestani, G., West, M. C., Maresca, T. J., Fissore, R. A., & Stratton, M. M. (2019). FRET-based sensor for CaMKII activity (FRESCA): A useful tool for assessing CaMKII activity in response to Ca(2+) oscillations in live cells. *J Biol Chem*, *294*(31), 11876-11891. https://doi.org/10.1074/jbc.RA119.009235

Armesilla, A. L., Williams, J. C., Buch, M. H., Pickard, A., Emerson, M., Cartwright, E. J., Oceandy, D., Vos, M. D., Gillies, S., Clark, G. J., & Neyses, L. (2004). Novel functional interaction between the plasma membrane Ca2+ pump 4b and the proapoptotic tumor suppressor Ras-associated factor 1 (RASSF1). *J Biol Chem*, *279*(30), 31318-31328. https://doi.org/10.1074/jbc.M307557200

Badura, A., Sun, X. R., Giovannucci, A., Lynch, L. A., & Wang, S. S. (2014). Fast calcium sensor proteins for monitoring neural activity. *Neurophotonics*, *1*(2), 025008. https://doi.org/10.1117/1.NPh.1.2.025008

Baune, B. T., Ponath, G., Golledge, J., Varga, G., Arolt, V., Rothermundt, M., & Berger, K. (2008). Association between IL-8 cytokine and cognitive performance in an elderly general population--the MEMO-Study. *Neurobiol Aging*, *29*(6), 937-944. https://doi.org/10.1016/j.neurobiolaging.2006.12.003

Beattie, E. C., Stellwagen, D., Morishita, W., Bresnahan, J. C., Ha, B. K., Von Zastrow, M., Beattie, M. S., & Malenka, R. C. (2002). Control of synaptic strength by glial TNFalpha. *Science*, *295*(5563), 2282-2285. https://doi.org/10.1126/science.1067859

Bernardino, L., Xapelli, S., Silva, A. P., Jakobsen, B., Poulsen, F. R., Oliveira, C. R., Vezzani, A., Malva, J. O., & Zimmer, J. (2005). Modulator effects of interleukin-1beta and tumor necrosis factor-alpha on AMPA-induced excitotoxicity in mouse organotypic hippocampal slice cultures. *J Neurosci*, *25*(29), 6734-6744. https://doi.org/10.1523/JNEUROSCI.1510-05.2005

Berridge, M. J., Bootman, M. D., & Lipp, P. (1998). Calcium--a life and death signal. *Nature*, *395*(6703), 645-648. https://doi.org/10.1038/27094

Berridge, M. J., Bootman, M. D., & Roderick, H. L. (2003). Calcium signalling: dynamics, homeostasis and remodelling. *Nat Rev Mol Cell Biol*, *4*(7), 517-529. https://doi.org/10.1038/nrm1155

Bhattacharya, S., Herrera-Molina, R., Sabanov, V., Ahmed, T., Iscru, E., Stober, F., Richter, K., Fischer, K. D., Angenstein, F., Goldschmidt, J., Beesley, P. W., Balschun, D., Smalla, K. H., Gundelfinger, E. D., & Montag, D. (2017). Genetically Induced Retrograde Amnesia of Associative Memories After Neuroplastin Ablation. *Biol Psychiatry*, *81*(2), 124-135. https://doi.org/10.1016/j.biopsych.2016.03.2107

Blaustein, M. P., & Lederer, W. J. (1999). Sodium/calcium exchange: its physiological implications. *Physiol Rev*, *79*(3), 763-854. https://doi.org/10.1152/physrev.1999.79.3.763

Bloodgood, B. L., Giessel, A. J., & Sabatini, B. L. (2009). Biphasic synaptic Ca influx arising from compartmentalized electrical signals in dendritic spines. *PLoS Biol*, *7*(9), e1000190. https://doi.org/10.1371/journal.pbio.1000190

Bloodgood, B. L., & Sabatini, B. L. (2007a). Ca(2+) signaling in dendritic spines. *Curr Opin Neurobiol*, *17*(3), 345-351. https://doi.org/10.1016/j.conb.2007.04.003

Bloodgood, B. L., & Sabatini, B. L. (2007b). Nonlinear regulation of unitary synaptic signals by CaV(2.3) voltage-sensitive calcium channels located in dendritic spines. *Neuron*, *53*(2), 249-260. https://doi.org/10.1016/j.neuron.2006.12.017

Boczek, T., Radzik, T., Ferenc, B., & Zylinska, L. (2019). The Puzzling Role of Neuron-Specific PMCA Isoforms in the Aging Process. *Int J Mol Sci*, *20*(24). https://doi.org/10.3390/ijms20246338

Boka, G., Anglade, P., Wallach, D., Javoy-Agid, F., Agid, Y., & Hirsch, E. C. (1994). Immunocytochemical analysis of tumor necrosis factor and its receptors in Parkinson's disease. *Neurosci Lett*, *172*(1-2), 151-154. https://doi.org/10.1016/0304-3940(94)90684-x

Bourgognon, J. M., & Cavanagh, J. (2020). The role of cytokines in modulating learning and memory and brain plasticity. *Brain Neurosci Adv*, *4*, 2398212820979802. https://doi.org/10.1177/2398212820979802

Boyken, J., Gronborg, M., Riedel, D., Urlaub, H., Jahn, R., & Chua, J. J. (2013). Molecular profiling of synaptic vesicle docking sites reveals novel proteins but few differences between glutamatergic and GABAergic synapses. *Neuron*, *78*(2), 285-297. https://doi.org/10.1016/j.neuron.2013.02.027

Breder, C. D., Tsujimoto, M., Terano, Y., Scott, D. W., & Saper, C. B. (1993). Distribution and characterization of tumor necrosis factor-alpha-like immunoreactivity in the murine central nervous system. *J Comp Neurol*, *337*(4), 543-567. https://doi.org/10.1002/cne.903370403

Breit, M., Kessler, M., Stepniewski, M., Vlachos, A., & Queisser, G. (2018). Spine-to-Dendrite Calcium Modeling Discloses Relevance for Precise Positioning of Ryanodine Receptor-Containing Spine Endoplasmic Reticulum. *Sci Rep*, *8*(1), 15624. https://doi.org/10.1038/s41598-018-33343-9

Brennan, F. X., Beck, K. D., & Servatius, R. J. (2004). Proinflammatory cytokines differentially affect leverpress avoidance acquisition in rats. *Behav Brain Res*, *153*(2), 351-355. https://doi.org/10.1016/j.bbr.2003.12.025

Brini, M. (2009). Plasma membrane Ca(2+)-ATPase: from a housekeeping function to a versatile signaling role. *Pflugers Arch*, *457*(3), 657-664. https://doi.org/10.1007/s00424-008-0505-6

Brini, M., Cali, T., Ottolini, D., & Carafoli, E. (2013). The plasma membrane calcium pump in health and disease. *FEBS J*, *280*(21), 5385-5397. https://doi.org/10.1111/febs.12193

Brini, M., & Carafoli, E. (2011). The plasma membrane Ca(2)+ ATPase and the plasma membrane sodium calcium exchanger cooperate in the regulation of cell calcium. *Cold Spring Harb Perspect Biol*, *3*(2). https://doi.org/10.1101/cshperspect.a004168

Bruce, J. I. E. (2018). Metabolic regulation of the PMCA: Role in cell death and survival. *Cell Calcium*, *69*, 28-36. https://doi.org/10.1016/j.ceca.2017.06.001

Buch, M. H., Pickard, A., Rodriguez, A., Gillies, S., Maass, A. H., Emerson, M., Cartwright, E. J., Williams, J. C., Oceandy, D., Redondo, J. M., Neyses, L., & Armesilla, A. L. (2005). The sarcolemmal calcium pump inhibits the calcineurin/nuclear factor of activated T-cell pathway via interaction with the calcineurin A catalytic subunit. *J Biol Chem*, *280*(33), 29479-29487. https://doi.org/10.1074/jbc.M501326200

Burette, A., Rockwood, J. M., Strehler, E. E., & Weinberg, R. J. (2003). Isoform-specific distribution of the plasma membrane Ca2+ ATPase in the rat brain. *J Comp Neurol*, *467*(4), 464-476. https://doi.org/10.1002/cne.10933

Burette, A., & Weinberg, R. J. (2007). Perisynaptic organization of plasma membrane calcium pumps in cerebellar cortex. *J Comp Neurol*, *500*(6), 1127-1135. https://doi.org/10.1002/cne.21237

Burette, A. C., Strehler, E. E., & Weinberg, R. J. (2009). "Fast" plasma membrane calcium pump PMCA2a concentrates in GABAergic terminals in the adult rat brain. *J Comp Neurol*, *512*(4), 500-513. https://doi.org/10.1002/cne.21909

Burette, A. C., Strehler, E. E., & Weinberg, R. J. (2010). A plasma membrane Ca2+ ATPase isoform at the postsynaptic density. *Neuroscience*, *169*(3), 987-993. https://doi.org/10.1016/j.neuroscience.2010.05.062

Butler, M. P., O'Connor, J. J., & Moynagh, P. N. (2004). Dissection of tumor-necrosis factor-alpha inhibition of long-term potentiation (LTP) reveals a p38 mitogen-activated protein kinase-dependent mechanism which maps to early-but not late-phase LTP. *Neuroscience*, *124*(2), 319-326. https://doi.org/10.1016/j.neuroscience.2003.11.040

Carafoli, E., Santella, L., Branca, D., & Brini, M. (2001). Generation, control, and processing of cellular calcium signals. *Crit Rev Biochem Mol Biol*, *36*(2), 107-260. https://doi.org/10.1080/20014091074183

Caride, A. J., Elwess, N. L., Verma, A. K., Filoteo, A. G., Enyedi, A., Bajzer, Z., & Penniston, J. T. (1999). The rate of activation by calmodulin of isoform 4 of the plasma membrane Ca(2+) pump is slow and is changed by alternative splicing. *J Biol Chem*, *274*(49), 35227-35232. https://doi.org/10.1074/jbc.274.49.35227

Caride, A. J., Penheiter, A. R., Filoteo, A. G., Bajzer, Z., Enyedi, A., & Penniston, J. T. (2001). The plasma membrane calcium pump displays memory of past calcium spikes. Differences between isoforms 2b and 4b. *J Biol Chem*, *276*(43), 39797-39804. https://doi.org/10.1074/jbc.M104380200

Caroni, P., & Carafoli, E. (1981). Regulation of Ca2+-pumping ATPase of heart sarcolemma by a phosphorylation-dephosphorylation Process. *J Biol Chem*, *256*(18), 9371-9373. https://www.ncbi.nlm.nih.gov/pubmed/6270081

Carrott, L., Bowl, M. R., Aguilar, C., Johnson, S. L., Chessum, L., West, M., Morse, S., Dorning, J., Smart, E., Hardisty-Hughes, R., Ball, G., Parker, A., Barnard, A. R., MacLaren, R. E., Wells, S., Marcotti, W., & Brown, S. D. (2016). Absence of Neuroplastin-65 Affects Synaptogenesis in Mouse Inner Hair Cells and Causes Profound Hearing Loss. *J Neurosci*, *36*(1), 222-234. https://doi.org/10.1523/JNEUROSCI.1808-15.2016

Chamberland, S., Zamora Moratalla, A., & Topolnik, L. (2019). Calcium extrusion mechanisms in dendrites of mouse hippocampal CA1 inhibitory interneurons. *Cell Calcium*, *77*, 49-57. https://doi.org/10.1016/j.ceca.2018.12.002

Chandler, L. J., Sutton, G., Dorairaj, N. R., & Norwood, D. (2001). N-methyl D-aspartate receptor-mediated bidirectional control of extracellular signal-regulated kinase activity in cortical neuronal cultures. *J Biol Chem*, *276*(4), 2627-2636. https://doi.org/10.1074/jbc.M003390200

Chen, H. Y., & Chesler, M. (2015). Autocrine boost of NMDAR current in hippocampal CA1 pyramidal neurons by a PMCA-dependent, perisynaptic, extracellular pH shift. *J Neurosci*, *35*(3), 873-877. https://doi.org/10.1523/JNEUROSCI.2293-14.2015

Chen, T. W., Wardill, T. J., Sun, Y., Pulver, S. R., Renninger, S. L., Baohan, A., Schreiter, E. R., Kerr, R. A., Orger, M. B., Jayaraman, V., Looger, L. L., Svoboda, K., & Kim, D. S. (2013). Ultrasensitive fluorescent proteins for imaging neuronal activity. *Nature*, *499*(7458), 295-300. https://doi.org/10.1038/nature12354

Choi, H. S., & Eisner, D. A. (1999). The role of sarcolemmal Ca2+-ATPase in the regulation of resting calcium concentration in rat ventricular myocytes. *J Physiol*, *515 (Pt 1)*, 109-118. https://doi.org/10.1111/j.1469-7793.1999.109ad.x

Choquette, D., Hakim, G., Filoteo, A. G., Plishker, G. A., Bostwick, J. R., & Penniston, J. T. (1984). Regulation of plasma membrane Ca2+ ATPases by lipids of the phosphatidylinositol cycle. *Biochem Biophys Res Commun*, *125*(3), 908-915. https://doi.org/10.1016/0006-291x(84)91369-x

Chung, I. Y., & Benveniste, E. N. (1990). Tumor necrosis factor-alpha production by astrocytes. Induction by lipopolysaccharide, IFN-gamma, and IL-1 beta. *J Immunol*, *144*(8), 2999-3007. https://www.ncbi.nlm.nih.gov/pubmed/2109008

Churchill, L., Rector, D. M., Yasuda, K., Fix, C., Rojas, M. J., Yasuda, T., & Krueger, J. M. (2008). Tumor necrosis factor alpha: activity dependent expression and promotion of cortical column sleep in rats. *Neuroscience*, *156*(1), 71-80. https://doi.org/10.1016/j.neuroscience.2008.06.066

Clarkson, B. D. S., Kahoud, R. J., McCarthy, C. B., & Howe, C. L. (2017). Inflammatory cytokine-induced changes in neural network activity measured by waveform analysis of high-content calcium imaging in murine cortical neurons. *Sci Rep*, *7*(1), 9037. https://doi.org/10.1038/s41598-017-09182-5

Cunningham, A. J., Murray, C. A., O'Neill, L. A., Lynch, M. A., & O'Connor, J. J. (1996). Interleukin-1 beta (IL-1 beta) and tumour necrosis factor (TNF) inhibit long-term potentiation in the rat dentate gyrus in vitro. *Neurosci Lett*, *203*(1), 17-20. https://doi.org/10.1016/0304-3940(95)12252-4

Dana, H., Sun, Y., Mohar, B., Hulse, B. K., Kerlin, A. M., Hasseman, J. P., Tsegaye, G., Tsang, A., Wong, A., Patel, R., Macklin, J. J., Chen, Y., Konnerth, A., Jayaraman, V., Looger, L. L., Schreiter, E. R., Svoboda, K., & Kim, D. S. (2019). High-performance calcium sensors for imaging activity in neuronal populations and microcompartments. *Nat Methods*, *16*(7), 649-657. https://doi.org/10.1038/s41592-019-0435-6

Davis, S., Vanhoutte, P., Pages, C., Caboche, J., & Laroche, S. (2000). The MAPK/ERK cascade targets both Elk-1 and cAMP response element-binding protein to control long-term potentiation-dependent gene expression in the dentate gyrus in vivo. *J Neurosci*, *20*(12), 4563-4572. https://www.ncbi.nlm.nih.gov/pubmed/10844026

DeMarco, S. J., & Strehler, E. E. (2001). Plasma membrane Ca2+-atpase isoforms 2b and 4b interact promiscuously and selectively with members of the membrane-associated guanylate kinase family of PDZ (PSD95/Dlg/ZO-1) domain-containing proteins. *J Biol Chem*, *276*(24), 21594-21600. https://doi.org/10.1074/jbc.M101448200

Deng, L., Chen, J., Wang, T., Chen, B., Yang, L., Liao, J., Chen, Y., Wang, J., Tang, H., Yi, J., Kang, K., Li, L., & Gou, D. (2021). PDGF/MEK/ERK axis represses Ca(2+) clearance via decreasing the abundance of plasma membrane Ca(2+) pump PMCA4 in pulmonary arterial smooth muscle cells. *Am J Physiol Cell Physiol*, *320*(1), C66-C79. https://doi.org/10.1152/ajpcell.00290.2020

Desrivieres, S., Lourdusamy, A., Tao, C., Toro, R., Jia, T., Loth, E., Medina, L. M., Kepa, A., Fernandes, A., Ruggeri, B., Carvalho, F. M., Cocks, G., Banaschewski, T., Barker, G. J., Bokde, A. L., Buchel, C., Conrod, P. J., Flor, H., Heinz, A., Gallinat, J., Garavan, H., Gowland, P., Bruhl, R., Lawrence, C., Mann, K., Martinot, M. L., Nees, F., Lathrop, M., Poline, J. B., Rietschel, M., Thompson, P., Fauth-Buhler, M., Smolka, M. N., Pausova, Z., Paus, T., Feng, J., Schumann, G., & Consortium, I. (2015). Single nucleotide polymorphism in the neuroplastin locus associates with cortical thickness and intellectual ability in adolescents. *Mol Psychiatry*, *20*(2), 263-274. https://doi.org/10.1038/mp.2013.197

Dou, Y., Tian, X., Zhang, J., Wang, Z., & Chen, G. (2018). Roles of TRAF6 in Central Nervous System. *Curr Neuropharmacol*, *16*(9), 1306-1313. https://doi.org/10.2174/1570159X16666180412094655

Dudek, S. M., & Fields, R. D. (2001). Mitogen-activated protein kinase/extracellular signal-regulated kinase activation in somatodendritic compartments: roles of action potentials, frequency, and mode of calcium entry. *J Neurosci*, *21*(2), RC122. https://www.ncbi.nlm.nih.gov/pubmed/11160456

Dunham, E. T., & Glynn, I. M. (1961). Adenosinetriphosphatase activity and the active movements of alkali metal ions. *J Physiol*, *156*, 274-293. https://doi.org/10.1113/jphysiol.1961.sp006675

Dupuis, J. P., Ladepeche, L., Seth, H., Bard, L., Varela, J., Mikasova, L., Bouchet, D., Rogemond, V., Honnorat, J., Hanse, E., & Groc, L. (2014). Surface dynamics of

GluN2B-NMDA receptors controls plasticity of maturing glutamate synapses. *EMBO J*, *33*(8), 842-861. https://doi.org/10.1002/embj.201386356

Empson, R. M., Buckby, L. E., Kraus, M., Bates, K. J., Crompton, M. R., Gundelfinger, E. D., & Beesley, P. W. (2006). The cell adhesion molecule neuroplastin-65 inhibits hippocampal long-term potentiation via a mitogen-activated protein kinase p38-dependent reduction in surface expression of GluR1-containing glutamate receptors. *J Neurochem*, *99*(3), 850-860. https://doi.org/10.1111/j.1471-4159.2006.04123.x

Empson, R. M., Garside, M. L., & Knopfel, T. (2007). Plasma membrane Ca2+ ATPase 2 contributes to short-term synapse plasticity at the parallel fiber to Purkinje neuron synapse. *J Neurosci*, *27*(14), 3753-3758. https://doi.org/10.1523/JNEUROSCI.0069-07.2007

Evans, R. C., & Blackwell, K. T. (2015). Calcium: amplitude, duration, or location? *Biol Bull*, *228*(1), 75-83. https://doi.org/10.1086/BBLv228n1p75

Ferragamo, M. J., Reinardy, J. L., & Thayer, S. A. (2009). Ca2+-dependent, stimulus-specific modulation of the plasma membrane Ca2+ pump in hippocampal neurons. *J Neurophysiol*, *101*(5), 2563-2571. https://doi.org/10.1152/jn.90774.2008

Fischer, M., Kaech, S., Wagner, U., Brinkhaus, H., & Matus, A. (2000). Glutamate receptors regulate actin-based plasticity in dendritic spines. *Nat Neurosci*, *3*(9), 887-894. https://doi.org/10.1038/78791

Fukazawa, Y., Saitoh, Y., Ozawa, F., Ohta, Y., Mizuno, K., & Inokuchi, K. (2003). Hippocampal LTP is accompanied by enhanced F-actin content within the dendritic spine that is essential for late LTP maintenance in vivo. *Neuron*, *38*(3), 447-460. https://doi.org/10.1016/s0896-6273(03)00206-x

Fukunaga, K., Muller, D., Ohmitsu, M., Bako, E., DePaoli-Roach, A. A., & Miyamoto, E. (2000). Decreased protein phosphatase 2A activity in hippocampal long-term potentiation. *J Neurochem*, *74*(2), 807-817. https://doi.org/10.1046/j.1471-4159.2000.740807.x

Garside, M. L., Turner, P. R., Austen, B., Strehler, E. E., Beesley, P. W., & Empson, R. M. (2009). Molecular interactions of the plasma membrane calcium ATPase 2 at pre- and post-synaptic sites in rat cerebellum. *Neuroscience*, *162*(2), 383-395. https://doi.org/10.1016/j.neuroscience.2009.04.059

Gasterstadt, I., Jack, A., Stahlhut, T., Rennau, L. M., Gonda, S., & Wahle, P. (2020). Genetically Encoded Calcium Indicators Can Impair Dendrite Growth of Cortical Neurons. *Front Cell Neurosci*, *14*, 570596. https://doi.org/10.3389/fncel.2020.570596

Gatto, C., & Milanick, M. A. (1993). Inhibition of the red blood cell calcium pump by eosin and other fluorescein analogues. *Am J Physiol*, *264*(6 Pt 1), C1577-1586. https://doi.org/10.1152/ajpcell.1993.264.6.C1577

Go, C. K., & Soboloff, J. (2018). Hold the door: hPMCA1/neuroplastin interactions regulate Ca(2+)-binding site accessibility. *Cell Calcium*, *76*, 135-136. https://doi.org/10.1016/j.ceca.2018.10.003

Gong, D., Chi, X., Ren, K., Huang, G., Zhou, G., Yan, N., Lei, J., & Zhou, Q. (2018). Structure of the human plasma membrane Ca(2+)-ATPase 1 in complex with its obligatory subunit neuroplastin. *Nat Commun*, *9*(1), 3623. https://doi.org/10.1038/s41467-018-06075-7

Groc, L., & Choquet, D. (2020). Linking glutamate receptor movements and synapse function. *Science*, *368*(6496). https://doi.org/10.1126/science.aay4631

Grosskreutz, J., Van Den Bosch, L., & Keller, B. U. (2010). Calcium dysregulation in amyotrophic lateral sclerosis. *Cell Calcium*, *47*(2), 165-174. https://doi.org/10.1016/j.ceca.2009.12.002

Grunditz, A., Holbro, N., Tian, L., Zuo, Y., & Oertner, T. G. (2008). Spine neck plasticity controls postsynaptic calcium signals through electrical compartmentalization. *J Neurosci*, *28*(50), 13457-13466. https://doi.org/10.1523/JNEUROSCI.2702-08.2008

Grutzendler, J., Kasthuri, N., & Gan, W. B. (2002). Long-term dendritic spine stability in the adult cortex. *Nature*, *420*(6917), 812-816. https://doi.org/10.1038/nature01276

Harvey, C. D., Ehrhardt, A. G., Cellurale, C., Zhong, H., Yasuda, R., Davis, R. J., & Svoboda, K. (2008). A genetically encoded fluorescent sensor of ERK activity. *Proc Natl Acad Sci U S A*, *105*(49), 19264-19269. https://doi.org/10.1073/pnas.0804598105

Harvey, C. D., Yasuda, R., Zhong, H., & Svoboda, K. (2008). The spread of Ras activity triggered by activation of a single dendritic spine. *Science*, *321*(5885), 136-140. https://doi.org/10.1126/science.1159675

Hegedus, L., Padanyi, R., Molnar, J., Paszty, K., Varga, K., Kenessey, I., Sarkozy, E., Wolf, M., Grusch, M., Hegyi, Z., Homolya, L., Aigner, C., Garay, T., Hegedus, B., Timar, J., Kallay, E., & Enyedi, A. (2017). Histone Deacetylase Inhibitor Treatment Increases the Expression of the Plasma Membrane Ca(2+) Pump PMCA4b and Inhibits the Migration of Melanoma Cells Independent of ERK. *Front Oncol*, *7*, 95. https://doi.org/10.3389/fonc.2017.00095

Hermes, M., Eichhoff, G., & Garaschuk, O. (2010). Intracellular calcium signalling in Alzheimer's disease. *J Cell Mol Med*, *14*(1-2), 30-41. https://doi.org/10.1111/j.1582-4934.2009.00976.x

Herrera-Molina, R., Mlinac-Jerkovic, K., Ilic, K., Stober, F., Vemula, S. K., Sandoval, M., Milosevic, N. J., Simic, G., Smalla, K. H., Goldschmidt, J., Bognar, S. K., & Montag, D. (2017). Neuroplastin deletion in glutamatergic neurons impairs selective brain functions and calcium regulation: implication for cognitive deterioration. *Sci Rep*, *7*(1), 7273. https://doi.org/10.1038/s41598-017-07839-9

Herrera-Molina, R., Sarto-Jackson, I., Montenegro-Venegas, C., Heine, M., Smalla, K. H., Seidenbecher, C. I., Beesley, P. W., Gundelfinger, E. D., & Montag, D. (2014). Structure of excitatory synapses and GABAA receptor localization at inhibitory synapses are regulated by neuroplastin-65. *J Biol Chem*, *289*(13), 8973-8988. https://doi.org/10.1074/jbc.M113.514992

Higley, M. J., & Sabatini, B. L. (2012). Calcium signaling in dendritic spines. *Cold Spring Harb Perspect Biol*, *4*(4), a005686. https://doi.org/10.1101/cshperspect.a005686

Hill, I. E., Selkirk, C. P., Hawkes, R. B., & Beesley, P. W. (1988). Characterization of novel glycoprotein components of synaptic membranes and postsynaptic densities, gp65 and gp55, with a monoclonal antibody. *Brain Res*, *461*(1), 27-43. https://doi.org/10.1016/0006-8993(88)90722-6

Holbro, N., Grunditz, A., & Oertner, T. G. (2009). Differential distribution of endoplasmic reticulum controls metabotropic signaling and plasticity at hippocampal synapses. *Proc Natl Acad Sci U S A*, *106*(35), 15055-15060. https://doi.org/10.1073/pnas.0905110106

Holtmaat, A. J., Trachtenberg, J. T., Wilbrecht, L., Shepherd, G. M., Zhang, X., Knott, G. W., & Svoboda, K. (2005). Transient and persistent dendritic spines in the neocortex in vivo. *Neuron*, *45*(2), 279-291. https://doi.org/10.1016/j.neuron.2005.01.003

Husi, H., Ward, M. A., Choudhary, J. S., Blackstock, W. P., & Grant, S. G. (2000). Proteomic analysis of NMDA receptor-adhesion protein signaling complexes. *Nat Neurosci*, *3*(7), 661-669. https://doi.org/10.1038/76615

Incontro, S., Diaz-Alonso, J., Iafrati, J., Vieira, M., Asensio, C. S., Sohal, V. S., Roche, K. W., Bender, K. J., & Nicoll, R. A. (2018). The CaMKII/NMDA receptor complex controls hippocampal synaptic transmission by kinase-dependent and independent mechanisms. *Nat Commun*, *9*(1), 2069. https://doi.org/10.1038/s41467-018-04439-7

Ivenshitz, M., & Segal, M. (2010). Neuronal density determines network connectivity and spontaneous activity in cultured hippocampus. *J Neurophysiol*, *104*(2), 1052-1060. https://doi.org/10.1152/jn.00914.2009

Jarrett, H. W., & Penniston, J. T. (1978). Purification of the Ca2+-stimulated ATPase activator from human erythrocytes. Its membership in the class of Ca2+-binding modulator proteins. *J Biol Chem*, *253*(13), 4676-4682. https://www.ncbi.nlm.nih.gov/pubmed/149133

Jensen, T. P., Filoteo, A. G., Knopfel, T., & Empson, R. M. (2007). Presynaptic plasma membrane Ca2+ ATPase isoform 2a regulates excitatory synaptic transmission in rat

hippocampal CA3. *J Physiol*, *579*(Pt 1), 85-99. https://doi.org/10.1113/jphysiol.2006.123901

Jiang, C. H., Wei, M., Zhang, C., & Shi, Y. S. (2021). The amino-terminal domain of GluA1 mediates LTP maintenance via interaction with neuroplastin-65. *Proc Natl Acad Sci U S A*, *118*(9). https://doi.org/10.1073/pnas.2019194118

Jones, S., Solomon, A., Sanz-Rosa, D., Moore, C., Holbrook, L., Cartwright, E. J., Neyses, L., & Emerson, M. (2010). The plasma membrane calcium ATPase modulates calcium homeostasis, intracellular signaling events and function in platelets. *J Thromb Haemost*, *8*(12), 2766-2774. https://doi.org/10.1111/j.1538-7836.2010.04076.x

Jost, N., Nagy, N., Corici, C., Kohajda, Z., Horvath, A., Acsai, K., Biliczki, P., Levijoki, J., Pollesello, P., Koskelainen, T., Otsomaa, L., Toth, A., Papp, J. G., Varro, A., & Virag, L. (2013). ORM-10103, a novel specific inhibitor of the Na+/Ca2+ exchanger, decreases early and delayed afterdepolarizations in the canine heart. *Br J Pharmacol*, *170*(4), 768-778. https://doi.org/10.1111/bph.12228

Kasahara, J., Fukunaga, K., & Miyamoto, E. (2001). Activation of calcium/calmodulin-dependent protein kinase IV in long term potentiation in the rat hippocampal CA1 region. *J Biol Chem*, *276*(26), 24044-24050. https://doi.org/10.1074/jbc.M100247200

Khairova, R. A., Machado-Vieira, R., Du, J., & Manji, H. K. (2009). A potential role for pro-inflammatory cytokines in regulating synaptic plasticity in major depressive disorder. *Int J Neuropsychopharmacol*, *12*(4), 561-578. https://doi.org/10.1017/S1461145709009924

Khazipov, R., Esclapez, M., Caillard, O., Bernard, C., Khalilov, I., Tyzio, R., Hirsch, J., Dzhala, V., Berger, B., & Ben-Ari, Y. (2001). Early development of neuronal activity in the primate hippocampus in utero. *J Neurosci*, *21*(24), 9770-9781. https://www.ncbi.nlm.nih.gov/pubmed/11739585

Kim, E., DeMarco, S. J., Marfatia, S. M., Chishti, A. H., Sheng, M., & Strehler, E. E. (1998). Plasma membrane Ca2+ ATPase isoform 4b binds to membrane-associated guanylate kinase (MAGUK) proteins via their PDZ (PSD-95/Dlg/ZO-1) domains. *J Biol Chem*, *273*(3), 1591-1595. https://doi.org/10.1074/jbc.273.3.1591

Kip, S. N., Gray, N. W., Burette, A., Canbay, A., Weinberg, R. J., & Strehler, E. E. (2006). Changes in the expression of plasma membrane calcium extrusion systems during the maturation of hippocampal neurons. *Hippocampus*, *16*(1), 20-34. https://doi.org/10.1002/hipo.20129

Kiryushko, D., Novitskaya, V., Soroka, V., Klingelhofer, J., Lukanidin, E., Berezin, V., & Bock, E. (2006). Molecular mechanisms of Ca(2+) signaling in neurons induced by the S100A4 protein. *Mol Cell Biol*, *26*(9), 3625-3638. https://doi.org/10.1128/MCB.26.9.3625-3638.2006

Knoblauch, A., & Sommer, F. T. (2016). Structural Plasticity, Effectual Connectivity, and Memory in Cortex. *Front Neuroanat*, *10*, 63. https://doi.org/10.3389/fnana.2016.00063

Kopec, C. D., Li, B., Wei, W., Boehm, J., & Malinow, R. (2006). Glutamate receptor exocytosis and spine enlargement during chemically induced long-term potentiation. *J Neurosci*, *26*(7), 2000-2009. https://doi.org/10.1523/JNEUROSCI.3918-05.2006

Korthals, M., Langnaese, K., Smalla, K. H., Kahne, T., Herrera-Molina, R., Handschuh, J., Lehmann, A. C., Mamula, D., Naumann, M., Seidenbecher, C., Zuschratter, W., Tedford, K., Gundelfinger, E. D., Montag, D., Fischer, K. D., & Thomas, U. (2017). A complex of Neuroplastin and Plasma Membrane Ca(2+) ATPase controls T cell activation. *Sci Rep*, *7*(1), 8358. https://doi.org/10.1038/s41598-017-08519-4

Kosk-Kosicka, D., & Bzdega, T. (1988). Activation of the erythrocyte Ca2+-ATPase by either self-association or interaction with calmodulin. *J Biol Chem*, *263*(34), 18184-18189. https://www.ncbi.nlm.nih.gov/pubmed/2973461

Kreutz, M. R., Langnaese, K., Dieterich, D. C., Seidenbecher, C. I., Zuschratter, W., Beesley, P. W., & Gundelfinger, E. D. (2001). Distribution of transcript and protein isoforms of the synaptic glycoprotein neuroplastin in rat retina. *Invest Ophthalmol Vis Sci*, *42*(8), 1907-1914. https://www.ncbi.nlm.nih.gov/pubmed/11431460

Kurnellas, M. P., Lee, A. K., Szczepanowski, K., & Elkabes, S. (2007). Role of plasma membrane calcium ATPase isoform 2 in neuronal function in the cerebellum and spinal cord. *Ann N Y Acad Sci*, *1099*, 287-291. https://doi.org/10.1196/annals.1387.025

Lan, J. Y., Skeberdis, V. A., Jover, T., Grooms, S. Y., Lin, Y., Araneda, R. C., Zheng, X., Bennett, M. V., & Zukin, R. S. (2001). Protein kinase C modulates NMDA receptor trafficking and gating. *Nat Neurosci*, *4*(4), 382-390. https://doi.org/10.1038/86028

Lang, C., Barco, A., Zablow, L., Kandel, E. R., Siegelbaum, S. A., & Zakharenko, S. S. (2004). Transient expansion of synaptically connected dendritic spines upon induction of hippocampal long-term potentiation. *Proc Natl Acad Sci U S A*, *101*(47), 16665-16670. https://doi.org/10.1073/pnas.0407581101

Langnaese, K., Beesley, P. W., & Gundelfinger, E. D. (1997). Synaptic membrane glycoproteins gp65 and gp55 are new members of the immunoglobulin superfamily. *J Biol Chem*, *272*(2), 821-827. https://doi.org/10.1074/jbc.272.2.821

Lehotsky, J., Raeymaekers, L., Missiaen, L., Wuytack, F., De Smedt, H., & Casteels, R. (1992). Stimulation of the catalytic cycle of the Ca2+ pump of porcine plasma-membranes by negatively charged phospholipids. *Biochim Biophys Acta*, *1105*(1), 118-124. https://doi.org/10.1016/0005-2736(92)90169-m

Leonoudakis, D., Braithwaite, S. P., Beattie, M. S., & Beattie, E. C. (2004). TNFalpha-induced AMPA-receptor trafficking in CNS neurons; relevance to excitotoxicity? *Neuron Glia Biol*, *1*(3), 263-273. https://doi.org/10.1017/S1740925X05000608

Li, H., Liu, Y., Gao, X., Liu, L., Amuti, S., Wu, D., Jiang, F., Huang, L., Wang, G., Zeng, J., Ma, B., & Yuan, Q. (2019). Neuroplastin 65 modulates anxiety- and depression-like behavior likely through adult hippocampal neurogenesis and central 5-HT activity. *FEBS J*, *286*(17), 3401-3415. https://doi.org/10.1111/febs.14865

Li, R., Yang, L., Lindholm, K., Konishi, Y., Yue, X., Hampel, H., Zhang, D., & Shen, Y. (2004). Tumor necrosis factor death receptor signaling cascade is required for amyloid-beta protein-induced neuron death. *J Neurosci*, *24*(7), 1760-1771. https://doi.org/10.1523/JNEUROSCI.4580-03.2004

Lieberman, A. P., Pitha, P. M., Shin, H. S., & Shin, M. L. (1989). Production of tumor necrosis factor and other cytokines by astrocytes stimulated with lipopolysaccharide or a neurotropic virus. *Proc Natl Acad Sci U S A*, *86*(16), 6348-6352. https://doi.org/10.1073/pnas.86.16.6348

Lin, X., Brunk, M. G. K., Yuanxiang, P., Curran, A. W., Zhang, E., Stober, F., Goldschmidt, J., Gundelfinger, E. D., Vollmer, M., Happel, M. F. K., Herrera-Molina, R., & Montag, D. (2021). Neuroplastin expression is essential for hearing and hair cell PMCA expression. *Brain Struct Funct*. https://doi.org/10.1007/s00429-021-02269-w

Lisek, M., Boczek, T., & Zylinska, L. (2018). Calcium as a Trojan horse in mental diseases-The role of PMCA and PMCA-interacting proteins in bipolar disorder and schizophrenia. *Neurosci Lett*, *663*, 48-54. https://doi.org/10.1016/j.neulet.2017.08.005

Lisek, M., Ferenc, B., Studzian, M., Pulaski, L., Guo, F., Zylinska, L., & Boczek, T. (2017). Glutamate Deregulation in Ketamine-Induced Psychosis-A Potential Role of PSD95, NMDA Receptor and PMCA Interaction. *Front Cell Neurosci*, *11*, 181. https://doi.org/10.3389/fncel.2017.00181

Liu, J., Fukunaga, K., Yamamoto, H., Nishi, K., & Miyamoto, E. (1999). Differential roles of Ca(2+)/calmodulin-dependent protein kinase II and mitogen-activated protein kinase activation in hippocampal long-term potentiation. *J Neurosci*, *19*(19), 8292-8299. https://www.ncbi.nlm.nih.gov/pubmed/10493730

Lock, J. T., Parker, I., & Smith, I. F. (2015). A comparison of fluorescent Ca(2)(+) indicators for imaging local Ca(2)(+) signals in cultured cells. *Cell Calcium*, *58*(6), 638-648. https://doi.org/10.1016/j.ceca.2015.10.003

MacDonald, J. F., Kotecha, S. A., Lu, W. Y., & Jackson, M. F. (2001). Convergence of PKC-dependent kinase signal cascades on NMDA receptors. *Curr Drug Targets*, *2*(3), 299-312. https://doi.org/10.2174/1389450013348452

Maggio, N., & Vlachos, A. (2018). Tumor necrosis factor (TNF) modulates synaptic plasticity in a concentration-dependent manner through intracellular calcium stores. *J Mol Med (Berl)*, *96*(10), 1039-1047. https://doi.org/10.1007/s00109-018-1674-1

Mahajan, G., & Nadkarni, S. (2019). Intracellular calcium stores mediate metaplasticity at hippocampal dendritic spines. *J Physiol*, *597*(13), 3473-3502. https://doi.org/10.1113/JP277726

Makani, S., & Chesler, M. (2010). Rapid rise of extracellular pH evoked by neural activity is generated by the plasma membrane calcium ATPase. *J Neurophysiol*, *103*(2), 667-676. https://doi.org/10.1152/jn.00948.2009

Marcos, D., Sepulveda, M. R., Berrocal, M., & Mata, A. M. (2009). Ontogeny of ATP hydrolysis and isoform expression of the plasma membrane Ca(2+)-ATPase in mouse brain. *BMC Neurosci*, *10*, 112. https://doi.org/10.1186/1471-2202-10-112

Marzban, H., Khanzada, U., Shabir, S., Hawkes, R., Langnaese, K., Smalla, K. H., Bockers, T. M., Gundelfinger, E. D., Gordon-Weeks, P. R., & Beesley, P. W. (2003). Expression of the immunoglobulin superfamily neuroplastin adhesion molecules in adult and developing mouse cerebellum and their localisation to parasagittal stripes. *J Comp Neurol*, *462*(3), 286-301. https://doi.org/10.1002/cne.10719

Matsuzaki, M., Honkura, N., Ellis-Davies, G. C., & Kasai, H. (2004). Structural basis of long-term potentiation in single dendritic spines. *Nature*, *429*(6993), 761-766. https://doi.org/10.1038/nature02617

McKay, S., Ryan, T. J., McQueen, J., Indersmitten, T., Marwick, K. F. M., Hasel, P., Kopanitsa, M. V., Baxter, P. S., Martel, M. A., Kind, P. C., Wyllie, D. J. A., O'Dell, T. J., Grant, S. G. N., Hardingham, G. E., & Komiyama, N. H. (2018). The Developmental Shift of NMDA Receptor Composition Proceeds Independently of GluN2 Subunit-Specific GluN2 C-Terminal Sequences. *Cell Rep*, *25*(4), 841-851 e844. https://doi.org/10.1016/j.celrep.2018.09.089

Michailidis, I. E., Helton, T. D., Petrou, V. I., Mirshahi, T., Ehlers, M. D., & Logothetis, D. E. (2007). Phosphatidylinositol-4,5-bisphosphate regulates NMDA receptor activity through alpha-actinin. *J Neurosci*, *27*(20), 5523-5532. https://doi.org/10.1523/JNEUROSCI.4378-06.2007

Minlebaev, M., Ben-Ari, Y., & Khazipov, R. (2007). Network mechanisms of spindle-burst oscillations in the neonatal rat barrel cortex in vivo. *J Neurophysiol*, *97*(1), 692-700. https://doi.org/10.1152/jn.00759.2006

Missiaen, L., Raeymaekers, L., Wuytack, F., Vrolix, M., de Smedt, H., & Casteels, R. (1989). Phospholipid-protein interactions of the plasma-membrane Ca2+-transporting ATPase. Evidence for a tissue-dependent functional difference. *Biochem J*, *263*(3), 687-694. https://doi.org/10.1042/bj2630687

Nagerl, U. V., Eberhorn, N., Cambridge, S. B., & Bonhoeffer, T. (2004). Bidirectional activity-dependent morphological plasticity in hippocampal neurons. *Neuron*, *44*(5), 759-767. https://doi.org/10.1016/j.neuron.2004.11.016

Ng, A. N., Doherty, A. J., Lombroso, P. J., Emptage, N. J., & Collingridge, G. L. (2014). Rapid regulation of endoplasmic reticulum dynamics in dendritic spines by NMDA receptor activation. *Mol Brain*, *7*, 60. https://doi.org/10.1186/s13041-014-0060-3

Niggli, V., Adunyah, E. S., Penniston, J. T., & Carafoli, E. (1981). Purified (Ca2+-Mg2+)-ATPase of the erythrocyte membrane. Reconstitution and effect of calmodulin and phospholipids. *J Biol Chem*, *256*(1), 395-401. https://www.ncbi.nlm.nih.gov/pubmed/6108953

Niggli, V., Penniston, J. T., & Carafoli, E. (1979). Purification of the (Ca2+-Mg2+)-ATPase from human erythrocyte membranes using a calmodulin affinity column. *J Biol Chem*, *254*(20), 9955-9958. https://www.ncbi.nlm.nih.gov/pubmed/158595

Ono, Y., Mori, Y., Egashira, Y., Sumiyama, K., & Takamori, S. (2019). Expression of plasma membrane calcium ATPases confers Ca(2+)/H(+) exchange in rodent synaptic vesicles. *Sci Rep*, *9*(1), 4289. https://doi.org/10.1038/s41598-019-40557-y

Opazo, P., Labrecque, S., Tigaret, C. M., Frouin, A., Wiseman, P. W., De Koninck, P., & Choquet, D. (2010). CaMKII triggers the diffusional trapping of surface AMPARs

through phosphorylation of stargazin. *Neuron*, *67*(2), 239-252. https://doi.org/10.1016/j.neuron.2010.06.007

Opitz, T., De Lima, A. D., & Voigt, T. (2002). Spontaneous development of synchronous oscillatory activity during maturation of cortical networks in vitro. *J Neurophysiol*, *88*(5), 2196-2206. https://doi.org/10.1152/jn.00316.2002

Owczarek, S., Kiryushko, D., Larsen, M. H., Kastrup, J. S., Gajhede, M., Sandi, C., Berezin, V., Bock, E., & Soroka, V. (2010). Neuroplastin-55 binds to and signals through the fibroblast growth factor receptor. *FASEB J*, *24*(4), 1139-1150. https://doi.org/10.1096/fj.09-140509

Owczarek, S., Soroka, V., Kiryushko, D., Larsen, M. H., Yuan, Q., Sandi, C., Berezin, V., & Bock, E. (2011). Neuroplastin-65 and a mimetic peptide derived from its homophilic binding site modulate neuritogenesis and neuronal plasticity. *J Neurochem*, *117*(6), 984-994. https://doi.org/10.1111/j.1471-4159.2011.07269.x

Pande, J., Mallhi, K. K., & Grover, A. K. (2005). A novel plasma membrane Ca(2+)-pump inhibitor: caloxin 1A1. *Eur J Pharmacol*, *508*(1-3), 1-6. https://doi.org/10.1016/j.ejphar.2004.11.057

Pande, J., Szewczyk, M. M., Kuszczak, I., Grover, S., Escher, E., & Grover, A. K. (2008). Functional effects of caloxin 1c2, a novel engineered selective inhibitor of plasma membrane Ca(2+)-pump isoform 4, on coronary artery. *J Cell Mol Med*, *12*(3), 1049-1060. https://doi.org/10.1111/j.1582-4934.2008.00140.x

Papatheodoropoulos, C., & Kouvaros, S. (2016). High-frequency stimulation-induced synaptic potentiation in dorsal and ventral CA1 hippocampal synapses: the involvement of NMDA receptors, mGluR5, and (L-type) voltage-gated calcium channels. *Learn Mem*, *23*(9), 460-464. https://doi.org/10.1101/lm.042531.116

Park, K. M., Yule, D. I., & Bowers, W. J. (2008). Tumor necrosis factor-alpha potentiates intraneuronal Ca2+ signaling via regulation of the inositol 1,4,5-trisphosphate receptor. *J Biol Chem*, *283*(48), 33069-33079. https://doi.org/10.1074/jbc.M802209200

Penheiter, A. R., Bajzer, Z., Filoteo, A. G., Thorogate, R., Torok, K., & Caride, A. J. (2003). A model for the activation of plasma membrane calcium pump isoform 4b by calmodulin. *Biochemistry*, *42*(41), 12115-12124. https://doi.org/10.1021/bi027098+

Penniston, J. T., & Enyedi, A. (1998). Modulation of the plasma membrane Ca2+ pump. *J Membr Biol*, *165*(2), 101-109. https://doi.org/10.1007/s002329900424

Penniston, J. T., Padanyi, R., Paszty, K., Varga, K., Hegedus, L., & Enyedi, A. (2014). Apart from its known function, the plasma membrane Ca(2)(+)ATPase can regulate Ca(2)(+) signaling by controlling phosphatidylinositol 4,5-bisphosphate levels. *J Cell Sci*, *127*(Pt 1), 72-84. https://doi.org/10.1242/jcs.132548

Pottorf, W. J., 2nd, Johanns, T. M., Derrington, S. M., Strehler, E. E., Enyedi, A., & Thayer, S. A. (2006). Glutamate-induced protease-mediated loss of plasma membrane Ca2+ pump activity in rat hippocampal neurons. *J Neurochem*, *98*(5), 1646-1656. https://doi.org/10.1111/j.1471-4159.2006.04063.x

Rimessi, A., Coletto, L., Pinton, P., Rizzuto, R., Brini, M., & Carafoli, E. (2005). Inhibitory interaction of the 14-3-3{epsilon} protein with isoform 4 of the plasma membrane Ca(2+)-ATPase pump. *J Biol Chem*, *280*(44), 37195-37203. https://doi.org/10.1074/jbc.M504921200

Riquelme, D., Alvarez, A., Leal, N., Adasme, T., Espinoza, I., Valdes, J. A., Troncoso, N., Hartel, S., Hidalgo, J., Hidalgo, C., & Carrasco, M. A. (2011). High-frequency field stimulation of primary neurons enhances ryanodine receptor-mediated Ca2+ release and generates hydrogen peroxide, which jointly stimulate NF-kappaB activity. *Antioxid Redox Signal*, *14*(7), 1245-1259. https://doi.org/10.1089/ars.2010.3238

Roome, C. J., & Empson, R. M. (2010). Assessment of the contribution of the plasma membrane calcium ATPase, PMCA, calcium transporter to synapse function using patch clamp electrophysiology and fast calcium imaging. *Methods Mol Biol*, *637*, 343-360. https://doi.org/10.1007/978-1-60761-700-6_19

Sabatini, B. L., Oertner, T. G., & Svoboda, K. (2002). The life cycle of Ca(2+) ions in dendritic spines. *Neuron*, *33*(3), 439-452. https://doi.org/10.1016/s0896-6273(02)00573-1

Saito, A., Fujikura-Ouchi, Y., Kuramasu, A., Shimoda, K., Akiyama, K., Matsuoka, H., & Ito, C. (2007). Association study of putative promoter polymorphisms in the neuroplastin gene and schizophrenia. *Neurosci Lett*, *411*(3), 168-173. https://doi.org/10.1016/j.neulet.2006.08.042

Sakaguchi, M., Yamamoto, M., Miyai, M., Maeda, T., Hiruma, J., Murata, H., Kinoshita, R., Winarsa Ruma, I. M., Putranto, E. W., Inoue, Y., Morizane, S., Huh, N. H., Tsuboi, R., & Hibino, T. (2016). Identification of an S100A8 Receptor Neuroplastin-beta and its Heterodimer Formation with EMMPRIN. *J Invest Dermatol*, *136*(11), 2240-2250. https://doi.org/10.1016/j.jid.2016.06.617

Sarto-Jackson, I., Milenkovic, I., Smalla, K. H., Gundelfinger, E. D., Kaehne, T., Herrera-Molina, R., Thomas, S., Kiebler, M. A., & Sieghart, W. (2012). The cell adhesion molecule neuroplastin-65 is a novel interaction partner of gamma-aminobutyric acid type A receptors. *J Biol Chem*, *287*(17), 14201-14214. https://doi.org/10.1074/jbc.M111.293175

Sato, M., Chen, C. C., Akiyama, K., & Otsuki, S. (1983). Acute exacerbation of paranoid psychotic state after long-term abstinence in patients with previous methamphetamine psychosis. *Biol Psychiatry*, *18*(4), 429-440. https://www.ncbi.nlm.nih.gov/pubmed/6860719

Schatzmann, H. J. (1966). ATP-dependent Ca++-extrusion from human red cells. *Experientia*, *22*(6), 364-365. https://doi.org/10.1007/BF01901136

Scheuss, V., Yasuda, R., Sobczyk, A., & Svoboda, K. (2006). Nonlinear [Ca2+] signaling in dendrites and spines caused by activity-dependent depression of Ca2+ extrusion. *J Neurosci*, *26*(31), 8183-8194. https://doi.org/10.1523/JNEUROSCI.1962-06.2006

Schmidt, N., Kollewe, A., Constantin, C. E., Henrich, S., Ritzau-Jost, A., Bildl, W., Saalbach, A., Hallermann, S., Kulik, A., Fakler, B., & Schulte, U. (2017). Neuroplastin and Basigin Are Essential Auxiliary Subunits of Plasma Membrane Ca(2+)-ATPases and Key Regulators of Ca(2+) Clearance. *Neuron*, *96*(4), 827-838 e829. https://doi.org/10.1016/j.neuron.2017.09.038

Schuh, K., Uldrijan, S., Gambaryan, S., Roethlein, N., & Neyses, L. (2003). Interaction of the plasma membrane Ca2+ pump 4b/CI with the Ca2+/calmodulin-dependent membrane-associated kinase CASK. *J Biol Chem*, *278*(11), 9778-9783. https://doi.org/10.1074/jbc.M212507200

Segal, M., & Korkotian, E. (2014). Endoplasmic reticulum calcium stores in dendritic spines. *Front Neuroanat*, *8*, 64. https://doi.org/10.3389/fnana.2014.00064

Selcher, J. C., Weeber, E. J., Christian, J., Nekrasova, T., Landreth, G. E., & Sweatt, J. D. (2003). A role for ERK MAP kinase in physiologic temporal integration in hippocampal area CA1. *Learn Mem*, *10*(1), 26-39. https://doi.org/10.1101/lm.51103

Sgambato-Faure, V., Xiong, Y., Berke, J. D., Hyman, S. E., & Strehler, E. E. (2006). The Homer-1 protein Ania-3 interacts with the plasma membrane calcium pump. *Biochem Biophys Res Commun*, *343*(2), 630-637. https://doi.org/10.1016/j.bbrc.2006.03.020

Shonesy, B. C., Jalan-Sakrikar, N., Cavener, V. S., & Colbran, R. J. (2014). CaMKII: a molecular substrate for synaptic plasticity and memory. *Prog Mol Biol Transl Sci*, *122*, 61-87. https://doi.org/10.1016/B978-0-12-420170-5.00003-9

Shull, G. E., & Greeb, J. (1988). Molecular cloning of two isoforms of the plasma membrane Ca2+-transporting ATPase from rat brain. Structural and functional domains exhibit similarity to Na+,K+- and other cation transport ATPases. *J Biol Chem*, *263*(18), 8646-8657. https://www.ncbi.nlm.nih.gov/pubmed/2837461

Sibarov, D. A., & Antonov, S. M. (2018). Calcium-Dependent Desensitization of NMDA Receptors. *Biochemistry (Mosc)*, *83*(10), 1173-1183. https://doi.org/10.1134/S0006297918100036

Simons, S. B., Escobedo, Y., Yasuda, R., & Dudek, S. M. (2009). Regional differences in hippocampal calcium handling provide a cellular mechanism for limiting plasticity.

Proc Natl Acad Sci U S A, *106*(33), 14080-14084. https://doi.org/10.1073/pnas.0904775106

Singh, A., Jones, O. D., Mockett, B. G., Ohline, S. M., & Abraham, W. C. (2019). Tumor Necrosis Factor-alpha-Mediated Metaplastic Inhibition of LTP Is Constitutively Engaged in an Alzheimer's Disease Model. *J Neurosci*, *39*(46), 9083-9097. https://doi.org/10.1523/JNEUROSCI.1492-19.2019

Smalla, K. H., Matthies, H., Langnase, K., Shabir, S., Bockers, T. M., Wyneken, U., Staak, S., Krug, M., Beesley, P. W., & Gundelfinger, E. D. (2000). The synaptic glycoprotein neuroplastin is involved in long-term potentiation at hippocampal CA1 synapses. *Proc Natl Acad Sci U S A*, *97*(8), 4327-4332. https://doi.org/10.1073/pnas.080389297

Smallwood, J. I., Gugi, B., & Rasmussen, H. (1988). Regulation of erythrocyte Ca2+ pump activity by protein kinase C. *J Biol Chem*, *263*(5), 2195-2202. https://www.ncbi.nlm.nih.gov/pubmed/2963001

Stawarski, M., Hernandez, R. X., Feghhi, T., Borycz, J. A., Lu, Z., Agarwal, A. B., Reihl, K. D., Tavora, R., Lau, A. W. C., Meinertzhagen, I. A., Renden, R., & Macleod, G. T. (2020). Neuronal Glutamatergic Synaptic Clefts Alkalinize Rather Than Acidify during Neurotransmission. *J Neurosci*, *40*(8), 1611-1624. https://doi.org/10.1523/JNEUROSCI.1774-19.2020

Stellwagen, D., Beattie, E. C., Seo, J. Y., & Malenka, R. C. (2005). Differential regulation of AMPA receptor and GABA receptor trafficking by tumor necrosis factor-alpha. *J Neurosci*, *25*(12), 3219-3228. https://doi.org/10.1523/JNEUROSCI.4486-04.2005

Stellwagen, D., & Malenka, R. C. (2006). Synaptic scaling mediated by glial TNF-alpha. *Nature*, *440*(7087), 1054-1059. https://doi.org/10.1038/nature04671

Strehler, E. E., Caride, A. J., Filoteo, A. G., Xiong, Y., Penniston, J. T., & Enyedi, A. (2007). Plasma membrane Ca2+ ATPases as dynamic regulators of cellular calcium handling. *Ann N Y Acad Sci*, *1099*, 226-236. https://doi.org/10.1196/annals.1387.023

Strehler, E. E., & Zacharias, D. A. (2001). Role of alternative splicing in generating isoform diversity among plasma membrane calcium pumps. *Physiol Rev*, *81*(1), 21-50. https://doi.org/10.1152/physrev.2001.81.1.21

Stuck, E. D., Christensen, R. N., Huie, J. R., Tovar, C. A., Miller, B. A., Nout, Y. S., Bresnahan, J. C., Beattie, M. S., & Ferguson, A. R. (2012). Tumor necrosis factor alpha mediates GABA(A) receptor trafficking to the plasma membrane of spinal cord neurons in vivo. *Neural Plast*, *2012*, 261345. https://doi.org/10.1155/2012/261345

Sumardika, I. W., Chen, Y., Tomonobu, N., Kinoshita, R., Ruma, I. M. W., Sato, H., Kondo, E., Inoue, Y., Yamauchi, A., Murata, H., Yamamoto, K. I., Tomida, S., Shien, K., Yamamoto, H., Soh, J., Futami, J., Putranto, E. W., Hibino, T., Nishibori, M., Toyooka, S., & Sakaguchi, M. (2019). Neuroplastin-beta mediates S100A8/A9-induced lung cancer disseminative progression. *Mol Carcinog*, *58*(6), 980-995. https://doi.org/10.1002/mc.22987

Sun, W., Suzuki, K., Toptunov, D., Stoyanov, S., Yuzaki, M., Khiroug, L., & Dityatev, A. (2019). In vivo Two-Photon Imaging of Anesthesia-Specific Alterations in Microglial Surveillance and Photodamage-Directed Motility in Mouse Cortex. *Front Neurosci*, *13*, 421. https://doi.org/10.3389/fnins.2019.00421

Svoboda, K., Tank, D. W., & Denk, W. (1996). Direct measurement of coupling between dendritic spines and shafts. *Science*, *272*(5262), 716-719. https://doi.org/10.1126/science.272.5262.716

Szewczyk, M. M., Pande, J., Akolkar, G., & Grover, A. K. (2010). Caloxin 1b3: a novel plasma membrane Ca(2+)-pump isoform 1 selective inhibitor that increases cytosolic Ca(2+) in endothelial cells. *Cell Calcium*, *48*(6), 352-357. https://doi.org/10.1016/j.ceca.2010.10.008

Tancredi, V., D'Arcangelo, G., Grassi, F., Tarroni, P., Palmieri, G., Santoni, A., & Eusebi, F. (1992). Tumor necrosis factor alters synaptic transmission in rat hippocampal slices. *Neurosci Lett*, *146*(2), 176-178. https://doi.org/10.1016/0304-3940(92)90071-e

Tang, S., & Yasuda, R. (2017). Imaging ERK and PKA Activation in Single Dendritic Spines during Structural Plasticity. *Neuron*, *93*(6), 1315-1324 e1313. https://doi.org/10.1016/j.neuron.2017.02.032

Tchelingerian, J. L., Quinonero, J., Booss, J., & Jacque, C. (1993). Localization of TNF alpha and IL-1 alpha immunoreactivities in striatal neurons after surgical injury to the hippocampus. *Neuron*, *10*(2), 213-224. https://doi.org/10.1016/0896-6273(93)90312-f

Thomas, G. M., & Huganir, R. L. (2004). MAPK cascade signalling and synaptic plasticity. *Nat Rev Neurosci*, *5*(3), 173-183. https://doi.org/10.1038/nrn1346

van Bommel, B., Konietzny, A., Kobler, O., Bar, J., & Mikhaylova, M. (2019). F-actin patches associated with glutamatergic synapses control positioning of dendritic lysosomes. *EMBO J*, *38*(15), e101183. https://doi.org/10.15252/embj.2018101183

Vemula, S. K., Malci, A., Junge, L., Lehmann, A. C., Rama, R., Hradsky, J., Matute, R. A., Weber, A., Prigge, M., Naumann, M., Kreutz, M. R., Seidenbecher, C. I., Gundelfinger, E. D., & Herrera-Molina, R. (2020). The Interaction of TRAF6 With Neuroplastin Promotes Spinogenesis During Early Neuronal Development. *Front Cell Dev Biol*, *8*, 579513. https://doi.org/10.3389/fcell.2020.579513

Verma, A. K., Filoteo, A. G., Stanford, D. R., Wieben, E. D., Penniston, J. T., Strehler, E. E., Fischer, R., Heim, R., Vogel, G., Mathews, S., & et al. (1988). Complete primary structure of a human plasma membrane Ca2+ pump. *J Biol Chem*, *263*(28), 14152-14159. https://www.ncbi.nlm.nih.gov/pubmed/2844759

Williams, J. C., Armesilla, A. L., Mohamed, T. M., Hagarty, C. L., McIntyre, F. H., Schomburg, S., Zaki, A. O., Oceandy, D., Cartwright, E. J., Buch, M. H., Emerson, M., & Neyses, L. (2006). The sarcolemmal calcium pump, alpha-1 syntrophin, and neuronal nitric-oxide synthase are parts of a macromolecular protein complex. *J Biol Chem*, *281*(33), 23341-23348. https://doi.org/10.1074/jbc.M513341200

Willmott, T., Skitsa, I., Hill, I., Mummery, R., & Beesley, P. W. (1992). Molecular characterisation and structural relationship of the synapse-enriched glycoproteins gp65 and gp55. *J Neurochem*, *58*(6), 2037-2043. https://doi.org/10.1111/j.1471-4159.1992.tb10944.x

Wilson, M. C., Kraus, M., Marzban, H., Sarna, J. R., Wang, Y., Hawkes, R., Halestrap, A. P., & Beesley, P. W. (2013). The neuroplastin adhesion molecules are accessory proteins that chaperone the monocarboxylate transporter MCT2 to the neuronal cell surface. *PLoS One*, *8*(11), e78654. https://doi.org/10.1371/journal.pone.0078654

Winnubst, J., Cheyne, J. E., Niculescu, D., & Lohmann, C. (2015). Spontaneous Activity Drives Local Synaptic Plasticity In Vivo. *Neuron*, *87*(2), 399-410. https://doi.org/10.1016/j.neuron.2015.06.029

Wu, G. Y., Deisseroth, K., & Tsien, R. W. (2001). Spaced stimuli stabilize MAPK pathway activation and its effects on dendritic morphology. *Nat Neurosci*, *4*(2), 151-158. https://doi.org/10.1038/83976

Yagi, T., Asada, R., Kanekura, K., Eesmaa, A., Lindahl, M., Saarma, M., & Urano, F. (2020). Neuroplastin Modulates Anti-inflammatory Effects of MANF. *iScience*, *23*(12), 101810. https://doi.org/10.1016/j.isci.2020.101810

Yuste, R., & Denk, W. (1995). Dendritic spines as basic functional units of neuronal integration. *Nature*, *375*(6533), 682-684. https://doi.org/10.1038/375682a0

Zeng, W. Z., Grillet, N., Dewey, J. B., Trouillet, A., Krey, J. F., Barr-Gillespie, P. G., Oghalai, J. S., & Muller, U. (2016). Neuroplastin Isoform Np55 Is Expressed in the Stereocilia of Outer Hair Cells and Required for Normal Outer Hair Cell Function. *J Neurosci*, *36*(35), 9201-9216. https://doi.org/10.1523/JNEUROSCI.0093-16.2016

Zhai, S., Ark, E. D., Parra-Bueno, P., & Yasuda, R. (2013). Long-distance integration of nuclear ERK signaling triggered by activation of a few dendritic spines. *Science*, *342*(6162), 1107-1111. https://doi.org/10.1126/science.1245622

Zhu, J. J., Qin, Y., Zhao, M., Van Aelst, L., & Malinow, R. (2002). Ras and Rap control AMPA receptor trafficking during synaptic plasticity. *Cell*, *110*(4), 443-455. https://doi.org/10.1016/s0092-8674(02)00897-8

Zou, J. Y., & Crews, F. T. (2005). TNF alpha potentiates glutamate neurotoxicity by inhibiting glutamate uptake in organotypic brain slice cultures: neuroprotection by NF kappa B inhibition. *Brain Res*, *1034*(1-2), 11-24. https://doi.org/10.1016/j.brainres.2004.11.014

Zvaritch, E., James, P., Vorherr, T., Falchetto, R., Modyanov, N., & Carafoli, E. (1990). Mapping of functional domains in the plasma membrane Ca2+ pump using trypsin proteolysis. *Biochemistry*, *29*(35), 8070-8076. https://doi.org/10.1021/bi00487a012

7. List of abbreviations

AMPAR	α-amino-3-hydroxy-5-methyl-4-isoxazolepropionic acid receptor
AP	Action potential
APV	2-Amino-5-phosphonovaleric acid
ATP	Adenosine triphosphate
BSA	Bovine serum albumin
Ca^{2+}	Calcium
CAM	Cell adhesion molecule
CaM	Calmodulin
CaMKII	Ca^{2+}/Calmodulin-dependent protein kinase II
cDNA	Complementary deoxyribonucleic acid
CNQX	6-cyano-7-nitroquinoxaline-2,3-dione
C-terminus	Carboxy terminus
DAG	Diacylglycerol
DIV	Day in vitro
DMEM	Dulbecco's modified eagle's medium
E. coli	Escherichia coli
EF	Endotoxin free
ER	Endoplasmic reticulum
ERK1/2	Extracellular signal-regulated protein kinases 1/2
FGFR	Fibroblast growth factor receptor
FRET	Fluorescence resonance energy transfer
$GABA_AR$	A-type of gamma-amino butyric acid receptor
GECIs	Genetically encoded fluorescent Ca^{2+} indicators
GFP	Green fluorescent protein
GRB2	Growth factor receptor-bound protein 2
HBSS	Hank's balanced salt solution
HEPES	4-(2-hydroxyethyl)-1-piperazineethanesulfonic acid
HEK	Human embryonic kidney cell
HFS	High-frequency-stimulation
Ig	Immunoglobulin
IP_3R	Inositol 1,4,5-trisphosphate receptor
JNK	c-Jun N-terminal kinase
KO	Knockout
LTD	Long term depression
LTP	Long term potentiation
MANF	Mesencephalic astrocyte-derived neurotrophic factor
MAPK	Mitogen-activated protein kinase

MAGUK	Membrane-associated guanylate kinase
MCT2	Monocarboxylate transporter 2
MCU	Mitochondrial calcium uniporter
mEPSC	Miniature excitatory postsynaptic current
NCX	Na^+/Ca^{2+}-exchanger
NFAT	Nuclear factor of activated T-cell
NF-κB	Nuclear factor-kappa B
NMDAR	The N-methyl-D-aspartate receptor
NOS-1	Nitric-oxide synthase-1
OGB-1	Oregon Green BAPTA-1
PI_3K	Phosphoinositide 3-kinase
$PtdIns(4,5)P_2$	Phosphatidylinositol 4,5- bisphosphate
PIP_2	Phosphatidylinositol-4,5-bisphosphate
PMCA	Plasma membrane calcium ATPase
PKA	Protein kinase A
PKC	Protein kinase C
PLC	Phospholipase C
PSD	Post-synaptic density
ROI	Region of interest
RT	Room temperature
SA	Spine apparatus
SDS-PAGE	Sodium dodecyl sulfate–polyacrylamide gel electrophoresis
SEM	Standard error of the mean
SERCA	Sarco/endoplasmic reticulum calcium ATPase
SNPs	Single nucleotide polymorphisms
STED	Stimulated emission depletion
TBS	Tris-buffered saline
TMD	Transmembrane domain
TNF	Tumor-necrosis factor
TRAF	Tumor-necrosis factor receptor associated factor
TTX	Tetrodotoxin
VGCC	Voltage-gated calcium channel
WLL	White light laser
WT	Wild-type

8. List of figures

9. List of tables

10. Appendix

Table 9. Normalized calcium kinetics upon stimulation with HFS in Figure 9

	Dendrites				Spines			
	-	**CE**	**Np65**	**Np65 +CE**	**-**	**CE**	**Np65**	**Np65 +CE**
Decay time	1.000 ± 0.06269	1.653 ± 0.1227	0.5923 ± 0.02370	1.882 ± 0.1197	1.008 ± 0.03106	1.441 ± 0.05445	0.6734 ± 0.01703	1.567 ± 0.07448
Half-width	1.00 ± 0.0358	1.11 ± 0.0445	0.7272 ± 0.01823	1.058 ± 0.04463	1.000 ± 0.02066	1.065 ± 0.02563	0.6962 ± 0.01467	0.9274 ± 0.03994
Peak amplitude	0.9261 ± 0.08931	1.701 ± 0.1882	0.4270 ± 0.03217	0.6604 ± 0.08712	0.9273 ± 0.04236	1.227 ± 0.06796	0.2658 ± 0.01329	0.2764 ± 0.01677
Rise time	0.9784 ± 0.04841	0.7957 ± 0.08293	0.9286 ± 0.06341	0.8083 ± 0.08722	1.000 ± 0.03793	0.9348 ± 0.05256	0.9357 ± 0.04171	1.351 ± 0.07846

Table 10. Normalized calcium kinetics of spontaneous activity in Figure 10

	Dendrites		Spines	
	-	**Np65**	**-**	**Np65**
Decay time	1.000 ± 0.03325	0.6779 ± 0.01040	1.000 ± 0.01802	0.7969 ± 0.007375
Half-width	1.000 ± 0.01916	0.9426 ± 0.009923	1.000 ± 0.01267	0.9771 ± 0.007507
Peak amplitude	0.9955 ± 0.03355	0.7725 ± 0.01650	1.000 ± 0.02281	0.8519 ± 0.01592
Rise time	0.9548 ± 0.01383	1.030 ± 0.01091	0.9517 ± 0.01267	1.047 ± 0.01022

Table 11. Synaptic localization of PMCA, Neuroplastin and NMDAR2A in Figure 12

	PMCA		Neuroplastin		NMDAR2A	
	-	**HFS**	**-**	**HFS**	**-**	**HFS**
N° clusters/µm²	62.11 ± 2.129	72.85 ± 2.250	49.60 ± 1.866	58.35 ± 2.027	50.05 ± 2.297	51.22 ± 2.241
Puncta (intensity x area)	8.485 ± 0.3605	10.74 ± 0.4839	3.550 ± 0.1702	3.649 ± 0.2286	6.896 ± 0.4970	7.272 ± 0.5196
Intensity (a.u.)	36.89 ± 1.790	39.90 ± 1.909	14.65 ± 0.3907	14.83 ± 0.4919	24.12 ± 1.382	22.55 ± 0.9605
Area (µm²/Shank2)	0.2525 ± 0.0102	0.2811 ± 0.0083	0.2410 ± 0.0086	0.2416 ± 0.0096	0.279 ± 0.0133	0.312 ± 0.0111

Table 12. Shank2 area in PMCA, Neuroplastin and NMDAR2A immunostainings

	-		APV&CNQX		Caloxins	
	-	HFS	-	HFS	-	HFS
Shank2 area (μm^2)	0.03363 ± 0.001236	0.03082 ± 0.0009580	0.03134 ± 0.0008642	0.03176 ± 0.001319	0.03168 ± 0.001271	0.03122 ± 0.001414

Table 13. Synaptic localization of PMCA, Neuroplastin and NMDAR2A in Figure 14

	PMCA				Neuroplastin				NMDAR2A			
	APV&CNQX		Caloxins		APV&CNQX		Caloxins		APV&CNQX		Caloxins	
	-	HFS	-	HFS	-	HFS	-	HFS	-	HFS	-	HFS
N° clusters/μm^2	73.31 ± 2.703	66.51 ± 1.703	64.53 ± 2.104	68.49 ± 2.638	56.75 ± 1.887	54.39 ± 1.986	52.99 ± 1.778	59.13 ± 3.134	56.25 ± 2.402	52.65 ± 2.798	52.46 ± 2.484	51.26 ± 2.547
Puncta (intensity x area)	10.07 ± 0.533	9.267 ± 0.460	9.756 ± 0.524	9.825 ± 0.541	3.525 ± 0.237	3.548 ± 0.253	4.342 ± 0.269	3.492 ± 0.183	7.515 ± 0.569	6.524 ± 0.654	6.915 ± 0.659	7.385 ± 0.512
Intensity (a.u.)	39.17 ± 1.935	38.31 ± 2.048	38.14 ± 1.847	38.74 ± 2.051	14.56 ± 0.519	14.49 ± 0.591	16.96 ± 0.718	13.90 ± 0.344	24.37 ± 0.932	20.48 ± 1.057	21.65 ± 1.192	23.56 ± 0.875
Area (μm^2/Shank2)	0.269 ± 0.008	0.257 ± 0.008	0.264 ± 0.009	0.269 ± 0.008	0.236 ± 0.009	0.236 ± 0.009	0.255 ± 0.007	0.253 ± 0.010	0.299 ± 0.015	0.304 ± 0.018	0.293 ± 0.019	0.304 ± 0.014

Table 14. Synaptic localization of PMCA, Neuroplastin and NMDAR2A seems to be regulated by glutamate receptor activity and PMCA activity in Figure 15

	PMCA-Neuroplastin				PMCA-NMDAR2A			
	APV&CNQX		Caloxins		APV&CNQX		Caloxins	
	-	HFS	-	HFS	-	HFS	-	HFS
Pearson coefficient	0.8039 ± 0.0086	0.8402 ± 0.0078	0.7968 ± 0.0089	0.8224 ± 0.0087	0.1742 ± 0.0093	0.1933 ± 0.0074	0.1771 ± 0.0102	0.1834 ± 0.0099
Shortest distance	0.1443 ± 0.0180	0.1697 ± 0.0204	0.2130 ± 0.0258	0.1220 ± 0.0085	0.2345 ± 0.0068	0.2206 ± 0.0046	0.2400 ± 0.0072	0.2203 ± 0.0045

Table 15. Normalized calcium kinetics upon stimulation with 5 APs in Figure 16

	Dendrites		Spines		Dendrites		Spines	
	-	CLX	-	CLX	-	Saline	-	Saline
Decay time	1.030 ± 0.06932	1.204 ± 0.06419	1.000 ± 0.05074	1.274 ± 0.05305	1.000 ± 0.1261	0.8539 ± 0.08016	0.9003 ± 0.08467	0.8312 ± 0.05224
Half-width	1.000 ± 0.05739	1.004 ± 0.05657	1.000 ± 0.04967	1.076 ± 0.05480	1.000 ± 0.08909	1.025 ± 0.06914	1.008 ± 0.05893	1.059 ± 0.07175
Rise time	0.9685 ± 0.03163	1.006 ± 0.03244	1.000 ± 0.03259	1.030 ± 0.04119	1.000 ± 0.09932	1.112 ± 0.07260	1.000 ± 0.06216	1.137 ± 0.05810
Baseline	1.000 ± 0.06428	0.9668 ± 0.06698	1.000 ± 0.05124	0.9367 ± 0.05394	1.000 ± 0.1258	0.9550 ± 0.1105	0.9747 ± 0.05395	0.9900 ± 0.04445

Table 16. Normalized calcium kinetics upon stimulation with 5 APs in Figure 18

	Dendrites			Spines		
	TTX ORM	CLX 5 min	CLX 10 min	TTX ORM	CLX 5 min	CLX 10 min
Decay time	1.000 ± 0.04902	1.291 ± 0.08181	1.108 ± 0.07473	1.000 ± 0.02764	1.350 ± 0.07334	1.068 ± 0.04516
Half-width	1.000 ± 0.04391	1.037 ± 0.04681	0.9550 ± 0.04008	1.000 ± 0.03461	1.061 ± 0.04127	1.019 ± 0.04641
Rise time	1.000 ± 0.02939	1.103 ± 0.03519	0.9919 ± 0.02648	1.000 ± 0.02620	1.045 ± 0.03136	1.045 ± 0.02911
Baseline	1.000 ± 0.04306	0.8520 ± 0.03422	0.8927 ± 0.03646	1.000 ± 0.03330	0.8966 ± 0.03248	0.9712 ± 0.03755

Table 17. Normalized calcium kinetics upon stimulation with 5-10 APs in Figure 19

	Dendrites				Spines			
	APV CNQX	CLX 2 min	CLX 5 min	CLX 10 min	APV CNQX	CLX 2 min	CLX 5 min	CLX 10 min
Decay time	1.000 ± 0.04235	1.025 ± 0.04287	1.045 ± 0.03991	0.9372 ± 0.04286	1.000 ± 0.02676	1.093 ± 0.03035	1.032 ± 0.02831	0.9323 ± 0.02283
Half-width	0.9738 ± 0.02732	1.007 ± 0.02699	0.9863 ± 0.02179	0.9554 ± 0.02595	1.000 ± 0.02286	1.016 ± 0.02625	0.9457 ± 0.02149	0.9458 ± 0.02200
Rise time	1.000 ± 0.01321	0.9526 ± 0.01408	1.000 ± 0.01949	0.9736 ± 0.01821	1.000 ± 0.01627	0.9791 ± 0.01678	0.9772 ± 0.01583	0.9741 ± 0.01612

Table 18. Normalized calcium kinetics upon stimulation with HFS in Figure 20

	Dendrites				Spines			
	-	CE	Np65	Np65 +CE	-	CE	Np65	Np65 +CE
Decay time	1.000 ± 0.06176	1.298 ± 0.07874	1.337 ± 0.08622	1.892 ± 0.1851	1.000 ± 0.03809	1.146 ± 0.04358	1.242 ± 0.05039	1.834 ± 0.1073
Half-width	1.000 ± 0.03168	1.004 ± 0.02151	0.9997 ± 0.03645	1.089 ± 0.05297	1.000 ± 0.01727	0.9370 ± 0.03057	0.9616 ± 0.02647	1.154 ± 0.02856
Peak amplitude	0.9305 ± 0.1367	0.7267 ± 0.07930	0.5059 ± 0.04665	0.5779 ± 0.06931	1.000 ± 0.07960	0.8015 ± 0.05750	0.7916 ± 0.04214	1.116 ± 0.04214
Rise time	1.000 ± 0.08512	0.7479 ± 0.05663	0.8894 ± 0.05595	0.6700 ± 0.07278	0.9943 ± 0.05325	0.6770 ± 0.03809	0.9431 ± 0.03597	0.8784 ± 0.05664

Table 19. Normalized calcium kinetics upon stimulation with HFS in Figure 21

	Dendrites				Spines			
	-		Np65		-		Np65	
	-	APV CNQX	-	APV CNQX	-	APV CNQX	-	APV CNQX
Decay time	1.010 ± 0.06032	0.7583 ± 0.05790	0.8097 ± 0.03950	0.6721 ± 0.04725	1.000 ± 0.03805	0.7763 ± 0.03782	0.8940 ± 0.02769	0.6870 ± 0.02822
Half-width	1.000 ± 0.05952	0.8222 ± 0.05831	0.9387 ± 0.04300	0.6644 ± 0.03009	1.000 ± 0.03780	0.8485 ± 0.04136	0.8683 ± 0.02423	0.6033 ± 0.01529
Peak amplitude	1.059 ± 0.1212	0.5464 ± 0.05762	0.4750 ± 0.03898	0.3065 ± 0.02278	1.000 ± 0.07381	0.7472 ± 0.05608	0.6015 ± 0.03349	0.4516 ± 0.02607
Rise time	1.000 ± 0.05275	1.405 ± 0.1098	0.9051 ± 0.02333	0.9095 ± 0.03200	1.000 ± 0.06410	1.095 ± 0.06784	0.8386 ± 0.02701	0.7805 ± 0.03271

Table 20. Normalized calcium kinetics upon stimulation with HFS in Figure 22

	Dendrites				Spines			
	-		APV+CNQX		-		APV+CNQX	
	-	CLX	-	CLX	-	CLX	-	CLX
Decay time	1.000 ± 0.05119	0.8777 ± 0.05563	0.7485 ± 0.07581	0.8699 ± 0.06339	1.000 ± 0.03716	0.8328 ± 0.02873	0.6922 ± 0.03444	0.8817 ± 0.05215
Half-width	1.000 ± 0.04651	0.9495 ± 0.04370	0.9540 ± 0.04125	0.9553 ± 0.03456	1.000 ± 0.02598	0.9318 ± 0.02889	0.8106 ± 0.02773	0.9152 ± 0.02565
Peak amplitude	1.030 ± 0.05984	1.177 ± 0.1219	0.6060 ± 0.05886	1.437 ± 0.1539	1.039 ± 0.03771	1.355 ± 0.07296	0.6189 ± 0.03957	1.223 ± 0.06498
Rise time	1.000 ± 0.1259	1.031 ± 0.1377	1.517 ± 0.1200	1.031 ± 0.09942	1.000 ± 0.06203	0.6273 ± 0.07145	1.516 ± 0.06933	1.033 ± 0.06229

Table 21. Synaptic localization of p-CaMKIIα and p-ERK1/2 in Figure 25

	p-CaMKII				p-ERK1/2			
	-		CLX		-		CLX	
	-	HFS	-	HFS	-	HFS	-	HFS
N° clusters/μm²	42.71 ± 1.842	49.06 ± 1.974	48.17 ± 2.982	53.78 ± 4.661	40.95 ± 2.088	50.83 ± 2.173	48.20 ± 2.808	59.78 ± 4.401
Puncta (intensity x area)	6.823 ± 0.6182	10.08 ± 0.7631	6.513 ± 0.5920	6.144 ± 0.4819	9.511 ± 0.8204	12.32 ± 0.8566	8.247 ± 0.6292	9.932 ± 0.9586
Intensity (a.u.)	45.57 ± 2.082	48.85 ± 2.036	43.17 ± 1.847	40.57 ± 1.697	47.29 ± 2.102	52.28 ± 2.011	47.40 ± 2.047	45.54 ± 2.199
Area (μm²/Shank2)	0.1486 ± 0.009498	0.2062 ± 0.01118	0.1501 ± 0.00999	0.1582 ± 0.01030	0.1995 ± 0.01178	0.2246 ± 0.01276	0.1685 ± 0.008234	0.1981 ± 0.01132

11. Ehrenerklärung

Ich versichere hiermit, dass ich die vorliegende Arbeit ohne unzulässige Hilfe Dritter und ohne Benutzung anderer als der angegebenen Hilfsmittel angefertigt habe; verwendete fremde und eigene Quellen sind als solche kenntlich gemacht.

Ich habe insbesondere nicht wissentlich:

- Ergebnisse erfunden oder widersprüchliche Ergebnisse verschwiegen,
- statistische Verfahren absichtlich missbraucht, um Daten in ungerechtfertigter Weise zu interpretieren,
- fremde Ergebnisse oder Veröffentlichungen plagiiert,
- fremde Forschungsergebnisse verzerrt wiedergegeben.

Mir ist bekannt, dass Verstöße gegen das Urheberrecht Unterlassungs- und Schadensersatzansprüche des Urhebers sowie eine strafrechtliche Androhung durch die Strafverfolgungsbehörden begründen kann.

Ich erkläre mich damit einverstanden, dass die Arbeit ggf. mit Mitteln der elektronischen Datenverarbeitung auf Plagiate überprüft werden kann.

Die Arbeit wurde bisher weder im Inland noch im Ausland in gleicher oder ähnlicher Form als Dissertation eingereicht und ist als Ganzes auch noch nicht veröffentlicht.

Magdeburg, 17.12.2021 Ayse Malci